

T-2987

ANALYTIC CONTINUATION OF
ELECTROMAGNETIC FIELDS

by

Kun Deuk Kim

ARTHUR LAKES LIBRARY
COLORADO SCHOOL of MINES
GOLDEN, COLORADO 80401

ProQuest Number: 10796254

All rights reserved

INFORMATION TO ALL USERS

The quality of this reproduction is dependent upon the quality of the copy submitted.

In the unlikely event that the author did not send a complete manuscript and there are missing pages, these will be noted. Also, if material had to be removed, a note will indicate the deletion.



ProQuest 10796254

Published by ProQuest LLC (2019). Copyright of the Dissertation is held by the Author.

All rights reserved.

This work is protected against unauthorized copying under Title 17, United States Code
Microform Edition © ProQuest LLC.

ProQuest LLC.
789 East Eisenhower Parkway
P.O. Box 1346
Ann Arbor, MI 48106 – 1346

T-2987

A thesis submitted to the Faculty and the Board of Trustees of the Colorado School of Mines in partial fulfillment of the requirements for the degree of Doctor of Philosophy (Geophysical Engineering).

Golden, Colorado

Date 26 Nov 84

Signed: Kim D. Kim
Kun D. Kim

Approved: George V. Keller
George V. Keller,
Thesis Advisor

Golden, Colorado

Date 26 Nov 84

PR Romig
Phillip R. Romig,
Head of Department
of Geophysics.

ABSTRACT

A scheme for interpretation of electromagnetic data by analytic continuation was studied.

Using the Stratton-Chu integrals, it is possible to express the electromagnetic field at a point inside the Earth in terms of the fields at the Earth's surface and at the lower side of the surface bounding the point. The Fourier expansion of the Green's function permits us to express the field inside the Earth in terms of the fields on the Earth's surface only.

The primary purpose of analytic continuation is to determine the location of inhomogeneities within the Earth through an increase in resolution. A fair estimate of the depth of inhomogeneities can be made from a visual examination alone of the continued data.

The noise test performed reveals that the analytic continuation can be used to extract a signal which is cluttered with random noise.

Since the analytic continuation works quite well in the problems of depth estimation, resolution, and signal enhancement, it offers a better approach to the interpretation of geoelectric problems than the method of a reconstruction of the electric conductivity is combined as a successive step of analytic continuation.

TABLE OF CONTENTS

ABSTRACT	iii
TABLE OF CONTENTS	iv
LIST OF FIGURES	v
ACKNOWLEDGEMENTS	x
INTRODUCTION	1
PHYSICAL BASIS OF THE PROBLEM	4
MATHEMATICAL FORMULATION AND COMPUTATION	8
1. Derivation of the equation of analytic continuation	8
2. Method of computation	19
APPLICATION OF THE ANALYTIC CONTINUATION	27
1. Signal enhancement and localization of an inhomogeneity	27
2. Resolution problem	45
3. Accuracy of scale or computer modeling	64
CONCLUSIONS	69
REFERENCES	71
APPENDIX A. INTERACTIVE USER'S MANUAL - SAMPLE SESSION FOR MODELING AND CONTINUATION FOR A MAGNETIC DIPOLE SOURCE	73
APPENDIX B. TEST DATA - MODELING AND CONTINUATION.	75
APPENDIX C. COMPUTER PROGRAM LISTINGS	93

LIST OF FIGURES

Fig.1.	Geometry of domains and boundaries	5
Fig.2.	Domains and boundaries in the geoelectric problem	5
Fig.3.	Flow chart of the program ACEF	20
Fig.4.	Schematic diagram of the two dipole model	23
Fig.5.	Contour of the in-phase component of Hz. The depth of dipoles is 120m.	24
Fig.6.	Contour of the in-phase component of Hz after downward continuation. The depth of continuation is 20m.....	25
Fig.7	Modeling data at the depth of 100m.	26
Fig.8.	Logarithmic amplitude of vertical magnetic field. The depth of dipole is 100m.	29
Fig.9.	Contour after downward continuation. The depth of continuation is 20m.	30
Fig.10.	Modeling data at the depth of 100m	31
Fig.11.	Profile after downward continuation. The depth of continuation is $z/d=0.1$, where d is the depth to the dipole.	35
Fig12.	Profile after downward continuation. The depth of continuation is $z/d=0.5$	36

Fig.13. Profile after downward continuation. The depth of continuation is $z/d=0.9$	37
Fig.14. Profile after downward continuation. The o-mark line is the theoretical data. The Δ -mark line is profile with spacing 25m	38
Fig.15. The effect of grid spacing. The o-mark line is profile with spacing 20m. The Δ -mark line is profile with spacing 25m.	39
Fig.16. The oscillations generated due to fine grid. The grid spacing is 10m.	40
Fig.17. Downward continuation beyond the source region. The depth of continuation is 120m.	41
Fig.18. Contour of the propagated field.	42
Fig.19. Contour after downward continuation. The depth of continuation is $z/d=0.2$	43
Fig.20. Contour of the modeling data at the depth of $z/d=0.8$	44
Fig.21. Resolution problem. The depth of dipoles is 120m. The o-mark line is the profile after downward continuation to the level $z=100m$	46
Fig.22. Real component of the noise generated.	47
Fig.23. Imaginary component of the noise generated	48

Fig.24. Resolution problem. S/N ratio is 40	51
Fig.25. Resolution problem. S/N ratio is 20	52
Fig.26. Resolution problem. S/N ratio is 10	53
Fig.27. Resolution problem. S/N ratio is 5	54
Fig.28. Amplitude spectrum of the surface data. The depth of dipoles is 120m.	57
Fig.29. Amplitude spectrum of the surface data after convolution in the frequency domain.	58
Fig.30. Amplitude spectrum of the modeling data at the depth of 100m.	59
Fig.31. Amplitude spectrum of the surface data with 10 percent noise.	60
Fig.32. Amplitude spectrum of the data with 10 percent noise after convolution in the frequency domain.	61
Fig.33. Three-dimensional view of the amplitude spectrum of the surface data with 10 percent noise.	62
Fig.34. Three-dimensional view of the amplitude spectrum after convolution in the frequency domain.	63
Fig.35. Schematic diagram of the plate model.	64
Fig.36. Comparison between the theoretical data and the continued data.	67
Fig.37. Convergence of the continued data.	68

LIST OF SYMBOLS

\vec{E}	- Electric field intensity
\vec{H}	- Magnetic field intensity
\vec{J}	- Electric current density
q	- density of electric charge
σ	- Conductivity
ϵ	- dielectric permeability
μ	- Magnetic permeability. $4\pi \times 10^{-7}$ henry/m
ω	- Angular frequency
k	- Propagation constant
G	- Free space Green function
δ	- Dirac delta function
\vec{E}_0	- Electric field intensity at the Earth's surface
\vec{H}_0	- Magnetic field intensity at the Earth's surface
\vec{n}	- Unit normal vector
S	- Surface of integration
V	- Volume of integration
Γ	- Outer boundary of the domain
γ	- Inner boundary of the domain
\vec{J}^{ex}	- Density of extrinsic electric currents
q^{ex}	- Density of extrinsic electric charge

T-2987

$i - \sqrt{-1}$

V_+ - Domain outside the Earth's surface

V_- - Domain inside the Earth's surface

\bar{C} - Arbitrary constant vector

\bar{z} - Coordinate of the receiver

ACKNOWLEDGEMENTS

I wish to express my appreciation to my thesis advisor Professor George V. Keller, for his guidance and encouragement during the preparation of this work.

I am very grateful to Professors Alexander A. Kaufmann, Catherine A. Skokan, Donald I. Dickinson, and Jack K. Cohen for many valuable suggestions and much assistance as my committee members.

I also thank the Department of Geophysics, which sponsored my thesis work at Colorado School of Mines.

INTRODUCTION

Inverse problems are current sources of ongoing research in every branch of geophysics. Methods of solution of the inverse problems of geoelectrics fall into two groups:

(1) reconstruction of the surface field by analytic continuation; (2) reconstruction of the geoelectrical cross section of an inhomogeneity. These are the two trends of modern geoelectrical development.

The method of analytic continuation has been widely used in seismic, gravity, and magnetic prospecting. In the seismic case, the analytic continuation permits to reconstruct the subsurface field from the surface data. After that, the reflectors are imaged at each step of continuation, which is the dominant method in the seismic data processing, known as migration. The question of analytic continuation of time-varying electromagnetic field has been studied to a much lesser degree.

The second problem, which is the reconstruction of the electric conductivity, has been solved for a two-dimensional problem by Weidelt (1975) and Vozoff (1977) using the iterative algorithm and finite difference method, respectively. Recently, the finite element method has been developed by Oristaglio and Worthington (1980), which improved the in-

stability problems of previous algorithms.

It seems that the interpretation of geoelectric problems should consist of these two successive steps.

In this thesis, the problem of analytic continuation has been studied for the purpose of developing a scheme for interpretation of electromagnetic data, and for deriving a better model to reconstruct the geoelectrical cross section.

Several papers by Kertz (1957), Hartmann (1963), and Roy (1968, 1969) consider some simple situations using the Taylor series. This method has practical difficulty, because the radius of convergence of Taylor series is small and we need to do successive expansion for further points, which produce great error and computing costs. It is possible to construct an analytical method which could be free of these limitations, i.e. a method by which we can express the EM field at a point in terms of the integrals on the boundary. Such a method may be elaborated on the basis of the Stratton-Chu integrals (Stratton, 1953; Zhdanov, 1976, 1978). The Stratton-Chu integral permits to express the electromagnetic field in some domain in terms of its values on the inner side of the surface bounding the domain. By implementing the integral in the domain of geoelectrical problem, the electromagnetic field inside the Earth can be reconstructed from the fields on the Earth's surface.

Generally, we use very low frequency in electromagnetic prospecting; however, in some cases such as tunnel detection or depth sounding in permafrost region, we can resort to very high frequency electromagnetic waves; then we must deal with the propagation problems. Therefore, the general theory of the analytic continuation has been developed using the Stratton-Chu integrals and applied to both diffusion and propagation problems.

In practical electromagnetic situations, the useful signal is often cluttered with random noise, at least part of which is not instrumental, which may be caused by random variations of all parameters of the electromagnetic field.

For this purpose, the effect of the random noise on the analytic continuation was investigated using the surface data which includes random noise for several different signal to noise ratios.

In the presentation, we will start with a discussion of the physical basis of the problem and the derivation of the equations of the analytic continuation.

The second chapter covers the methods of computation and the description of the computer program.

Finally, I discuss the application of the analytic continuation to several practical problems.

PHYSICAL BASIS OF THE PROBLEM

The problem lies in continuing the electromagnetic field observed on the Earth's surface upwards into the air or downwards into the Earth and in constructing a horizontal section of the field.

Let the domain V bounded by the surface Γ be filled with a homogeneous medium of constant electrical conductivity, as shown in Fig.1. The electromagnetic field is excited externally. The electromagnetic fields \bar{E} and \bar{H} in domain V and on boundary Γ satisfy the Helmholtz equations:

$$\nabla^2 \bar{E} + k^2 \bar{E} = 0$$

$$\nabla^2 \bar{H} + k^2 \bar{H} = 0.$$

Take any internal point M_0 within V and circumscribe therefrom a sphere γ lying inside V . Then, we can use the Stratton-Chu integral formula to express the electromagnetic field at some point M' in γ in terms of its values on γ (Stratton, 1953).

The Stratton-Chu formula may be interpreted in a simple physical way. Let electric and magnetic currents and charges of the surface densities \bar{J}_e , \bar{J}_h and q_e , q_h be distributed over the closed surface Γ . They excite an electromagnetic field inside V :

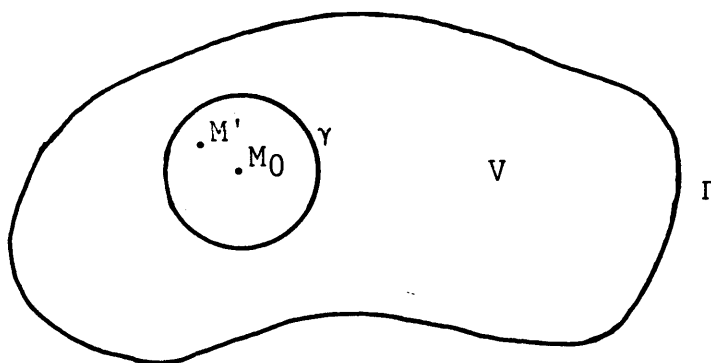


Fig.1. Geometry of domains and boundaries.

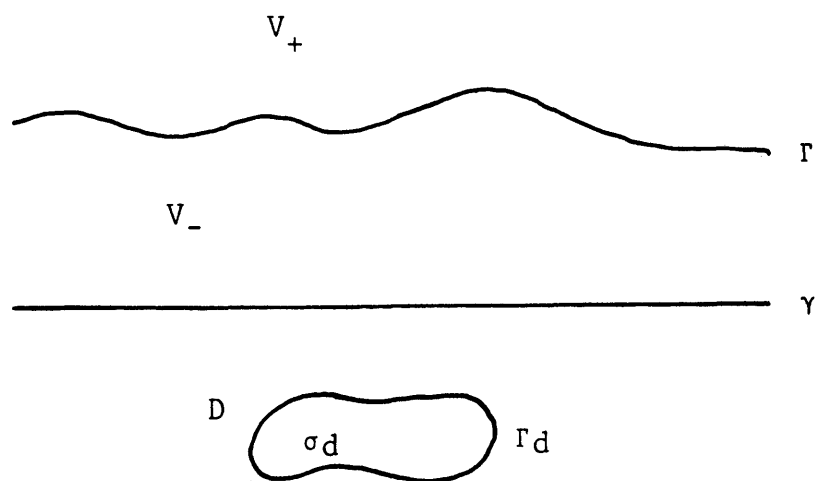


Fig.2. Domains and boundaries in the geoelectric problem.

$$\begin{aligned}\bar{E}(\bar{z}') &= \int_{\Gamma} \left\{ \frac{q_e \text{ grad } G}{\epsilon} - \bar{J}_h \times \text{grad } G + i\omega\mu \bar{J}_e G \right\} dS \\ \bar{H}(\bar{z}') &= \int_{\Gamma} \left\{ \frac{q_h \text{ grad } G}{\mu} + \bar{J}_e \times \text{grad } G - (\sigma - i\omega\epsilon)\bar{J}_h G \right\} dS\end{aligned}$$

where E, H are the electric and magnetic field, respectively; σ , ϵ , μ are electric conductivity, dielectric, and magnetic permeabilities of a medium, respectively; G is the free space Green's function.

Let us compare these expressions with equations (22) and (27) in the next chapter, which are Stratton-Chu integrals derived from the Gauss's formula. The electromagnetic field in V coincides with the field excited by the currents and charges distributed on Γ with identity

$$\begin{aligned}\bar{J}_e &= \{ \bar{n} \times \bar{H} \} & \bar{J}_h &= -\{ \bar{n} \times \bar{E} \} \\ q_e &= \epsilon \{ \bar{n} \cdot \bar{E} \} & q_h &= \mu \{ \bar{n} \cdot \bar{H} \} .\end{aligned}$$

Thus, in the Stratton-Chu formula, the real sources distributed outside V are replaced by equivalent fictitious sources distributed on the surface Γ .

In geoelectric problems, this can be described as follows. A homogeneous Earth with a known electric conductivity $\sigma_- = \text{constant}$ contains an inhomogeneity D of unknown shape or a variable conductivity $\sigma_d \neq \sigma_-$, as shown in Fig.2

The electromagnetic fields E_0 and H_0 have been specified on the Earth's surface Γ . Inside the near-surface domain V_- ,

the fields \bar{E} and \bar{H} must satisfy the Helmholtz equations and on the Earth's surface must coincide with \bar{E}_0 and \bar{H}_0 .

The field \bar{E}_0, \bar{H}_0 is to be continued into some domain V_+ of the Earth. As we pointed out before, the electromagnetic field within V_+ can be expressed in terms of its boundary value on γ and Γ , using the Stratton-Chu integrals.

The electromagnetic fields on Γ are known by measurement; however, the fields on γ are unknown. The integrals on γ can be transformed into the integrals over the Earth's surface Γ via the Fourier expansion of the Green function (Morse and Feshbach, 1953).

Then, the data on the plane γ in the Earth can be represented by the integrals over the Earth's surface Γ , which permits exact formulation of the analytic continuation.

MATHEMATICAL FORMULATION AND COMPUTATION

1. Derivation of the equation of analytic continuation.

In an isotropic medium, the electromagnetic field is governed by the Maxwell equations:

$$\text{curl } \bar{H} = \sigma \bar{E} + \epsilon \frac{\partial \bar{E}}{\partial t} + \bar{J}^{\text{ex}}$$

$$\text{curl } \bar{E} = -\mu \frac{\partial \bar{H}}{\partial t}$$

$$\text{div } \bar{H} = 0$$

$$\text{div } \epsilon \bar{E} = q + q^{\text{ex}}, \quad (1)$$

where \bar{E} , \bar{H} are the electric and magnetic field, respectively; σ , ϵ , μ are electric conductivity, dielectric, and magnetic permeabilities of a medium, respectively; q is the density of free electric charge; \bar{J}^{ex} , q^{ex} are the densities of extrinsic electric currents and charges, respectively.

The values of \bar{J}^{ex} and q^{ex} are related by the continuity equation

$$\text{div } \bar{J}^{\text{ex}} = - \frac{\partial q^{\text{ex}}}{\partial t}. \quad (2)$$

The density of conduction currents is expressed via the electric field by means of Ohm's law

$$\bar{J} = \sigma \bar{E}. \quad (3)$$

Let us confine ourselves to consideration of non-magnetic media and, hence, assume that

$$\mu = 4\pi \times 10^{-7} \text{ henry/m.} \quad (4)$$

Using the Fourier transform, we can represent the electromagnetic field as a sum of harmonic fields, whose time dependence is expressed by the factor $e^{-i\omega t}$. The harmonics of the field satisfy the equations

$$\text{curl } \bar{H} = \sigma \bar{E} - i\omega \epsilon \bar{E} + \bar{J}^{\text{ext}}$$

$$\text{curl } \bar{E} = i\omega \mu \bar{H}$$

$$\text{div } \bar{H} = 0$$

$$\text{div } \bar{E} = - \frac{1}{\sigma - i\omega \epsilon} (\bar{E} \cdot \text{grad}(\sigma - i\omega \epsilon) + i\omega q^{\text{ex}}). \quad (5)$$

Equations (5) for σ , μ , $\epsilon = \text{constant}$ and for no extrinsic currents or extrinsic charges are

$$\text{curl } \bar{H} = \sigma \bar{E} - i\omega \epsilon \bar{E}$$

$$\text{curl } \bar{E} = i\omega \mu \bar{H}$$

$$\text{div } \bar{H} = 0$$

$$\text{div } \bar{E} = 0. \quad (6)$$

Therefore, in this region, the electric field \bar{E} and the magnetic field \bar{H} satisfy the Helmholtz equations

$$\nabla^2 \bar{E} + k^2 \bar{E} = 0$$

$$\nabla^2 \bar{H} + k^2 \bar{H} = 0 \quad (7)$$

where $k^2 = i\omega\mu\sigma + \omega^2\mu\epsilon$.

Thus, in the region in Fig.1, the electromagnetic fields in V and Γ satisfy equations (6) and (7).

By means of the Stratton-Chu formulas, one can express the electromagnetic field \bar{E} and \bar{H} in some domain V in terms of their values on a inner side of the surface Γ bounding this domain.

Resort to the Gauss formula,

$$\int_V \operatorname{div} \bar{F} \, dV = \int_\Gamma \bar{F} \cdot \bar{dS} \quad (8)$$

and assume that

$$\bar{F} = (\bar{C} \cdot \bar{E}) \operatorname{grad}(u) + (\bar{C} \cdot \bar{E}) \operatorname{grad}(u) - i\omega\mu(\bar{C} \cdot \bar{H})u \quad (9)$$

where \bar{C} is an arbitrary constant vector, and u is a twice continually differentiable function.

Then,

$$\operatorname{div} \bar{F} = (\bar{C} \cdot \bar{E}) \nabla^2 u + \operatorname{grad}(u) \operatorname{curl}(\bar{C} \times \bar{E}) - i\omega\mu \{ (u \bar{H} \cdot \operatorname{curl} \bar{C} - u \bar{C} \cdot \operatorname{curl} \bar{H}) + (\bar{C} \times \bar{H}) \operatorname{grad}(u) \} . \quad (10)$$

Since $\operatorname{curl} \bar{H} = \sigma \bar{E} - i\omega\epsilon \bar{E}$

$$\operatorname{curl} \bar{C} = 0, \quad (11)$$

$$\begin{aligned} \operatorname{div} \bar{F} &= (\bar{C} \cdot \bar{E}) \nabla^2 u + (i\sigma\mu\omega + \omega^2\mu\epsilon)u(\bar{C} \cdot \bar{E}) \\ &= (\bar{C} \cdot \bar{E})(\nabla^2 u + k^2 u) \end{aligned} \quad (12)$$

where $k^2 = i\sigma\mu\omega + \omega^2\mu\epsilon$.

$$\text{and } \bar{\mathbf{F}} \cdot d\bar{\mathbf{S}} = (\bar{\mathbf{C}} \text{ grad } u)(d\bar{\mathbf{S}} \cdot \bar{\mathbf{E}}) + \bar{\mathbf{C}} (d\bar{\mathbf{S}} \cdot \bar{\mathbf{E}} \text{ grad } u) \\ + i\omega\mu\bar{\mathbf{C}} (d\bar{\mathbf{S}} \cdot \bar{\mathbf{H}})u. \quad (13)$$

Then, the divergence theorem (8) becomes

$$\int_V (\bar{\mathbf{C}} \cdot \bar{\mathbf{E}})(\nabla^2 u + k^2 u) dV = \int_\Gamma (\bar{\mathbf{C}} \cdot \text{grad } u)(d\bar{\mathbf{S}} \cdot \bar{\mathbf{E}}) + \\ (d\bar{\mathbf{S}} \times \bar{\mathbf{E}} \times \text{grad } u) + i\omega\mu(d\bar{\mathbf{S}} \times \bar{\mathbf{H}})u \quad (14)$$

$$\text{Hence, } \bar{\mathbf{C}} \cdot \left(\int_V \bar{\mathbf{E}}(\nabla^2 u + k^2 u) \right) = \bar{\mathbf{C}} \cdot \left(\int_\Gamma \text{grad } u(d\bar{\mathbf{S}} \cdot \bar{\mathbf{E}}) + \right. \\ \left. d\bar{\mathbf{S}} \times \bar{\mathbf{E}} \times \text{grad } u + i\omega\mu(d\bar{\mathbf{S}} \times \bar{\mathbf{H}})u \right) \quad (15)$$

Let us introduce unit vector $\bar{\mathbf{n}}$ which is inner normal of the surface Γ , then

$$d\bar{\mathbf{S}} = -\bar{\mathbf{n}} dS \quad (16)$$

Since $\bar{\mathbf{C}}$ is an arbitrary constant vector, (15) becomes

$$\int_V \bar{\mathbf{E}}(\nabla^2 u + k^2 u) dV = -\int_\Gamma \{ (\bar{\mathbf{n}} \cdot \bar{\mathbf{E}}) \text{grad } u + (\bar{\mathbf{n}} \cdot \bar{\mathbf{E}}) \\ \text{grad } u + i\omega\mu(\bar{\mathbf{n}} \times \bar{\mathbf{H}})u \} dS \quad (17)$$

This relation can be treated as the electrodynamic analog of the Green's formula. Take the fundamental Green's function

$$G = \frac{\exp(i k |\bar{\mathbf{z}}' - \bar{\mathbf{z}}|)}{4\pi |\bar{\mathbf{z}}' - \bar{\mathbf{z}}|} \quad (18)$$

which satisfies the equation

$$\nabla^2 G(\bar{\mathbf{z}}'/\bar{\mathbf{z}}) + k^2 G(\bar{\mathbf{z}}'/\bar{\mathbf{z}}) = -\delta(\bar{\mathbf{z}}' - \bar{\mathbf{z}}) \quad (19)$$

where \mathbf{z} and \mathbf{z}' are the radii vectors of the points M and M' .

} / constant

δ is the Dirac function.

Substituting (19) into (17) and using the equation

$$\int_V \bar{E}(-\delta(\bar{z}-\bar{z}'))dV = -\bar{E}(\bar{z}') \quad M' \in V$$

$$0 \quad M' \notin V, \quad (21)$$

we arrive at the integral Stratton-Chu formula for the electric field

$$\bar{E}(\bar{z}') = \int_{\Gamma} \{ (\bar{n} \cdot \bar{E}) \text{grad } G + (\bar{n} \times \bar{E}) \times \text{grad } G +$$

$$i\omega\mu(\bar{n} \times \bar{H})G \} dS \quad \text{for } M' \in V$$

$$0 \text{ for } M' \notin V \quad (22)$$

For the case of magnetic field, we define

$$\bar{F} = (\bar{C} \cdot \bar{H}) \text{grad } u + (\bar{C} \times \bar{H}) \times \text{grad } u - (\sigma - i\omega\epsilon)(\bar{C} \times \bar{E})u \quad (23)$$

$$\text{Then, } \text{div } \bar{F} = (\bar{C} \cdot \bar{H})(\nabla^2 u + k^2 u) \quad (24)$$

$$\bar{F} \cdot \bar{dS} = -\bar{C} \cdot \int_{\Gamma} \{ (\bar{n} \cdot \bar{H}) \text{grad } u + (\bar{n} \times \bar{H}) \times \text{grad } u + (\sigma - i\omega\epsilon)$$

$$(\bar{n} \times \bar{E})u \} dS \quad (25)$$

$$\text{Hence, } \int_V \bar{H}(\nabla^2 u + k^2 u)dV = -\int_{\Gamma} \{ (\bar{n} \cdot \bar{H}) \text{grad } u + (\bar{n} \times \bar{H}) \times$$

$$\text{grad } u + (\sigma - i\omega\epsilon)(\bar{n} \times \bar{E})u \} dS. \quad (26)$$

By taking the free space Green function (18), we have

$$\bar{H}(\bar{z}') = \int_{\Gamma} \{ (\bar{n} \cdot \bar{H}) \text{grad } G + (\bar{n} \times \bar{H}) \times \text{grad } G + (\sigma - i\omega\epsilon) \cdot$$

$$(\bar{n} \times \bar{E})G \} dS \quad \text{for } M' \in V$$

$$0 \text{ for } M' \notin V. \quad (27)$$

$$\begin{matrix} \hat{x} & \hat{y} & \hat{z} \\ \bar{E}_x & \bar{E}_y & \bar{E}_z \\ \bar{E}_v & \bar{E}_y & \bar{E}_z \end{matrix}$$

Equations (22) and (27) are the Stratton-Chu integral equations which describe the electromagnetic fields \bar{E} , \bar{H} in some homogeneous, isotropic, and source-free domain V in terms of its values on the surface Γ bounding the domain V .

Let us consider the geoelectric problem which is shown in Fig.2, using these Stratton-Chu integrals.

According to the Statton-Chu integrals (22) and (27), at $z' \in V_-$, we have

$$\begin{aligned} \bar{E}(\bar{z}') &= \int_{\Gamma} \{(\bar{n} \cdot \bar{E}_0) \text{grad } G + (\bar{n} \times \bar{E}_0) \times \text{grad } G \\ &\quad + i\omega\mu(\bar{n} \times \bar{H}_0)G\} dS \\ &\quad + \int_{\gamma} \{(\bar{n} \cdot \bar{E}) \text{grad } G + (\bar{n} \times \bar{E}) \times \text{grad } G + i\omega\mu(\bar{n} \times \bar{H})G\} dS. \end{aligned} \quad (28)$$

$$\begin{aligned} \bar{H}(\bar{z}') &= \int_{\Gamma} \{(\bar{n} \cdot \bar{H}_0) \text{grad } G + (\bar{n} \times \bar{H}_0) \times \text{grad } G \\ &\quad + (\sigma - i\omega\epsilon)(\bar{n} \times \bar{E})G\} dS \\ &\quad + \int_{\gamma} \{(\bar{n} \cdot \bar{H}) \text{grad } G + (\bar{n} \times \bar{H}) \times \text{grad } G \\ &\quad + (\sigma - i\omega\epsilon)(\bar{n} \times \bar{E})G\} dS. \end{aligned} \quad (29)$$

and \bar{E}_0 and \bar{H}_0 are the field values at the surface. The field values \bar{E}_0 and \bar{H}_0 are known by measurement, however, we have two unknown field values at \bar{z}' and at the surface \bar{z} in each equation.

The integrals over the plane γ can be transformed into the integrals over the Earth's surface Γ using Fourier expansion of the Green's function (Morse and Feshbach, 1953).

The Green function G in the integral over the plane γ depends on the positions of the points $z' \in V_-$ and $z \in \Gamma$. The coordinates z' and z of these points satisfy the condition $z' < z$, under which

$$G = \frac{1}{8\pi^2} \int_{-\infty}^{\infty} \frac{f(z')g(z)}{\eta} dk_x dk_y \quad (30)$$

where f, g describe non-uniform plane waves.

$$\begin{aligned} f(z') &= e^{-i(k_x x' + k_y y')} e^{\eta z'} \\ g(z) &= e^{i(k_x x + k_y y)} e^{-\eta z} \\ \eta &= \sqrt{k_x^2 + k_y^2 - k^2} \\ k^2 &= i\sigma\mu\omega + \omega^2\epsilon\mu \end{aligned} \quad (31)$$

Substituting (30) into the integrals in (28) and (29), we have

$$\begin{aligned} & \int_{\gamma} \{(\bar{\mathbf{n}} \cdot \bar{\mathbf{E}}) \text{grad } G + (\bar{\mathbf{n}} \times \bar{\mathbf{E}}) \times \text{grad } G + i\omega\mu(\bar{\mathbf{n}} \times \mathbf{H})G\} dS \\ &= \frac{1}{8\pi^2} \int_{-\infty}^{\infty} \frac{f}{\eta} dk_x dk_y \int_{\gamma} \{(\bar{\mathbf{n}} \cdot \bar{\mathbf{E}}) \text{grad } g + (\bar{\mathbf{n}} \times \bar{\mathbf{E}}) \times \text{grad } g \\ & \quad + i\omega\mu(\bar{\mathbf{n}} \times \bar{\mathbf{H}})g\} dS \end{aligned} \quad (32)$$

and for magnetic field

$$\begin{aligned} & \int_{\gamma} \{(\bar{\mathbf{n}} \cdot \bar{\mathbf{H}}) \text{grad } G + (\bar{\mathbf{n}} \times \bar{\mathbf{H}}) \times \text{grad } G + \sigma(\bar{\mathbf{n}} \times \bar{\mathbf{E}})G\} dS \\ &= \frac{1}{8\pi^2} \int_{-\infty}^{\infty} \frac{f}{\eta} dk_x dk_y \int_{\gamma} \{(\bar{\mathbf{n}} \cdot \bar{\mathbf{H}}) \text{grad } g + (\bar{\mathbf{n}} \times \bar{\mathbf{H}}) \times \text{grad } g \\ & \quad + (\sigma - i\omega\epsilon)(\bar{\mathbf{n}} \times \bar{\mathbf{E}})g\} dS \end{aligned} \quad (33)$$

Let us transform the integral over Γ into the integral over γ in (32) and (33).

Take the Green formulas (17) and (26) and apply them to the region V_- with $u = g$, then

$$\begin{aligned} & \int_{V_-} \bar{\mathbf{E}}(\nabla^2 g + k^2 g) dV \\ &= -\int_{\Gamma} \{(\bar{\mathbf{n}} \cdot \bar{\mathbf{E}}_0) \text{grad } g + (\bar{\mathbf{n}} \times \bar{\mathbf{E}}_0) \times \text{grad } g + i\omega\mu(\bar{\mathbf{n}} \times \mathbf{H})g\} dS \\ & \quad - \int_{\Upsilon} \{(\bar{\mathbf{n}} \cdot \bar{\mathbf{E}}) \text{grad } g + (\bar{\mathbf{n}} \times \bar{\mathbf{E}}) \text{grad } g + i\omega\mu(\bar{\mathbf{n}} \times \bar{\mathbf{H}})g\} dS \end{aligned} \quad (34)$$

and

$$\begin{aligned} & \int_{V_-} \bar{\mathbf{H}}(\nabla^2 g + k^2 g) dV \\ &= -\int_{\Gamma} \{(\bar{\mathbf{n}} \cdot \bar{\mathbf{H}}_0) \text{grad } g + (\bar{\mathbf{n}} \times \bar{\mathbf{H}}_0) \times \text{grad } g + \sigma(\bar{\mathbf{n}} \times \bar{\mathbf{E}}_0)g\} dS \\ & \quad - \int_{\Upsilon} \{(\bar{\mathbf{n}} \cdot \bar{\mathbf{H}}) \text{grad } g + (\bar{\mathbf{n}} \times \bar{\mathbf{H}}) \times \text{grad } g + (\sigma - i\omega\epsilon)(\bar{\mathbf{n}} \times \bar{\mathbf{E}})g\} dS \end{aligned} \quad (35)$$

The harmonic g defined by (31) satisfies the Helmholtz equation, that is,

$$\nabla^2 g + k^2 g = 0 \quad \text{in } V_- \quad (36)$$

Then (34) and (35) become

$$\begin{aligned} & \int_{\Upsilon} \{(\bar{\mathbf{n}} \cdot \bar{\mathbf{E}}) \text{grad } g + (\bar{\mathbf{n}} \times \bar{\mathbf{H}}) \times \text{grad } g + (\sigma - i\omega\epsilon)(\bar{\mathbf{n}} \times \bar{\mathbf{E}})g\} dS \\ &= -\int_{\Gamma} \{(\bar{\mathbf{n}} \cdot \bar{\mathbf{E}}_0) \text{grad } g + (\bar{\mathbf{n}} \times \bar{\mathbf{E}}_0) \times \text{grad } g + i\omega\mu(\bar{\mathbf{n}} \times \bar{\mathbf{H}}_0)g\} dS \end{aligned} \quad (37)$$

and

$$\begin{aligned} & \int_{\Upsilon} \{(\bar{\mathbf{n}} \cdot \bar{\mathbf{H}}) \text{grad } g + (\bar{\mathbf{n}} \times \bar{\mathbf{H}}) \times \text{grad } g + (\sigma - i\omega\epsilon)(\bar{\mathbf{n}} \times \bar{\mathbf{E}})g\} dS \\ &= -\int_{\Gamma} \{(\bar{\mathbf{n}} \cdot \bar{\mathbf{H}}_0) \text{grad } g + (\bar{\mathbf{n}} \times \bar{\mathbf{H}}_0) \times \text{grad } g + (\sigma - i\omega\epsilon)(\bar{\mathbf{n}} \times \bar{\mathbf{E}}_0)g\} dS. \end{aligned} \quad (38)$$

Substituting (37) and (38) into (32) and (33), respectively, we have

$$\begin{aligned} & \int_{\gamma} \{(\bar{\mathbf{n}} \cdot \bar{\mathbf{E}}) \text{grad } G + (\bar{\mathbf{n}} \times \bar{\mathbf{E}}) \times \text{grad } G + i\omega\mu(\bar{\mathbf{n}} \times \bar{\mathbf{H}})G\} dS \\ &= -\frac{1}{8\pi} \int_{-\infty}^{\infty} \frac{f}{\eta} dk_x dk_y \int_{\Gamma} \{(\bar{\mathbf{n}} \cdot \bar{\mathbf{E}}_0) \text{grad } g + (\bar{\mathbf{n}} \times \bar{\mathbf{E}}_0) \times \text{grad } g \\ & \quad + i\omega\mu(\bar{\mathbf{n}} \times \bar{\mathbf{H}}_0)g\} dS \end{aligned} \quad (39)$$

$$\begin{aligned} & \int_{\gamma} \{(\bar{\mathbf{n}} \cdot \bar{\mathbf{H}}) \text{grad } G + (\bar{\mathbf{n}} \times \bar{\mathbf{H}}) \times \text{grad } G + \sigma(\bar{\mathbf{n}} \times \bar{\mathbf{E}})G\} dS \\ &= -\frac{1}{8\pi} \int_{-\infty}^{\infty} \frac{f}{\eta} dk_x dk_y \int_{\Gamma} \{(\bar{\mathbf{n}} \cdot \bar{\mathbf{H}}_0) \text{grad } g + (\bar{\mathbf{n}} \times \bar{\mathbf{H}}_0) \times \text{grad } g \\ & \quad + (\sigma - i\omega\epsilon)(\bar{\mathbf{n}} \times \bar{\mathbf{E}}_0)g\} dS. \end{aligned} \quad (40)$$

In (39) and (40), the integrals over γ are expressed by the integrals over Γ .

Substituting (39) and (40) into (28) and (29), respectively, we have

$$\begin{aligned} E(z') &= \int_{\Gamma} \{(\bar{\mathbf{n}} \cdot \bar{\mathbf{E}}_0) \text{grad } G + (\bar{\mathbf{n}} \times \bar{\mathbf{E}}_0) \times \text{grad } G + i\omega\mu(\bar{\mathbf{n}} \times \bar{\mathbf{H}}_0)G\} dS \\ & \quad - \frac{1}{8\pi} \int_{-\infty}^{\infty} \frac{f}{\eta} dk_x dk_y \int_{\Gamma} \{(\bar{\mathbf{n}} \cdot \bar{\mathbf{E}}_0) \text{grad } g + (\bar{\mathbf{n}} \times \bar{\mathbf{E}}_0) \times \text{grad } g \\ & \quad + i\omega\mu(\bar{\mathbf{n}} \times \bar{\mathbf{H}}_0)g\} dS \end{aligned} \quad (41)$$

$$\begin{aligned} H(z') &= \int_{\Gamma} \{(\bar{\mathbf{n}} \cdot \bar{\mathbf{H}}_0) \text{grad } G + (\bar{\mathbf{n}} \times \bar{\mathbf{H}}_0) \times \text{grad } G \\ & \quad + (\sigma - i\omega\epsilon)(\bar{\mathbf{n}} \times \bar{\mathbf{E}}_0)\} dS \\ & \quad - \frac{1}{8\pi} \int_{-\infty}^{\infty} \frac{f}{\eta} dk_x dk_y \int_{\Gamma} \{(\bar{\mathbf{n}} \cdot \bar{\mathbf{H}}_0) \text{grad } g + (\bar{\mathbf{n}} \times \bar{\mathbf{H}}_0) \times \text{grad } g \\ & \quad + (\sigma - i\omega\epsilon)(\bar{\mathbf{n}} \times \bar{\mathbf{E}}_0)g\} dS. \end{aligned} \quad (42)$$

The Green function in the first integral in (41) and (42) can also be expanded.

Since the z coordinate of points $z' \in V_-$ and $z \in \Gamma$ and $z' > z$, the Fourier expansion of the Green function takes the form (Morse and Feshbach, 1953, Markov, 1967)

$$G = \frac{1}{8\pi^2} \int_{-\infty}^{\infty} \frac{\tilde{f}(z') \tilde{g}(z)}{\eta} dk_x dk_y \quad (43)$$

where

$$\begin{aligned} \tilde{f}(z') &= e^{i(k_x x' + k_y y')} e^{-\eta z'} \\ \tilde{g}(z) &= e^{-i(k_x x + k_y y)} e^{\eta z} \end{aligned} \quad \left| \begin{array}{l} \\ z' > z. \end{array} \right. \quad (44)$$

Substituting (43) into the first integral of (41) and (42), we have

$$\begin{aligned} E(\bar{z}') &= \frac{1}{8\pi^2} \int \frac{\tilde{f}}{\eta} dk_x dk_y \int_{\Gamma} \{ (\bar{\mathbf{n}} \cdot \bar{\mathbf{E}}_0) \text{grad } \tilde{g} + (\bar{\mathbf{n}} \times \bar{\mathbf{E}}_0) \times \text{grad } \tilde{g} \\ &\quad + i\omega\mu (\bar{\mathbf{n}} \times \bar{\mathbf{H}}_0) g \} dS \\ &\quad - \frac{1}{8\pi^2} \int_{-\infty}^{\infty} \frac{\tilde{f}}{\eta} dk_x dk_y \int_{\Gamma} \{ (\bar{\mathbf{n}} \cdot \bar{\mathbf{E}}_0) \text{grad } g + (\bar{\mathbf{n}} \times \bar{\mathbf{E}}_0) \times \text{grad } g \\ &\quad + i\omega\mu (\bar{\mathbf{n}} \times \bar{\mathbf{H}}_0) g \} dS \end{aligned} \quad (45)$$

$$\begin{aligned} H(\bar{z}') &= \frac{1}{8\pi^2} \int \frac{\tilde{f}}{\eta} dk_x dk_y \int_{\Gamma} \{ (\bar{\mathbf{n}} \cdot \bar{\mathbf{H}}_0) \text{grad } \tilde{g} + (\bar{\mathbf{n}} \times \bar{\mathbf{H}}_0) \times \text{grad } \tilde{g} \\ &\quad + (\sigma - i\omega\epsilon) (\bar{\mathbf{n}} \times \bar{\mathbf{E}}_0) \tilde{g} \} dS \\ &\quad - \frac{1}{8\pi^2} \int_{-\infty}^{\infty} \frac{\tilde{f}}{\eta} dk_x dk_y \int_{\Gamma} \{ (\bar{\mathbf{n}} \cdot \bar{\mathbf{H}}_0) \text{grad } g + (\bar{\mathbf{n}} \times \bar{\mathbf{H}}_0) \times \text{grad } g \\ &\quad + (\sigma - i\omega\epsilon) (\bar{\mathbf{n}} \times \bar{\mathbf{E}}_0) g \} dS. \end{aligned} \quad (46)$$

Discarding the atmospheric electrical conductivity, assume that $\bar{\mathbf{n}} \cdot \bar{\mathbf{E}}_0|_{\Gamma} = 0$, and take $z = 0$ at the surface Γ , we obtain

$$E_x(\bar{z}') = \frac{1}{4\pi^2} \int_{-\infty}^{\infty} \left\{ e_x^0 \cosh nz' + i\omega\mu h_y^0 \frac{\sinh nz'}{n} \right\} e^{-i(k_x x' + k_y y')} dk_x dk_y$$

$$E_y(\bar{z}') = \frac{1}{4\pi^2} \int_{-\infty}^{\infty} \left\{ e_y^0 \cosh nz' - i\omega\mu h_x^0 \frac{\sinh nz'}{n} \right\} e^{-i(k_x x' + k_y y')} dk_x dk_y$$

$$E_z(\bar{z}') = \frac{1}{4\pi^2} \int_{-\infty}^{\infty} (k_x e_x^0 + k_y e_y^0) \frac{\sinh nz'}{n} e^{-i(k_x x' + k_y y')} dk_x dk_y$$

$$H_x(\bar{z}') = \frac{1}{4\pi^2} \int_{-\infty}^{\infty} \left\{ h_x^0 \cosh nz' + ((\sigma - i\omega\epsilon)e_y^0 - ik_x h_z^0) \frac{\sinh nz'}{n} \right\} e^{-i(k_x x' + k_y y')} dk_x dk_y$$

$$H_y(\bar{z}') = \frac{1}{4\pi^2} \int_{-\infty}^{\infty} \left\{ h_y^0 \cosh nz' - ((\sigma - i\omega\epsilon)e_x^0 + ik_y h_z^0) \frac{\sinh nz'}{n} \right\} e^{-i(k_x x' + k_y y')} dk_x dk_y$$

$$H_z(\bar{z}') = \frac{1}{4\pi^2} \int_{-\infty}^{\infty} \left\{ h_z^0 \cosh nz' + i(k_x h_x^0 + k_y h_y^0) \frac{\sinh nz'}{n} \right\} e^{-i(k_x x' + k_y y')} dk_x dk_y$$

where \bar{e}^0 and \bar{h}^0 are the Fourier transform of the field at the surface \bar{E}^0 , \bar{H}^0 .

2. Method of computation

The algorithms for analytic continuation of the electromagnetic field have been implemented in the computer program ACEF. This program is designed for a two- or three-dimensional analytic continuation of the electromagnetic field.

The generalized flow of program ACEF is given in Fig.3. The first operation involves reading the surface data and parameters.

Surface data is read in row by row, with the x coordinate(horizontal) governed by the I index and the y coordinate by the J index. Row length and number of rows are designated by NX, NY parameters. A maximum number of 128x128 map values can be read in for each component of a surface data.

The surface data is next transformed to the frequency domain using the subroutine FOURT, and the values are stored in a two dimensional array. The data is next convolved with a set of Green's functions and then inverse transformed back to the space domain.

The processing results are represented either in profile form or contour form. Graphs of transformed electromagnetic fields and maps of contours of various field components are constructed using the program TOPO and GRAPH. Thus, ACEF

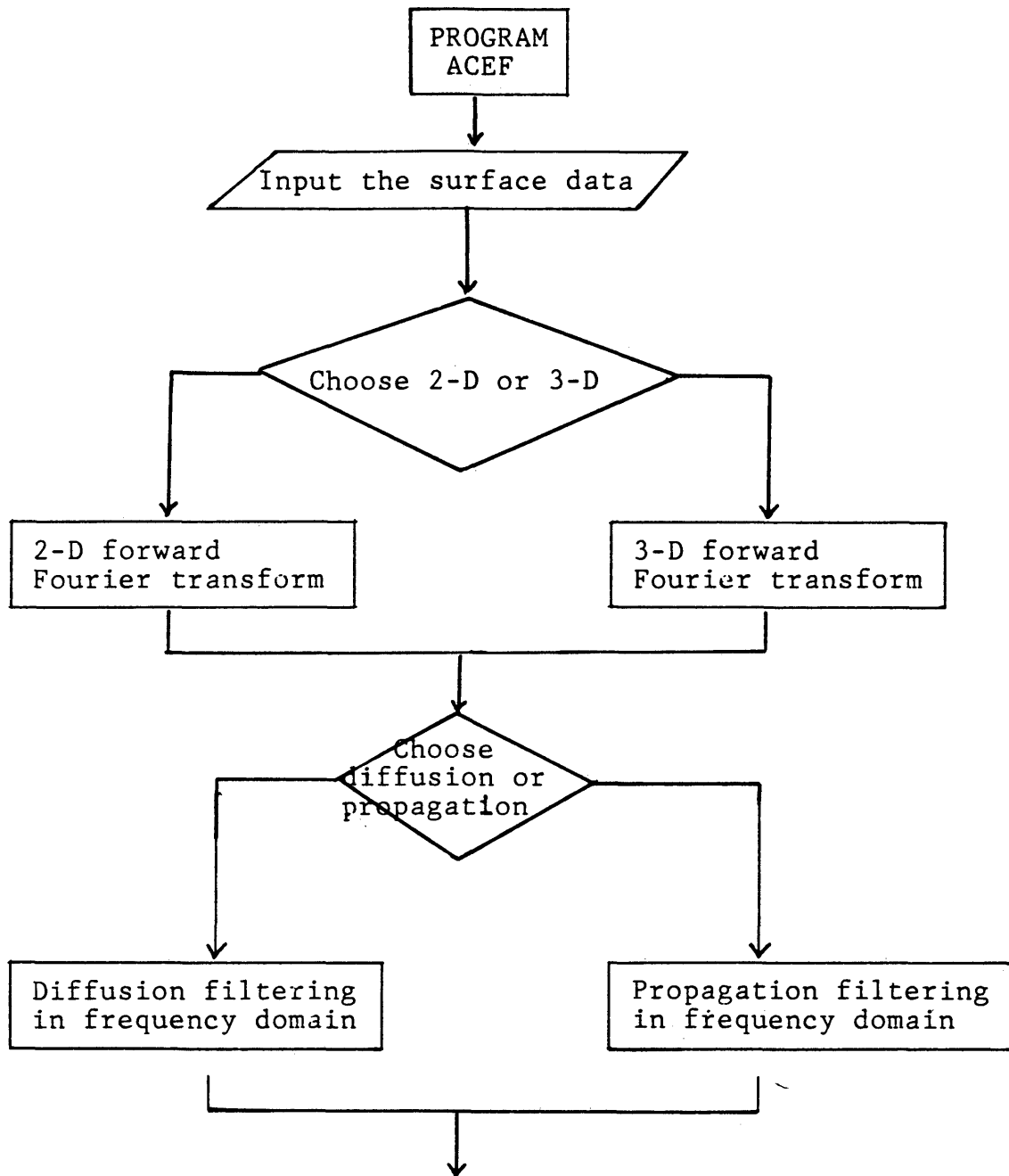


Fig.3. Flow chart of the program ACEF.

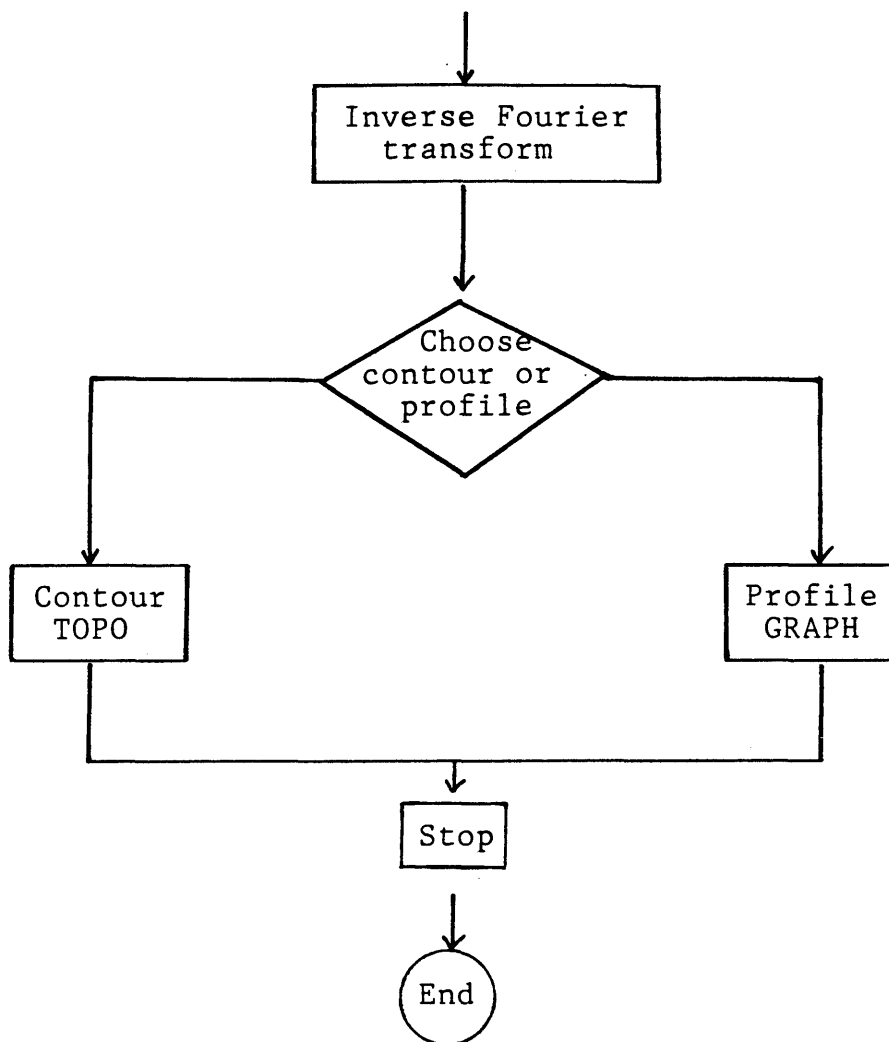


Fig.3. - Continued.

automates completely the analytic continuation of two- and three-dimensional electromagnetic fields.

Running time required is 120 seconds on a Dec-10 computer for an input array of 41x41 size.

Fig.4. is the model for testing the algorithm and the program ACEF. The input data is a field computed over two magnetic dipoles which are 100m apart. The depth of dipoles are 120m. All the parameters of this model are known, and the downward continuation was made by the program ACEF for the field at a depth of 100m.

Fig.5. shows the contour of the in-phase component when the depth of dipoles are 120m. The surface anomaly has been continued into the Earth to the level $z=100m$, which is shown in Fig.6. The calculated value of the contour and the continued value are almost identical, as shown in Fig.6 and Fig.7, demonstrating the veridity of the program ACEF and supporting the reliability of the algorithm which uses the Stratton-Chu integrals.

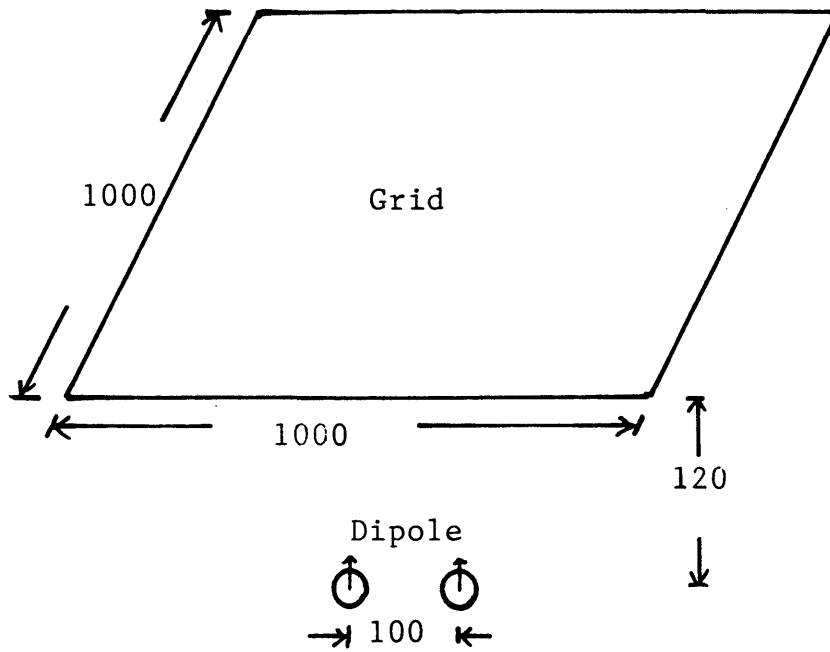


Fig.4. Schematic diagram of the two dipole model.

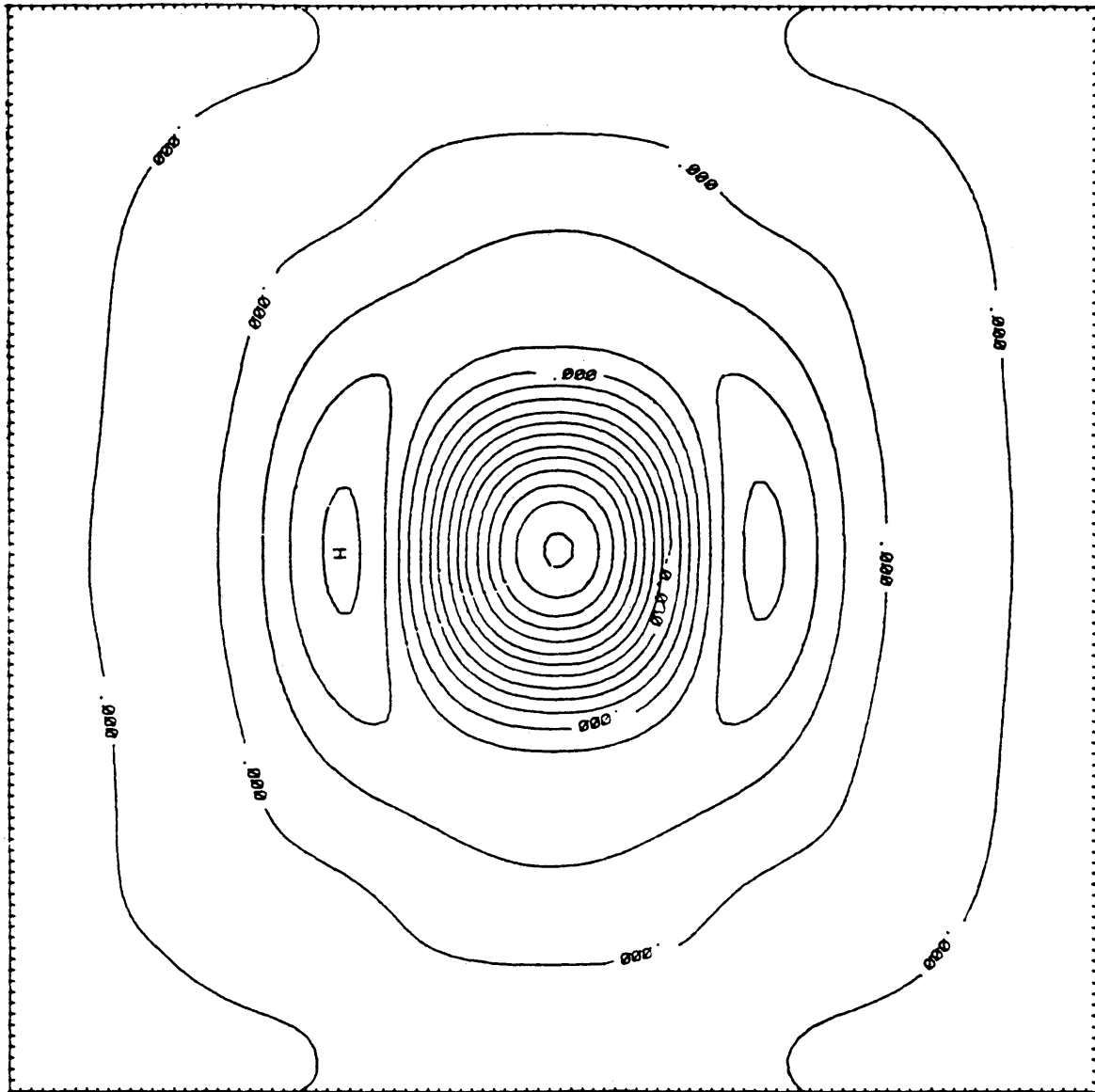


Fig.5. Contour of the in-phase component of H_z . The depth of dipoles is 120m.

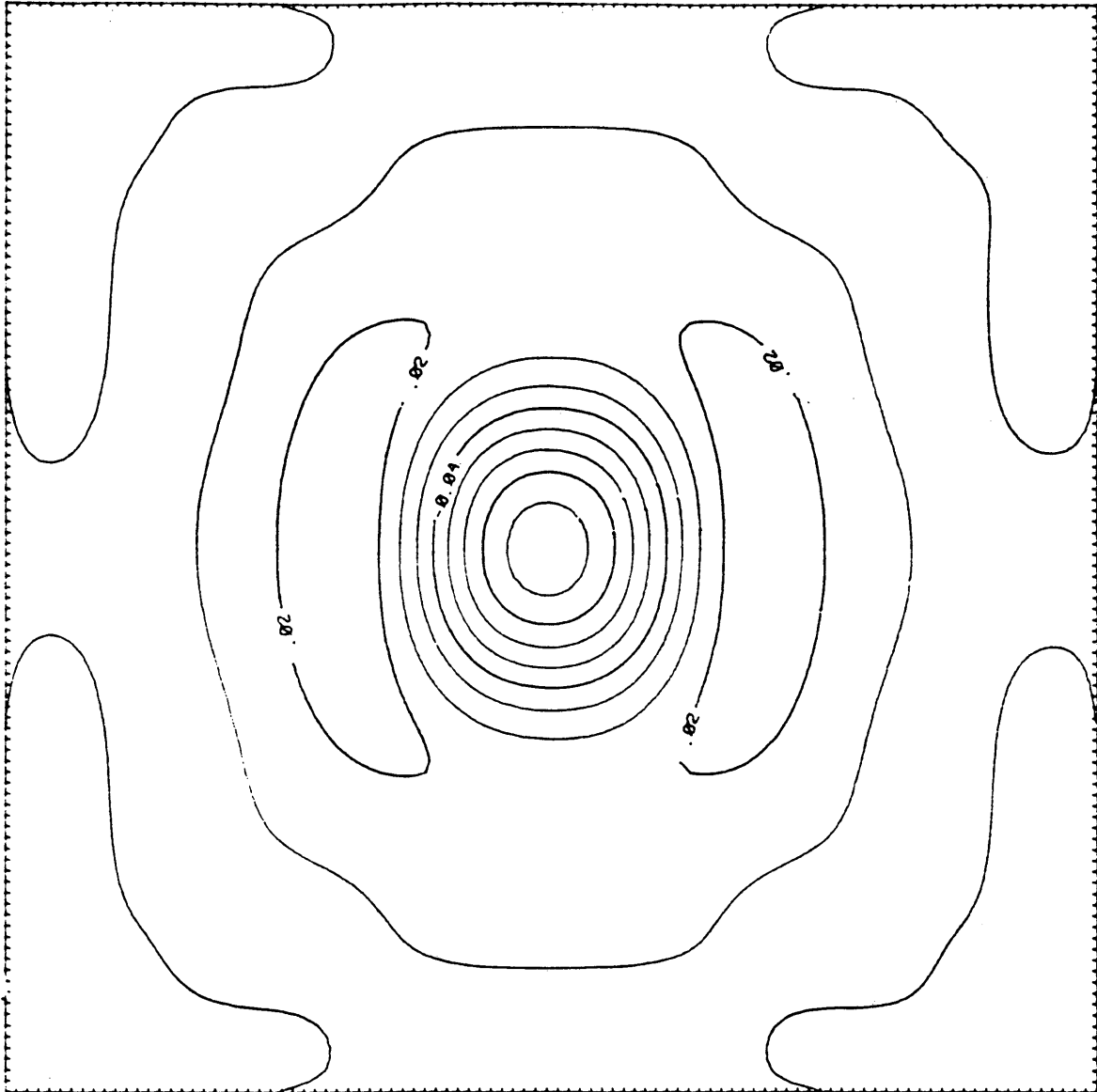


Fig.6. Contour of the in-phase component of H_z after downward continuation. The depth of continuation is 20m.

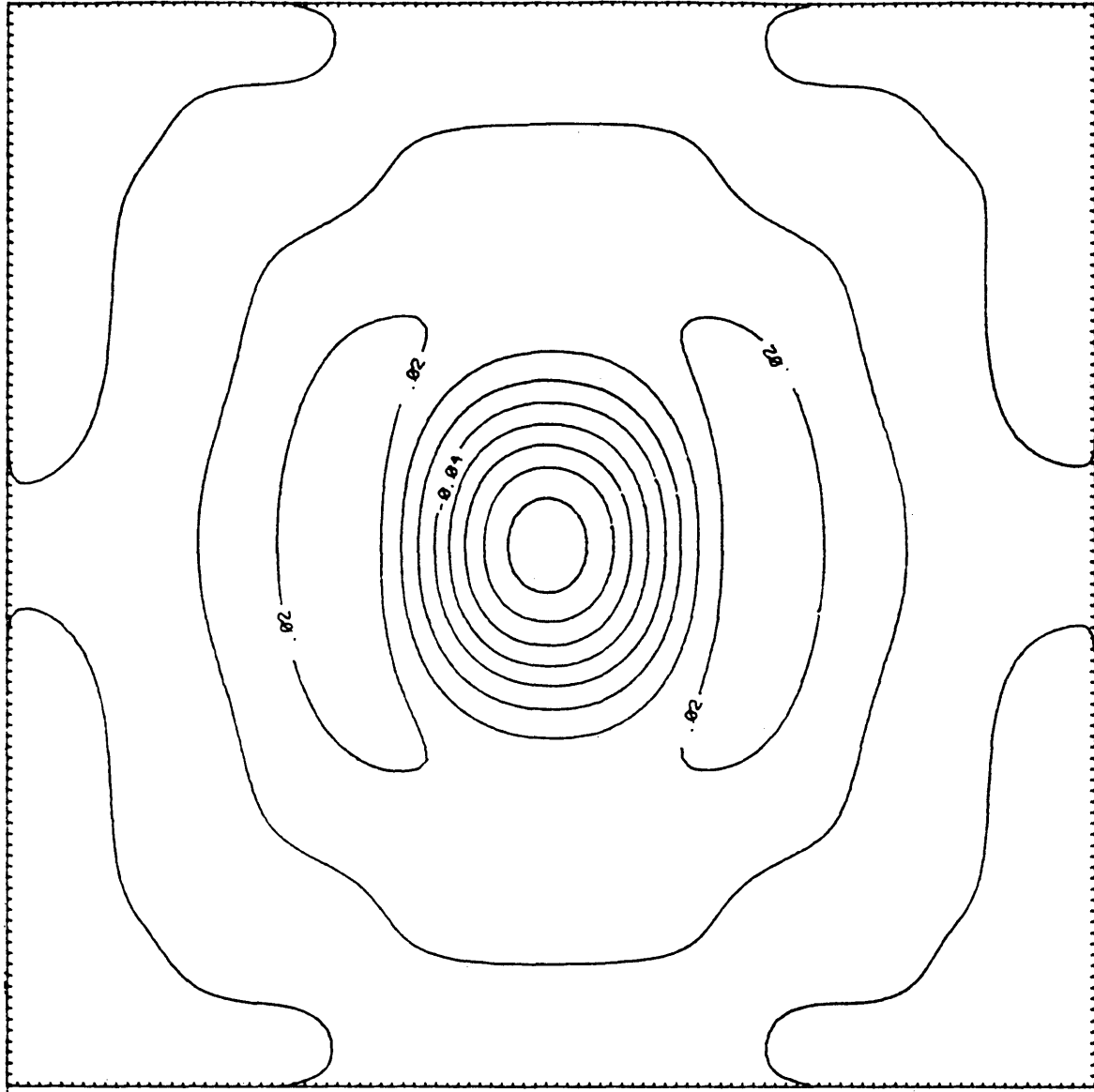


Fig.7. Modeling data at the depth of 100m.

APPLICATION OF THE ANALYTIC CONTINUATION

We will examine the process of analytic continuation in detail in this chapter, in an attempt to choose criteria suitable for interpreting the analytic continued field. We will try to investigate these matters by carrying out the computations for several theoretical models.

1. Signal enhancement and localization of inhomogeneity.

The problem is to locate the source of the secondary electromagnetic field from the fields measured on the Earth's surface. In a geopotential problem, the analytic continuation makes it possible to detect its singular points confined to geological structures. In a geoelectric problem, the fields are reconstructed by the fields \bar{E} , \bar{H} specified on the Earth's surface and the reconstructed fields describe fictitious electromagnetic fields through the surface of a geoelectrical inhomogeneity. These fields may have singular points which are confined within geological structures. The relationship between the singular points of the electromagnetic field and the geoelectric inhomogeneities has been investigated using several models.

This analysis of location of inhomogeneities has been

performed in a three-dimensional electromagnetic field.

Fig.8. shows the log plot of the amplitude response of a dipole when the depth of dipole is 100m. In Figs 8 to 10, only the case of diffusion was considered, which involves a quasi-static approximation both in modeling and continuation. The field was calculated on a regularly spaced square grid of 20m intervals. In order to see the variations at the edge of the grid, the logarithmic contour was plotted.

The surface anomaly has been continued into the Earth to the level $z = 80\text{m}$, which is shown in Fig.9. The amplitude of the anomalies rapidly increases with depth. The calculated values of contours and the continued values are almost identical except the distortions at corners. This distortion comes from the round-off error in Dec-10 computer during the modeling and continuation, because the amplitude at the edge is about 10^{-12} , as shown in the logarithmic plot in Fig.8. Since the amplitude at the center is about 10, this distortion can be neglected, as shown in the linear contour in Figs. 5 to 7.

Next, we considered the propagation problems in Figs. 11 to 13. The exciting frequency of 57 M Hz was used, because that is the normal frequency used in the tunnel detection. The surface anomaly has been continued into the Earth to the levels $z/d=0.1, 0.5, \text{ and } 0.9$, where d is the depth to the source and z is the depth of continuation.

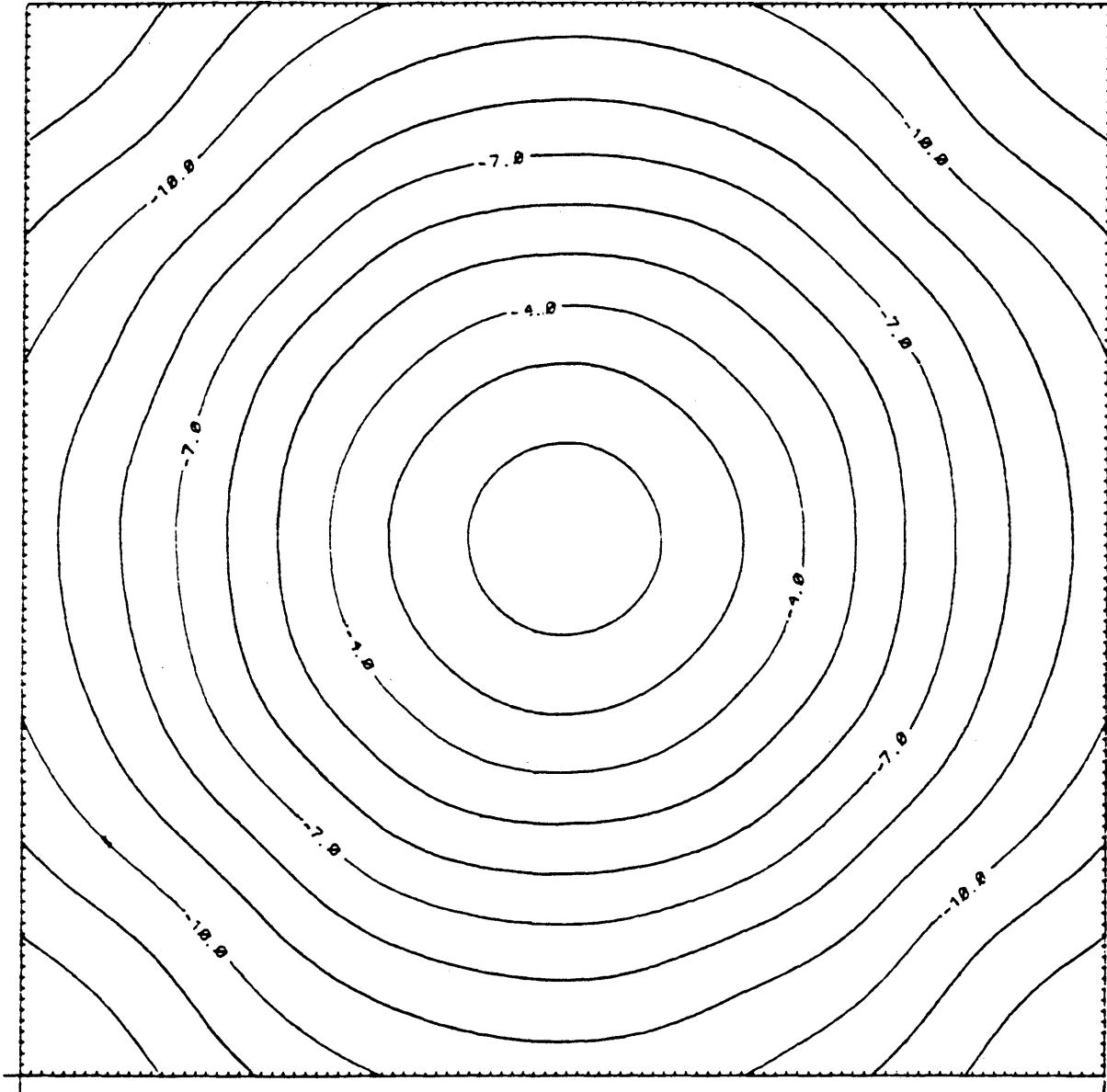


Fig. 8. Logarithmic amplitude of vertical magnetic field.
Depth of dipole is 100 m.

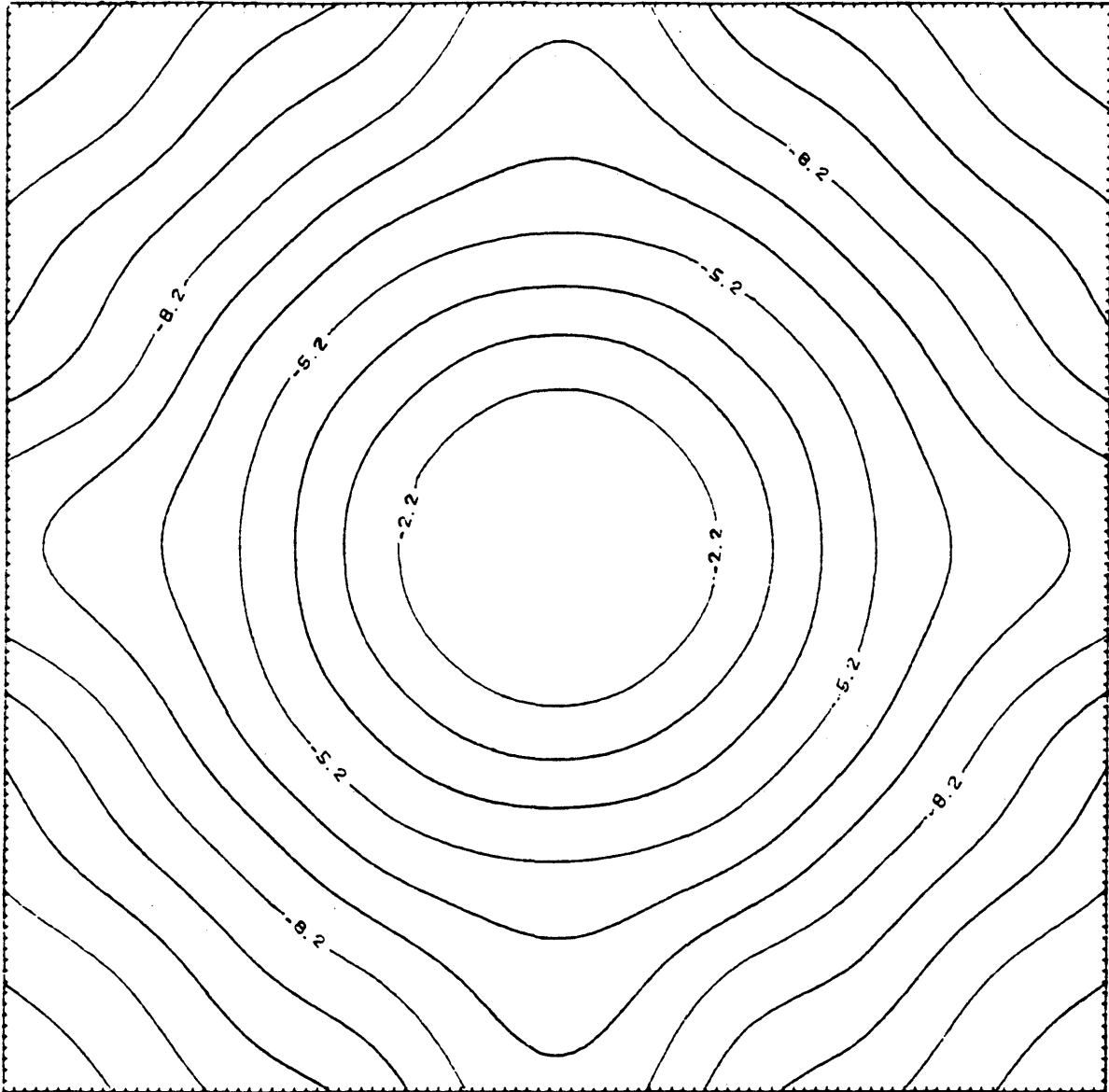


Fig.9. Contours after downward continuation. The depth of continuation is 20 m.

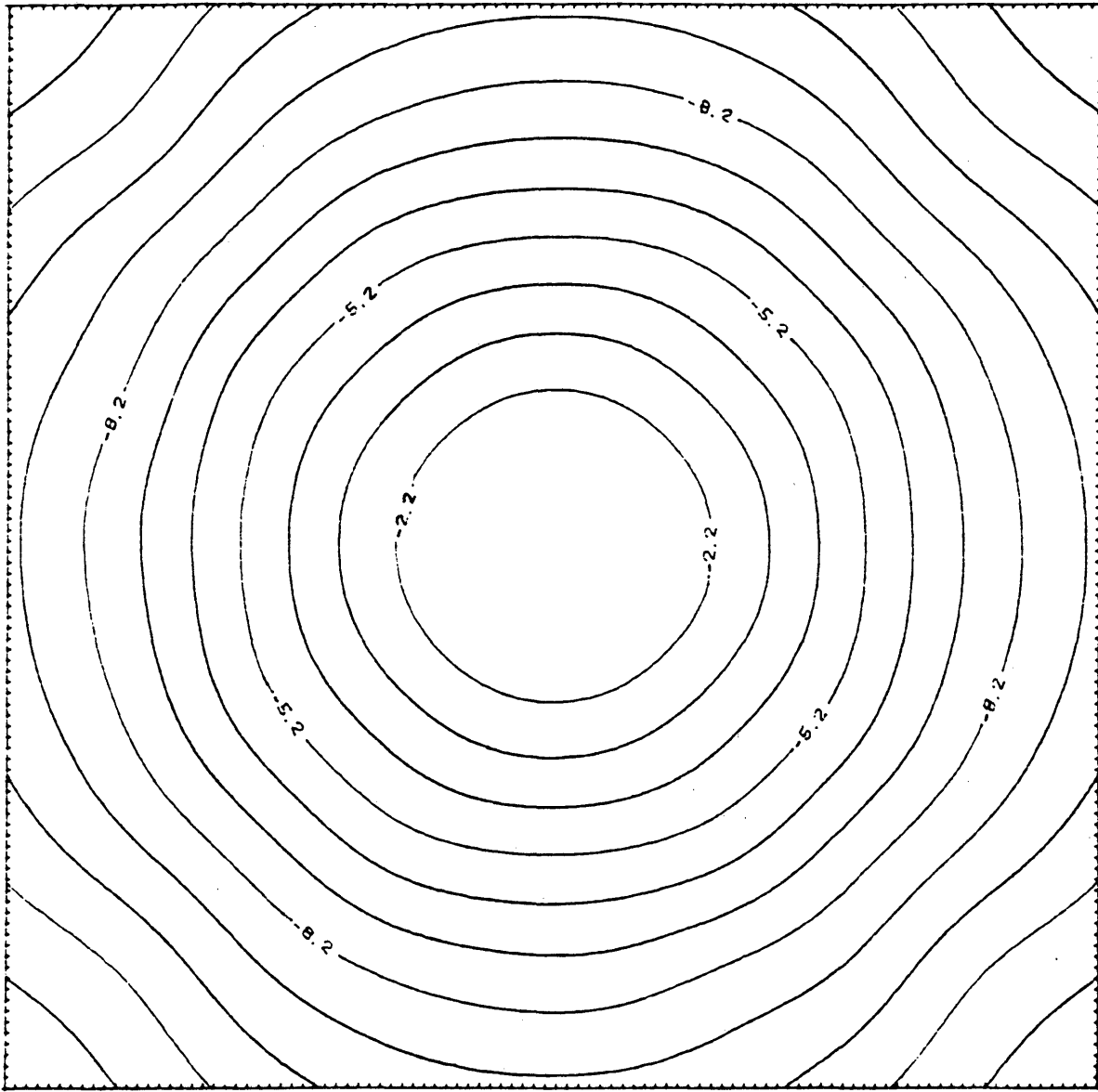


Fig.10. Modeling data at the depth of 80 m.

The magnitude of anomalies rapidly increases with depth. It is well seen in Figs. 11 to 13 where the curves of in-phase component of H_z are presented. The deep anomaly is several times larger than the surface anomaly. At the level of $z/d=0.5$, it is seen that the continued data still agrees well with the modeling data at the depth, as shown in the x-mark line and Δ -mark line in Fig.12. At this level, there is no indication of instability or oscillation, and the curve still retains its original character, although the amplitude increases further. Further continuation of the field near the source gives fields that show oscillations as shown in Fig.13. This final continuation of the fields produces no major changes in the peak anomaly, although the anomaly is surrounded by oscillations which indicate that the depth of continuation is near the source.

We investigate this problem further with two dipole model, which is shown in Fig.4, for the case of diffusion. In this model, the surface anomaly has been continued into the Earth to the level $z=90\text{m}$, near the source at 100m .

In Fig.14, we observe that the Δ -mark line, which is the continued data with spacing 20m , does not converge to that with spacing 25m near the source region. We also note that the continued data does not agree with the theoretical

data at the depth, which is the o-mark line in Fig.14.

This phenomenon is more clear when the spacing is increased to 50m, as shown in the rectangular mark line in Fig.15.

The oscillations become bigger as the spacing decreases from 25m to 20m as shown in Figs 14 to 15. If the spacing is decreased further to 10m, the anomaly is cluttered with big vibrations as shown in Fig.16.

The oscillations generated due to the fine grid can be eliminated by increasing the grid spacing; however, near the source region, the two sets of data does not converge each other. This phenomenon is a definitive sign that the depth of continuation is near the source.

Further continuation of the surface data beyond the source region yields larger oscillations, as shown in Fig. 17.

From what has been said above, it appears that we can choose two qualitative criteria for the location of an inhomogeneity. First, it is the basic change in the shape of the continued anomaly curve as compared to that of the surface curve. As the surface curve is continued farther and farther down, the peaks and troughs of the original observed anomaly will become sharper and sharper. The second one is the appearance of the oscillations and divergence. When the secondary peaks and troughs outnumber the primary peaks or

troughs and does not show convergence, they are the definitive sign that the depth of continuation is near the source.

It should be noted that the depth determined in this way gives a maximum depth beyond which the actual body cannot occur. In electromagnetic prospecting, the anomalies are caused by secondary currents concentrated within the conducting ore body. The limiting depth determined by downward continuation would, therefore, correspond to the depth of the maximum current concentration in a particular case, which ordinarily, occurs near the top of the target body.

Figs 18 to 20 show the log contour of the propagated field. We again note the distortions at corners of the grid. In Fig.19, which is the continued data to the level $z/d=0.8$, we observe that the amplitude at the center of the grid is about 10^9 , while the value from which the distortion appear is about 10^2 . Therefore, the distortion which appear at corners on the logarithmic contour can be neglected in the linear scale for both diffusion and propagation problems.

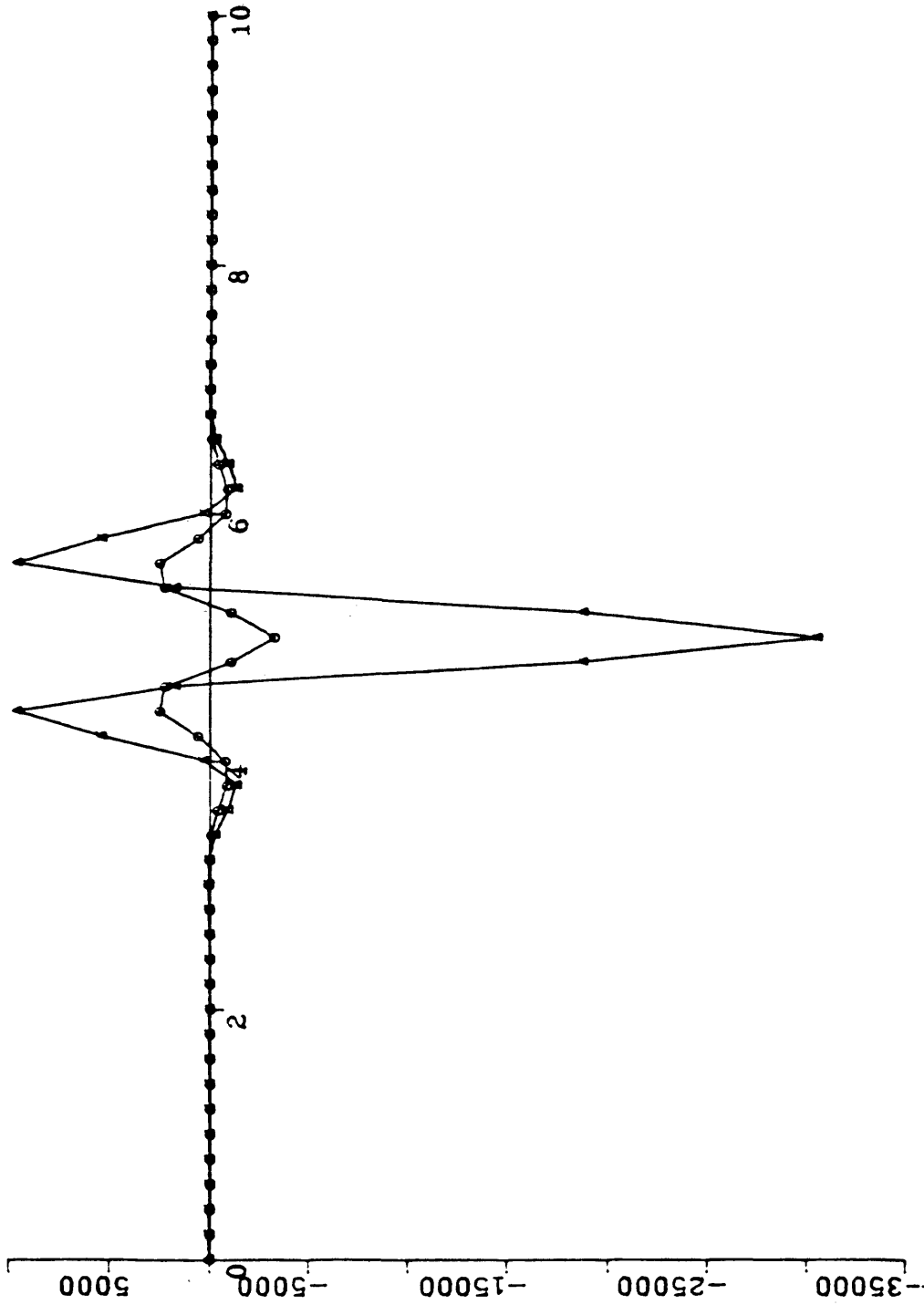


Fig.11. Profile after downward continuation. The depth of continuation is $z/d=0.1$.

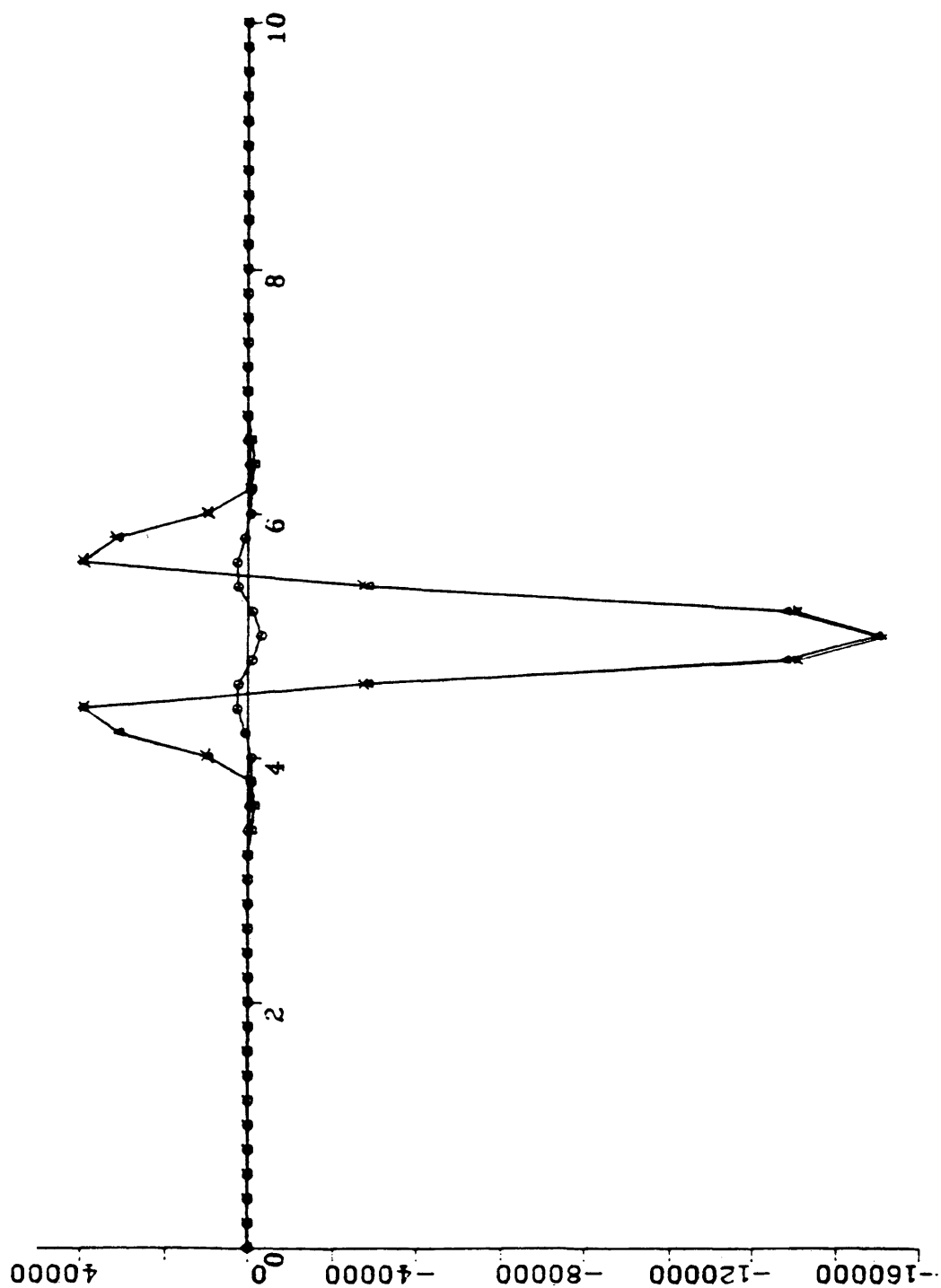


Fig.12. Profile after downward continuation. The depth of continuation is $z/d=0.5$.

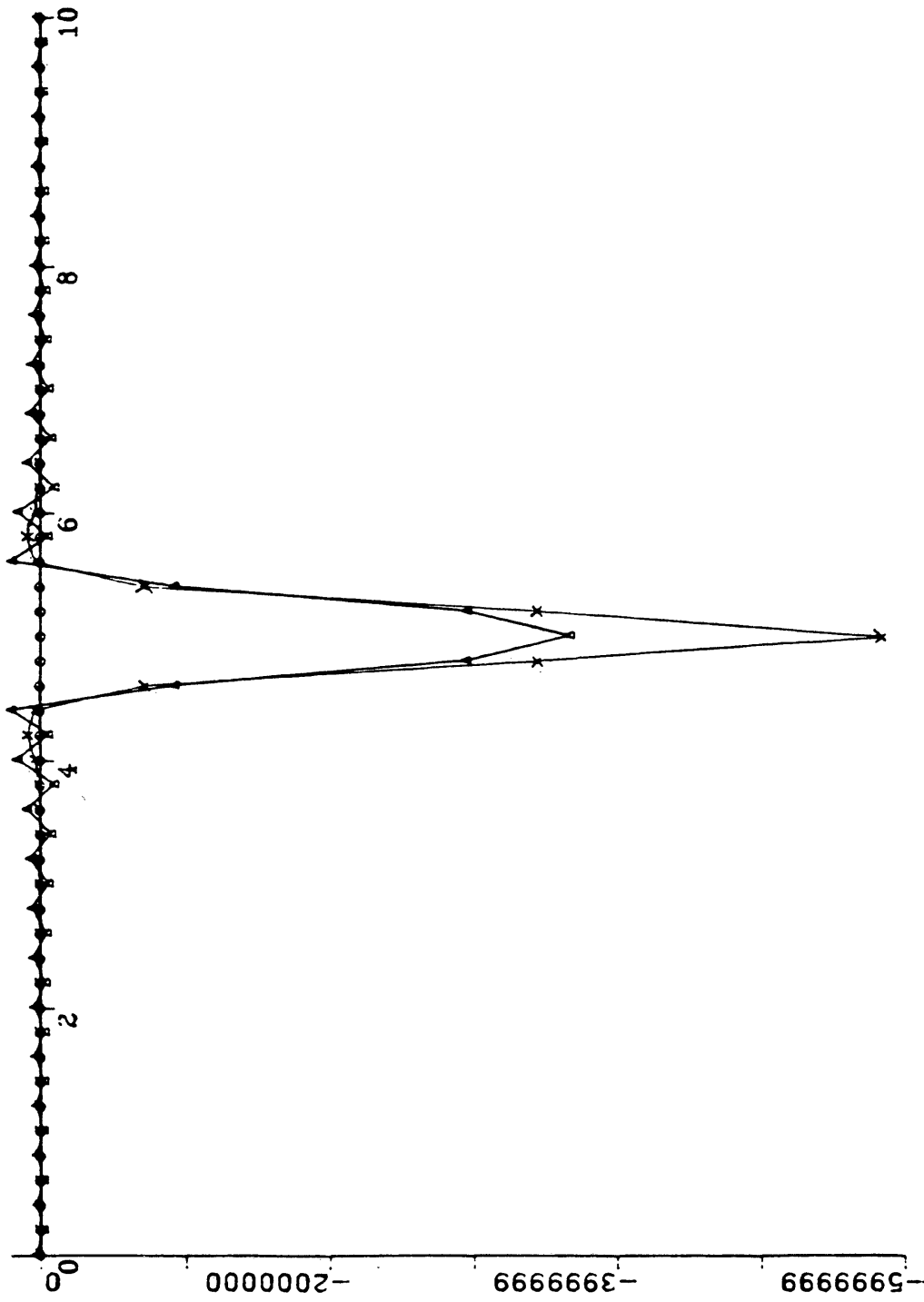


Fig.13. Profile after downward continuation. The depth of continuation is $z/d=0.9$.

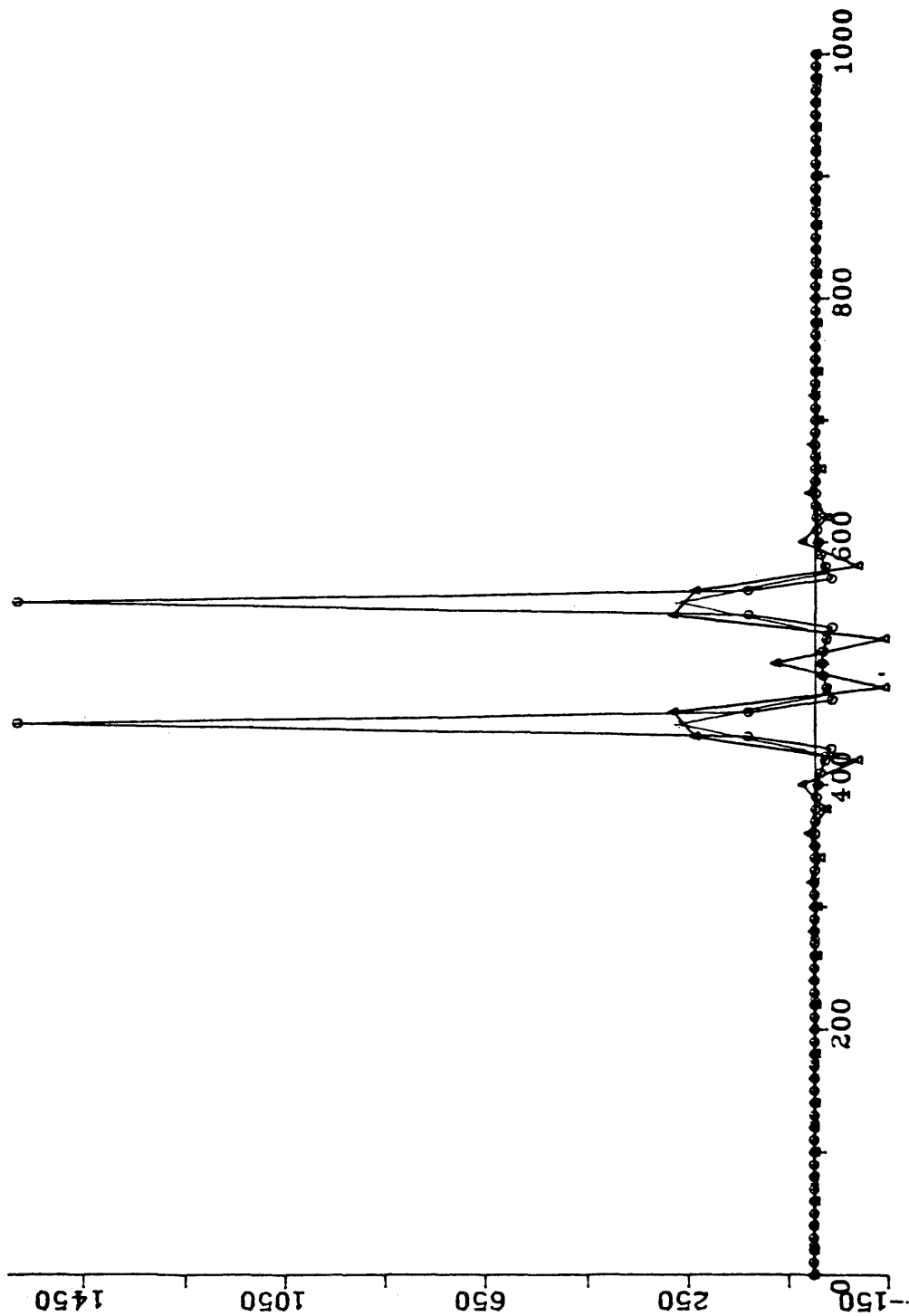


Fig.14. Profile after downward continuation. 0-mark line is the theoretical data and -mark line is the continued data with spacing 25m.

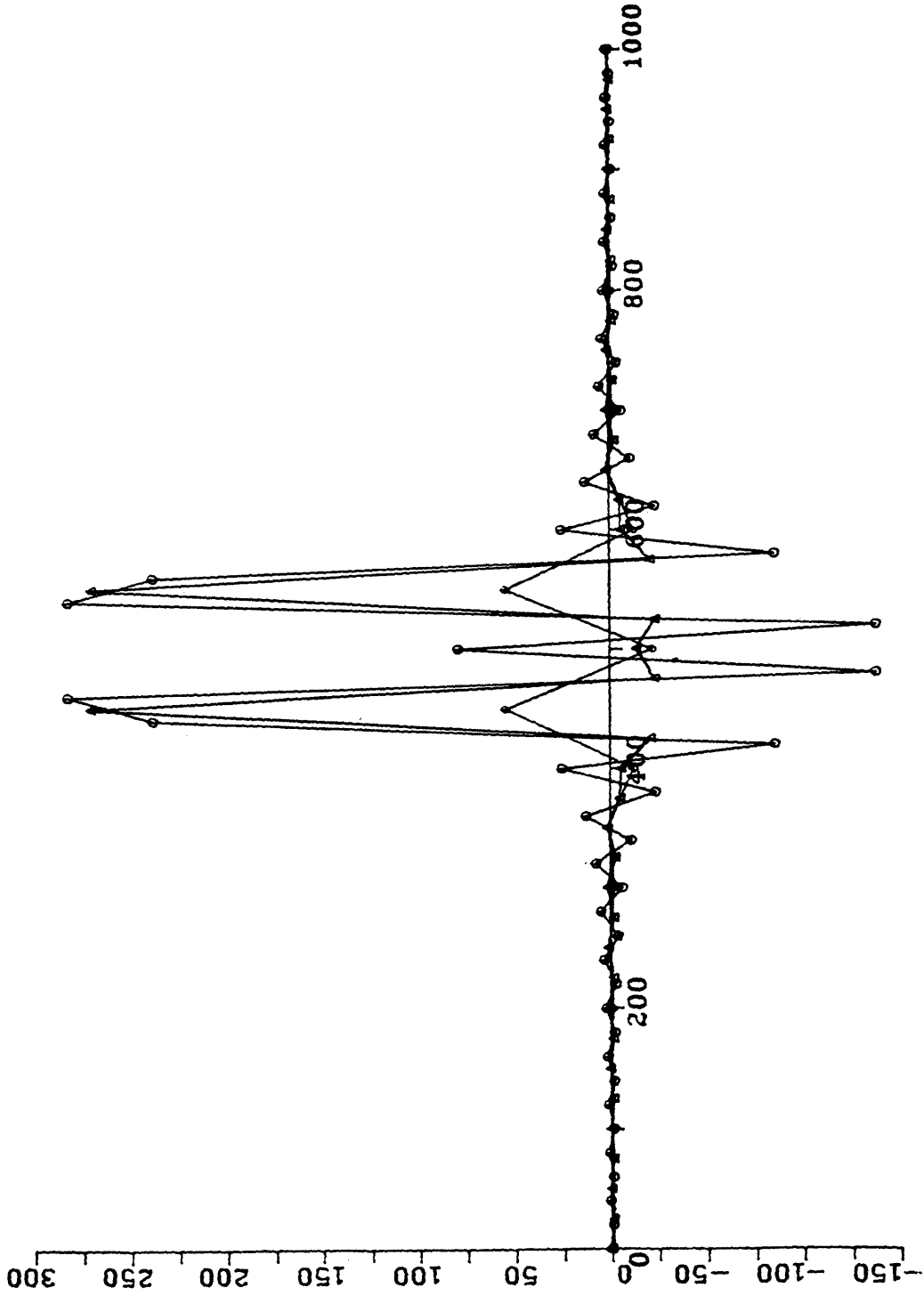


Fig.15. The effect of grid spacing. o-mark line is 20m spacing and -mark line is 25m spacing.

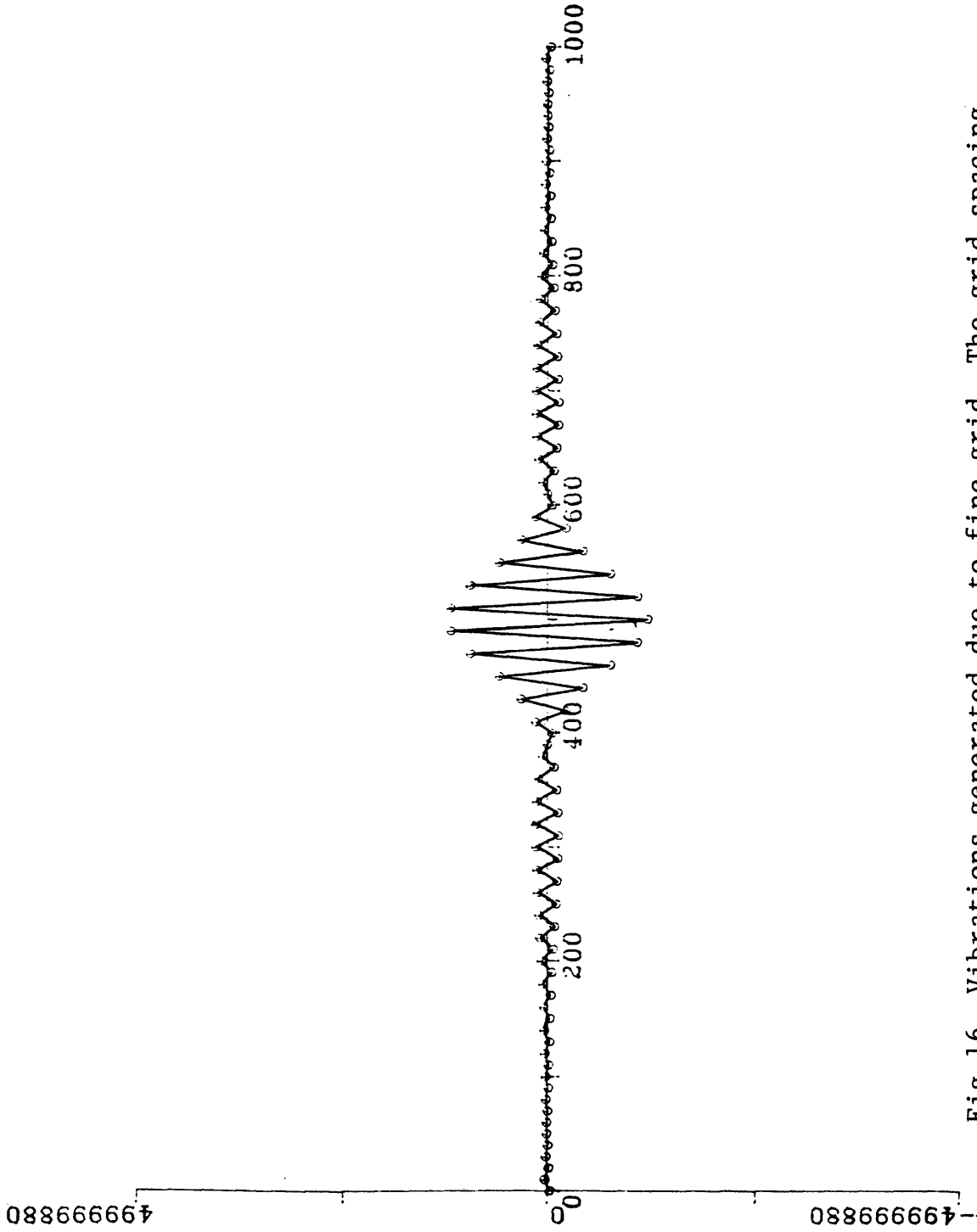


Fig.16. Vibrations generated due to fine grid. The grid spacing is 10m.

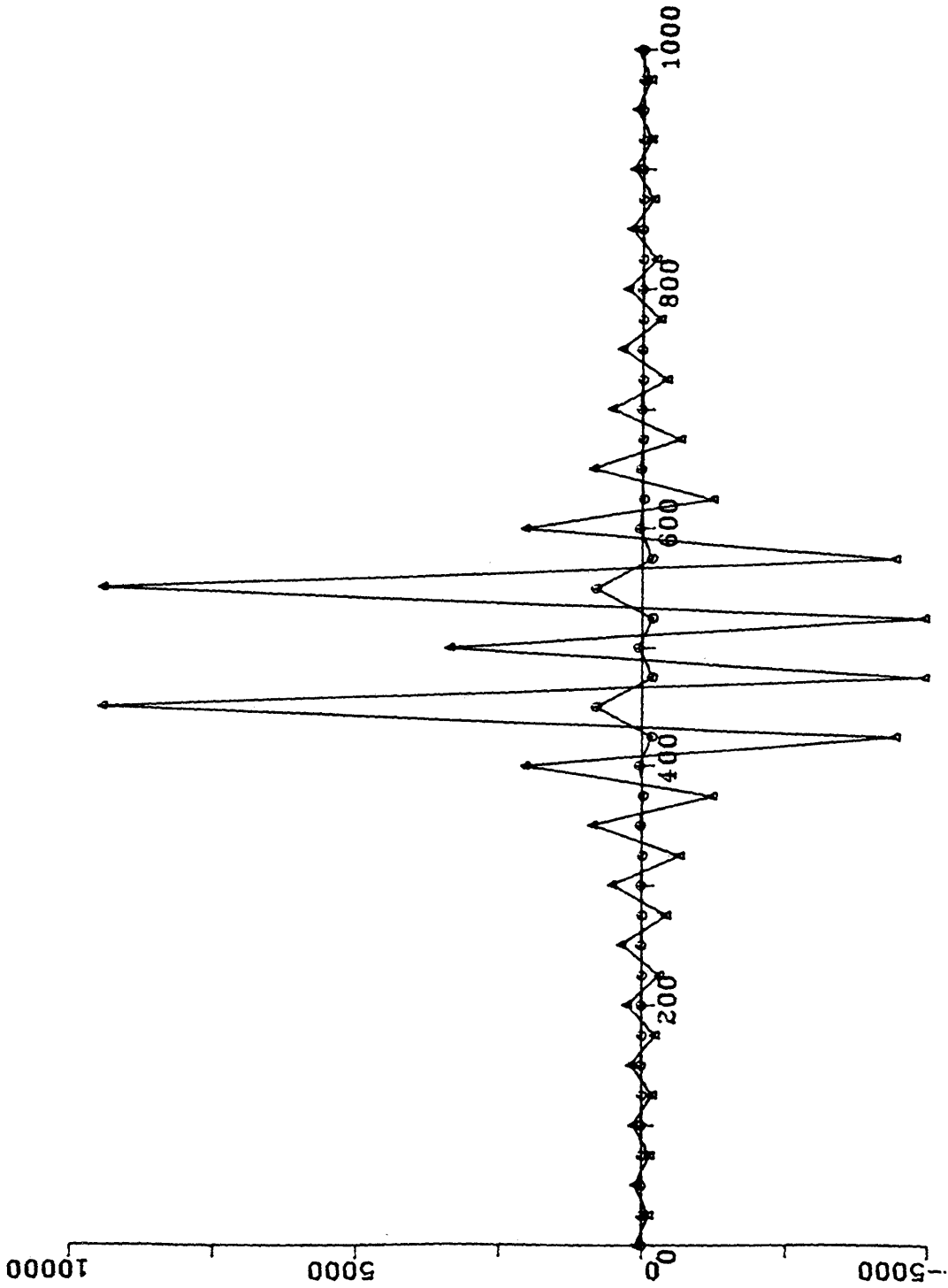


Fig.17. Downward continuation beyond the source region. The depth of continuation is 120m.

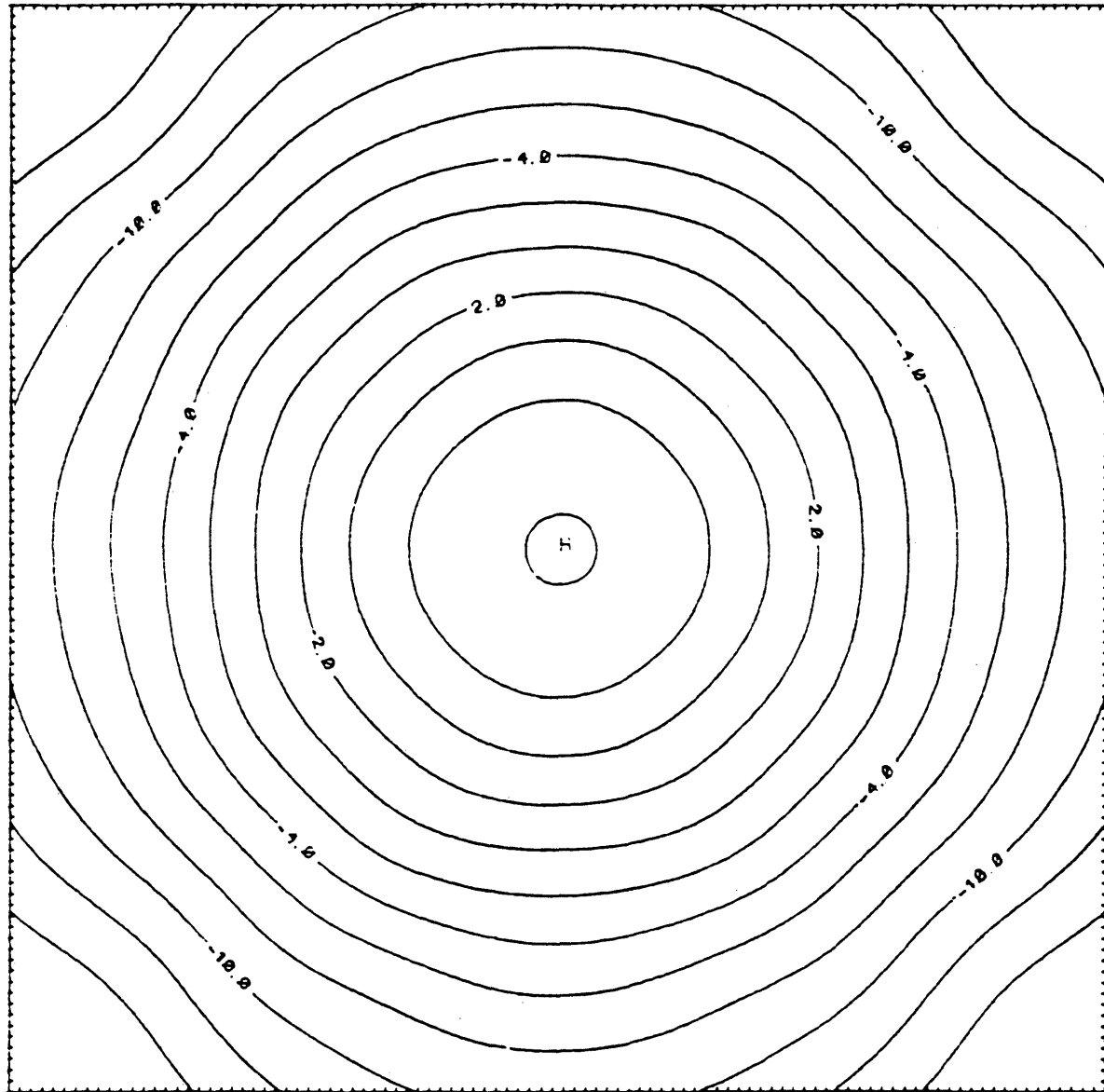


Fig.18. Contour of propagated field.

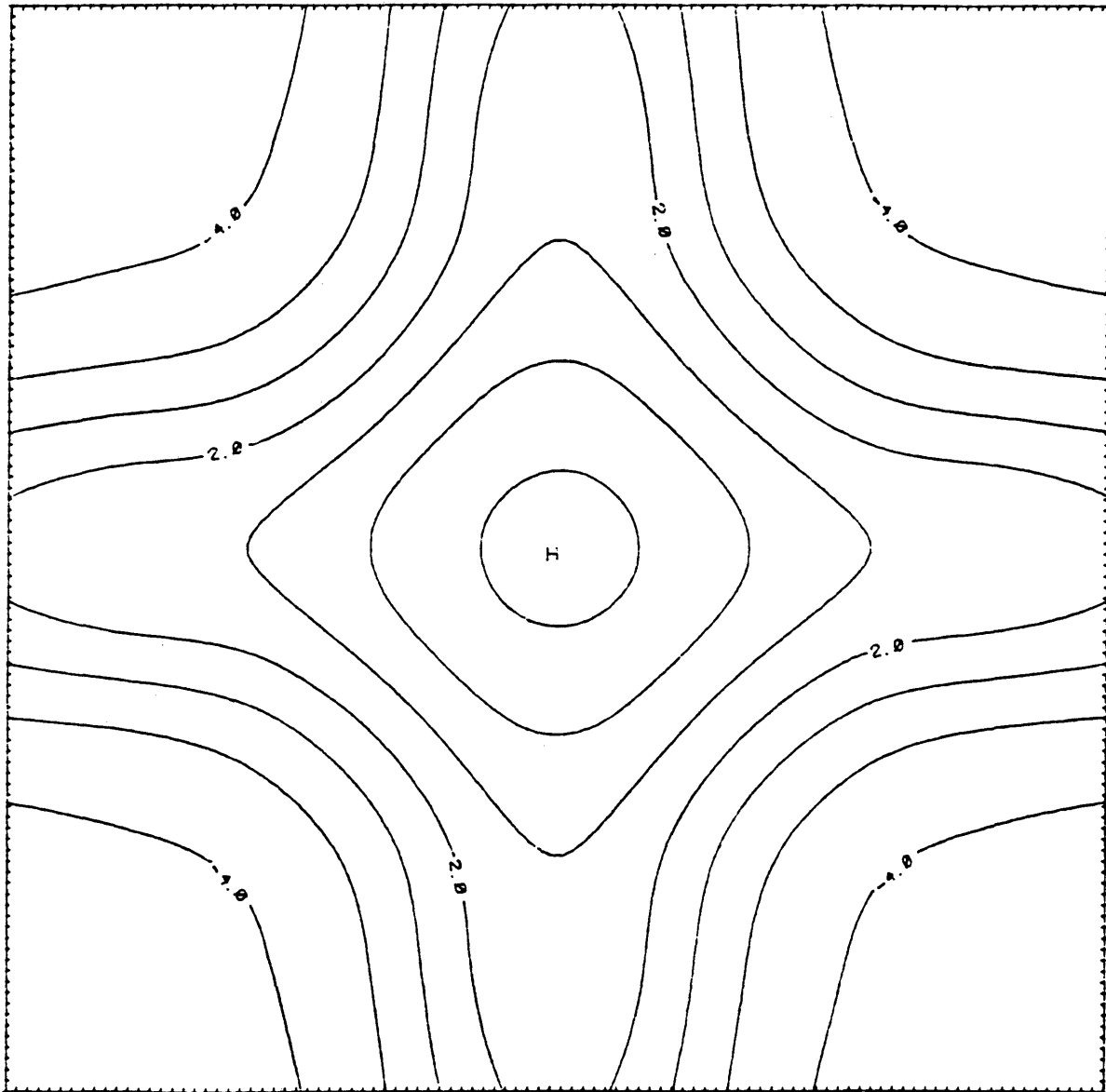


Fig.19. Contour after downward continuation. The depth of continuation is 0.2.

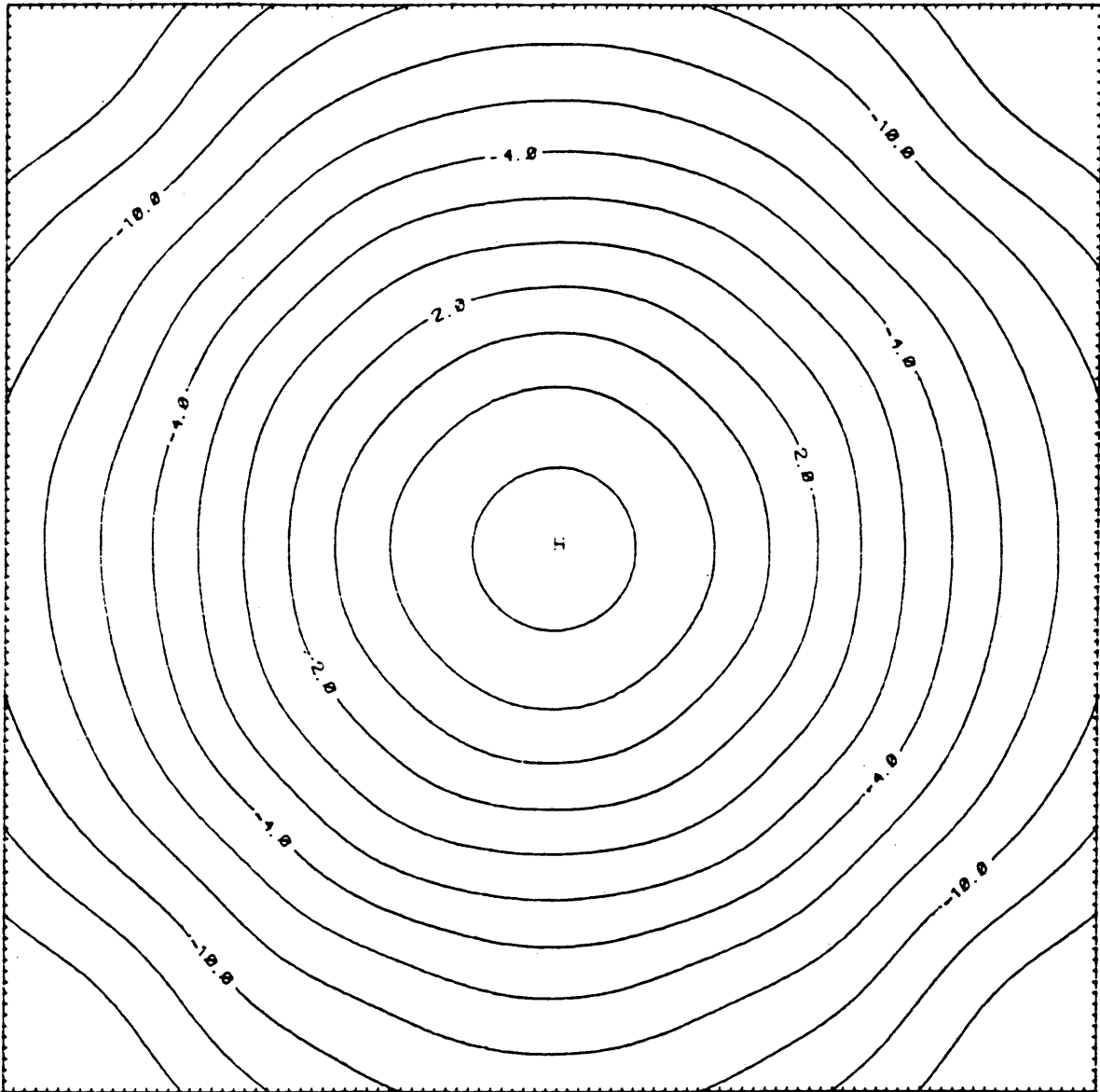


Fig.20. Modeling data at the depth of 0.2.

2. Resolution problem

Consider the model in Fig.4. The electromagnetic field is excited by two magnetic dipoles which are 100m apart. The depth of the dipoles is 120m.

The field at the surface may be analyzed as if it originated from one source since the profile has one signal maximum at the center, as shown in the line with Δ -mark in Fig.21. The field continued downward 20m shows changes of the location of signal maxima, which indicates the anomaly originates from two sources. The appearance of this feature is credited to the increased resolution of the downward continuation process.

In practical electromagnetic situations, a recording on the Earth's surface will contain noise which represents all the events in the recorded data which do not satisfy the wave equation. The useful signal is often cluttered with random noise, at least part of which is not instrumental, which may be caused by random variations of all the parameters of the electromagnetic field.

For this purpose, the grids of random electromagnetic errors to be used were generated by using the random number generator function RAN in Dec-10 computer. The grids formed in this manner are shown in Figs. 22 and 23. The grids of

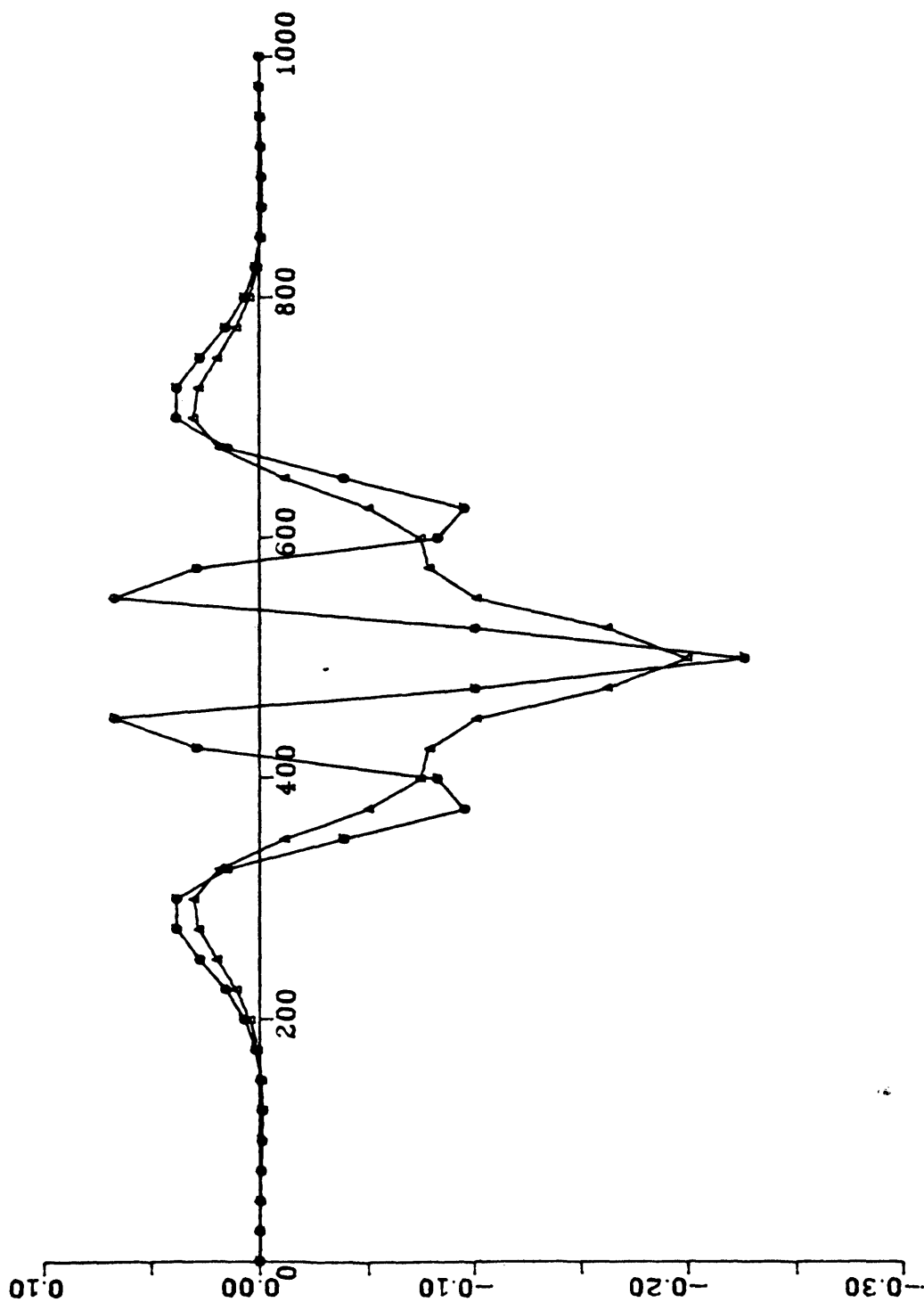


Fig.21. Resolution problem. The continued data agrees well with the modeling data and the two dipoles are resolved.

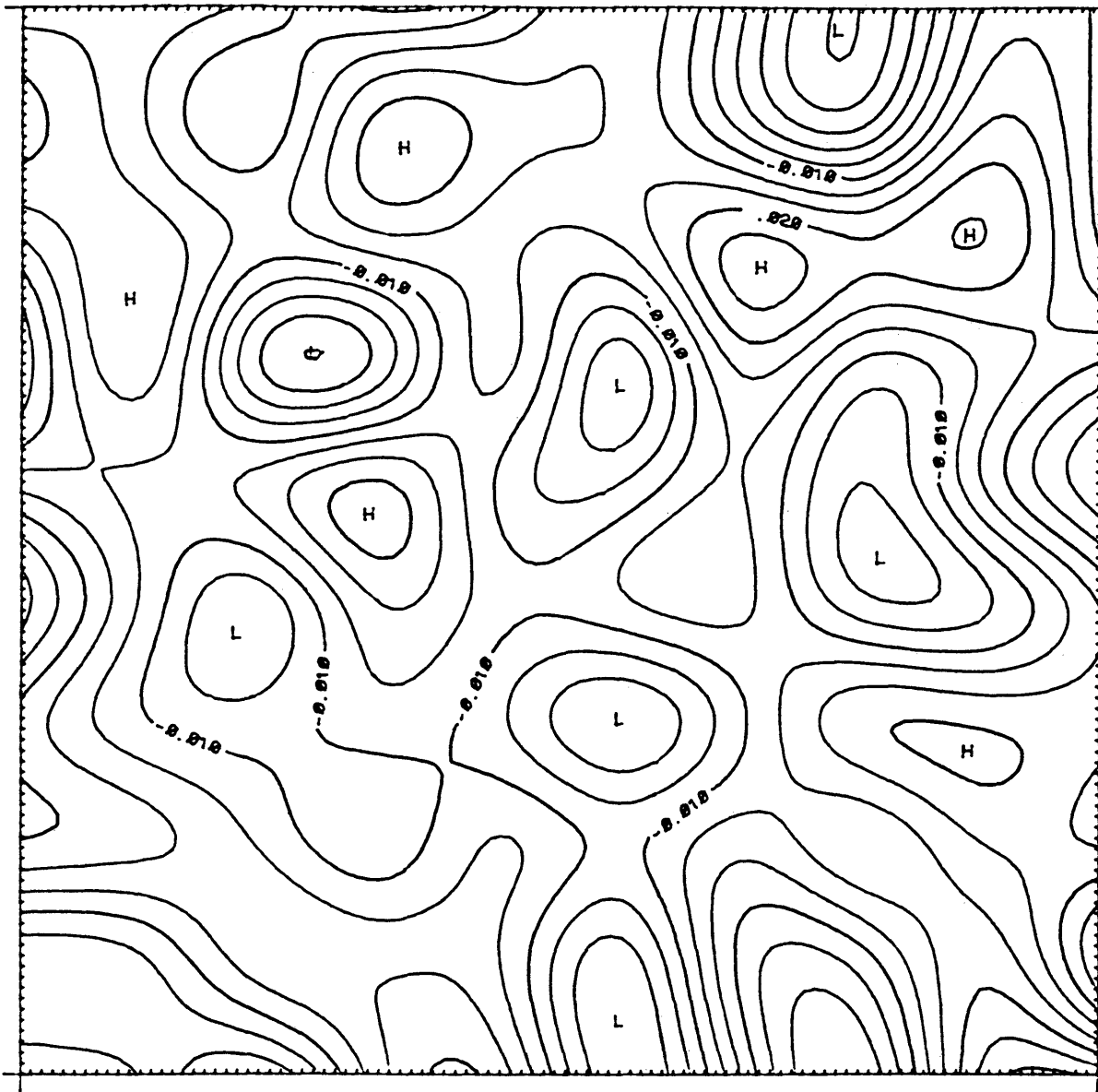


Fig.22. Real component of the noise generated.

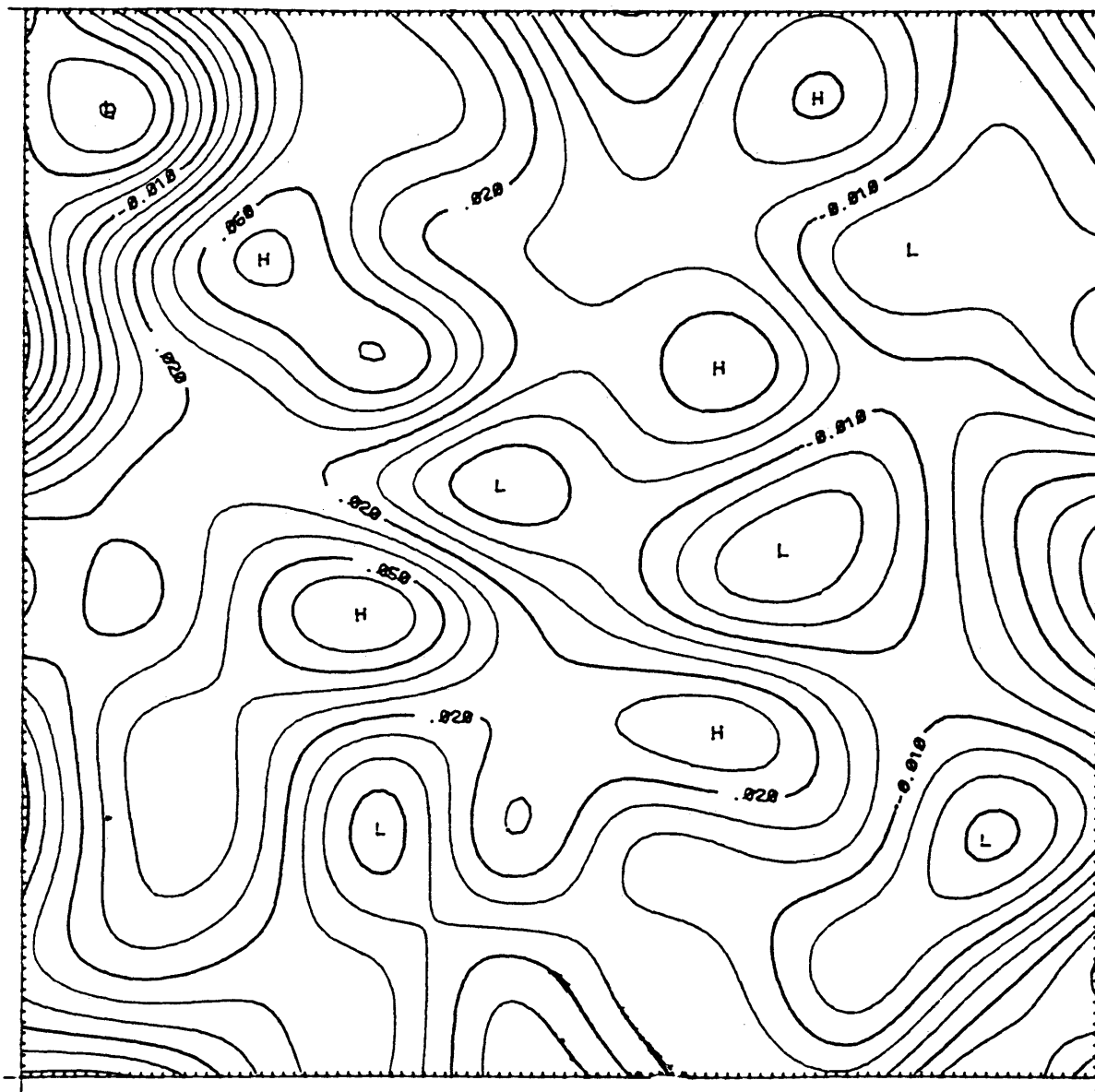


Fig.23. Imaginary component of the noise generated.

41 x 41 values were prepared for each in-phase and quadrature components of the electromagnetic fields.

It will be noted in Figs 22 and 23 that there is a sort of directional effect which may cause random error anomalies to have trends. However, we use three components of the electromagnetic fields in analytic continuation which corresponds to over ten thousand random numbers; therefore, it is to be expected that the statistical properties of the noise generated would reflect the measurement error and the geological noise.

The investigation of the effect of the random noise on the analytic continuation was performed by decreasing the signal to noise ratios from 40 to 5, as shown in Figs. 24 to 27.

The signal to noise ratios were calculated as follows,

$$E = \frac{\sum S_{ij}^2}{\sum N_{ij}^2}$$

where E represents the signal to noise ratio and S_{ij} and N_{ij} are the signal strength and noise strength at each grid point, respectively. If a different signal to noise ratio is desired, it is only necessary to multiply the grid values by the ratio R, which is

$$R = \sqrt{E'/E}$$

where E' is the new signal to noise ratio. Then the new signal to noise ratio is

$$E' = \frac{(S_{ij} R)^2}{N_{ij}^2} .$$

The original surface data without noise shows a symmetric and smooth pattern, as shown by the o-mark line in Fig.21. As the signal to noise ratio decreases from 40 to 5, the asymmetry and the random oscillations of the surface data become larger, as shown by the Δ -mark line in Figs. 24 to 27.

The x-mark line in Figs.24 to 27 show the data sets which are continued downward 20m for the signal to noise ratios from 40 to 5. We note that the random variations start to appear when the signal to noise ratio decreases to 5. The peaks and troughs of the continued data agree well with the theoretically computed data at the depth, which are the o-mark lines in Figs. 24 to 27. Therefore, the analytic continuation scheme still works well in the resolution problems even for surface data with much noise.

In a usual electromagnetic survey, the random error is often as much as 5 percent, which corresponds to a S/N ratio 20. In Fig.25, which shows the surface data of S/N ratio 20, we note that the downward continued data agrees well with the theoretical data except for small random variations of the continued data at the edge of the profile.

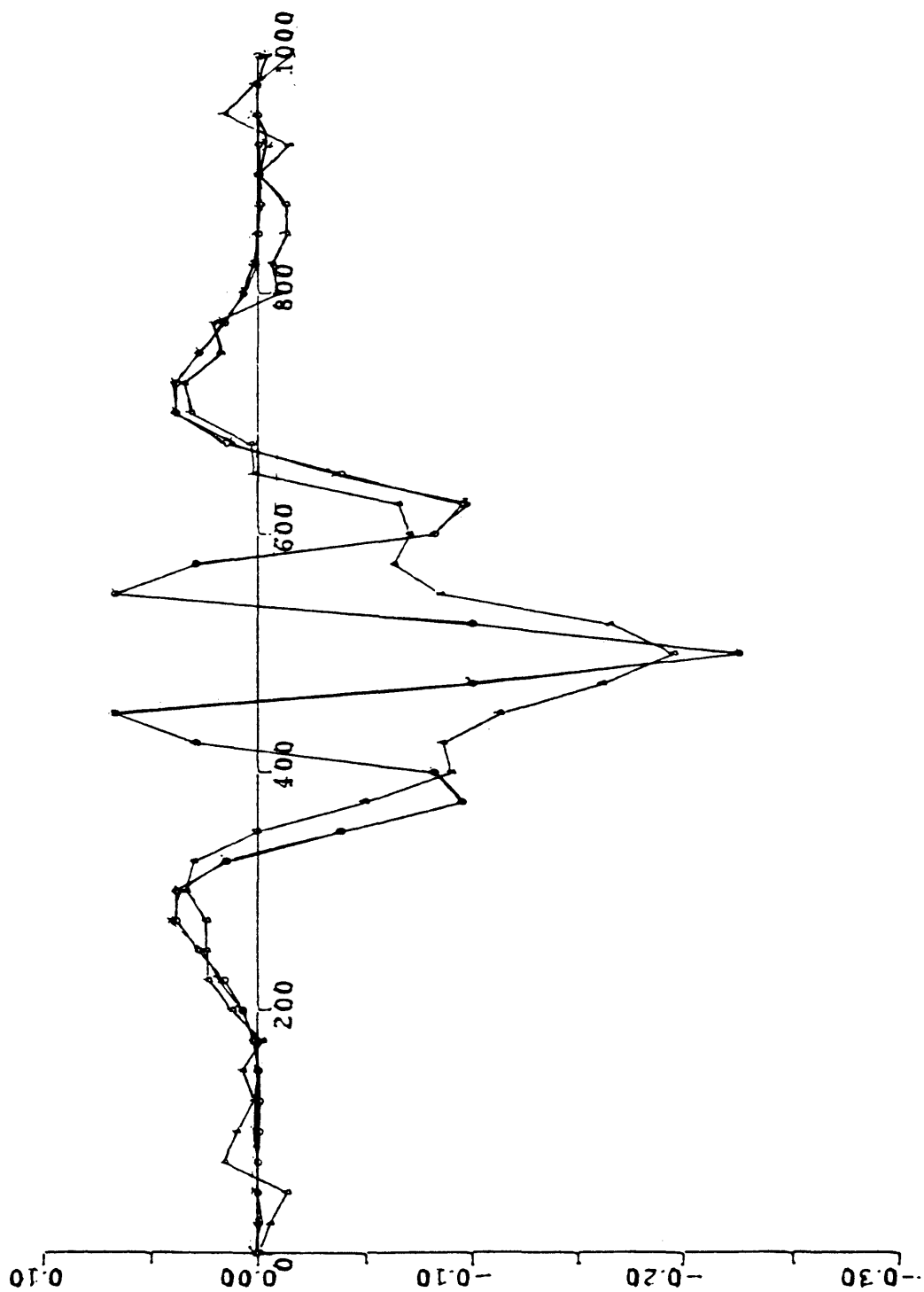


Fig.24. Resolution problem. S/N ratio is 40.

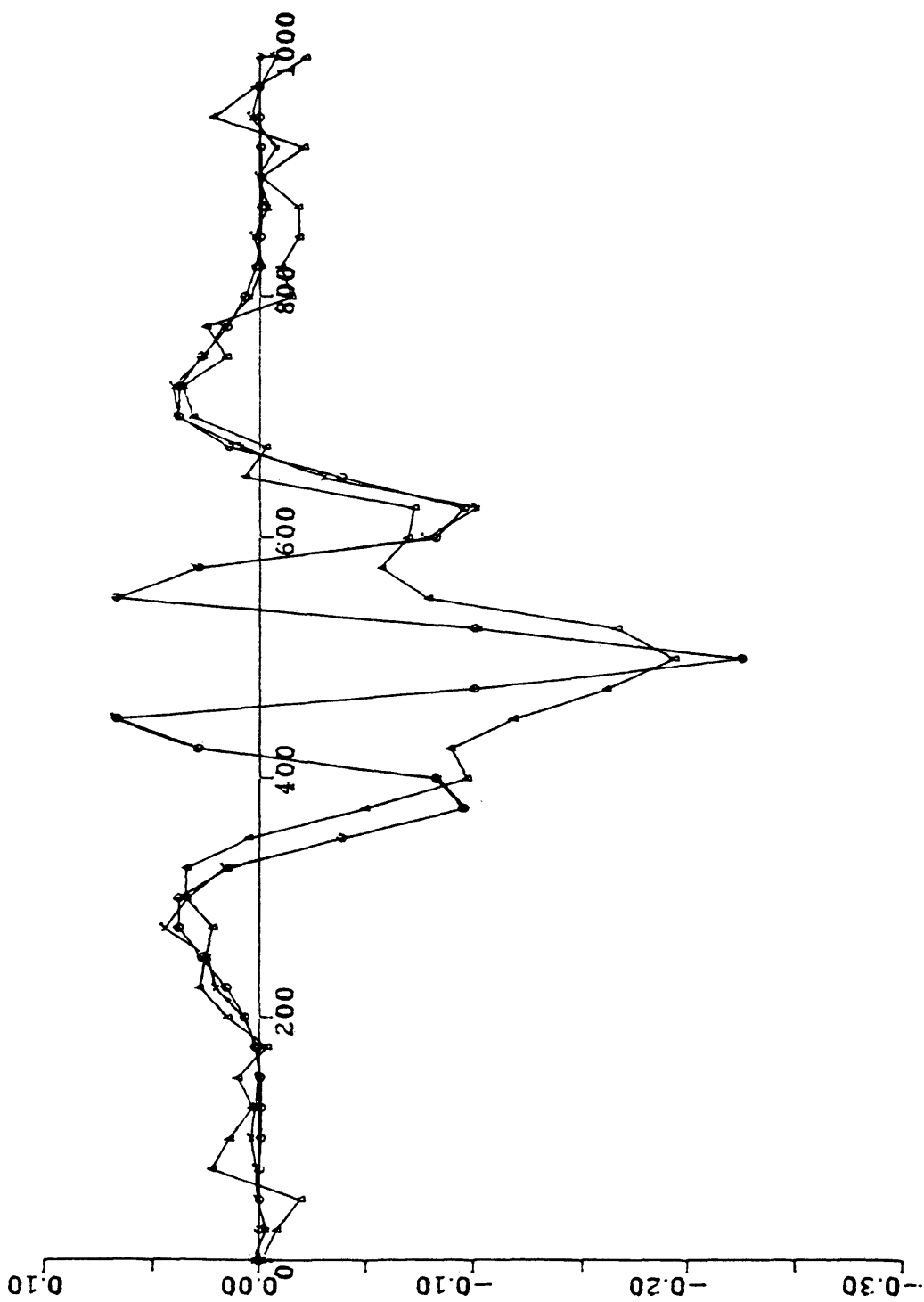


Fig.25. Resolution problem. S/N ratio is 20.

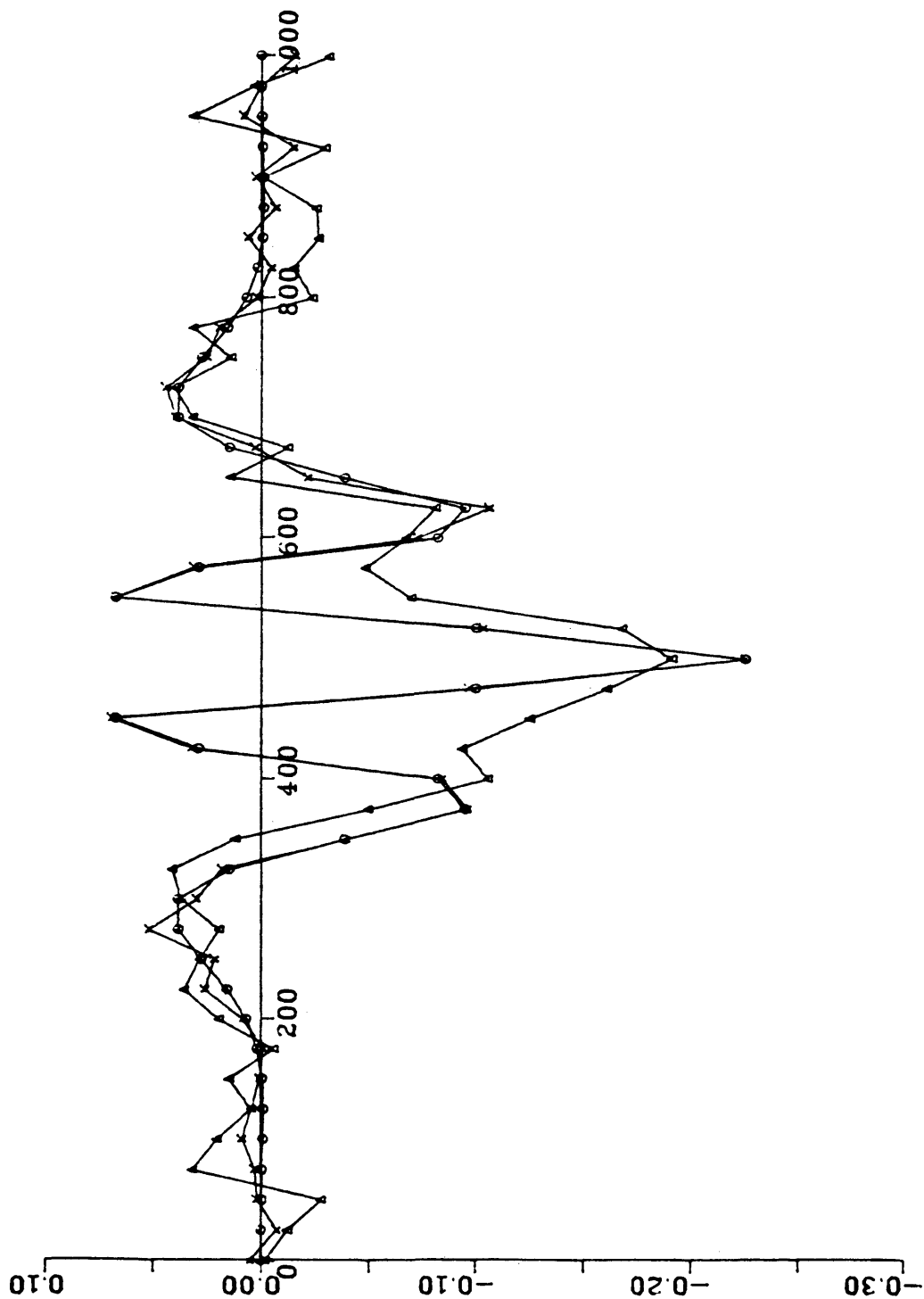


Fig.26. Resolution problem. S/N ratio is 10.

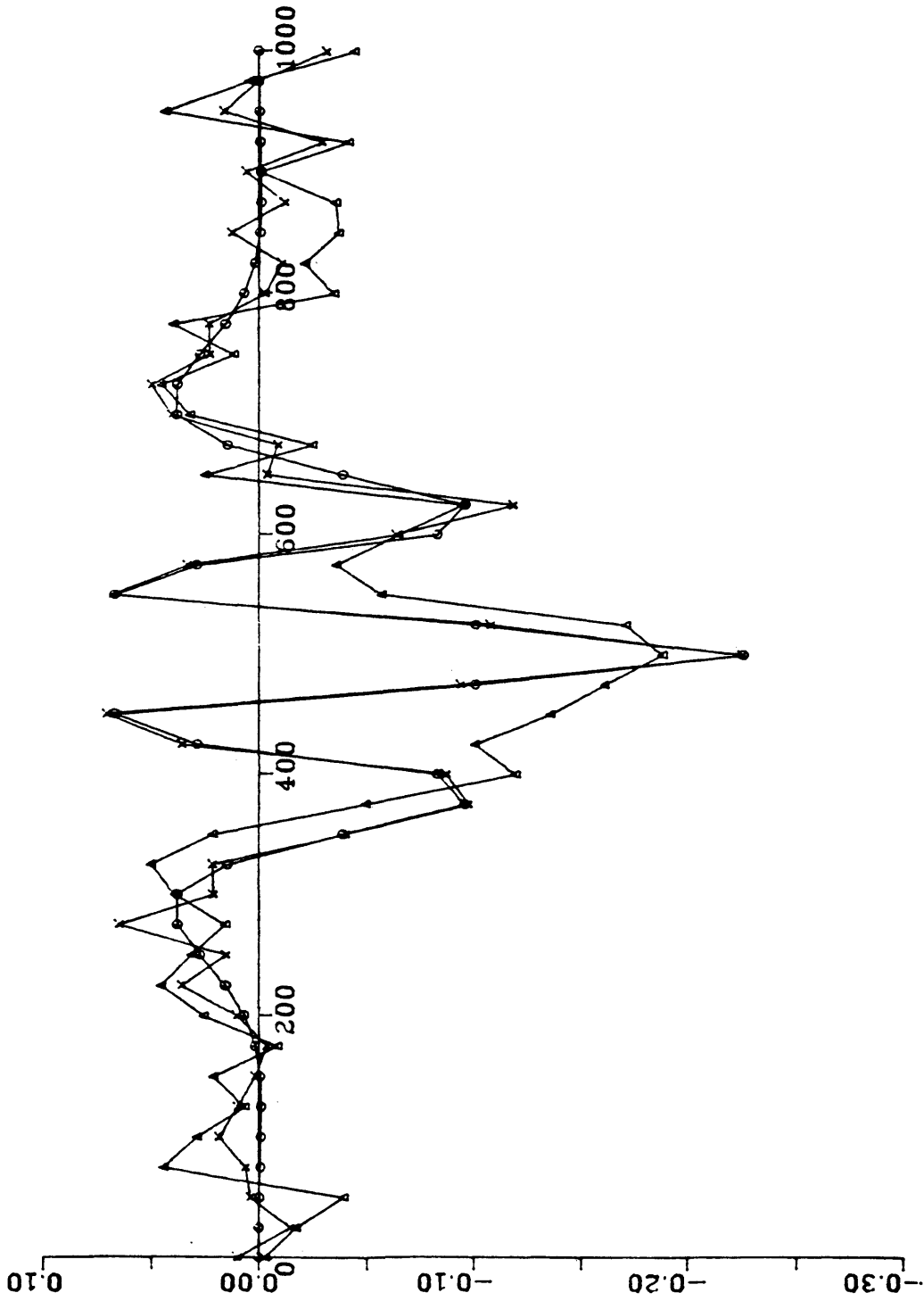


Fig.27. Resolution problem. S/N ratio is 5.

Considering the large noise in the surface data, this can be credited to the enhancement of the S/N ratio by the analytic continuation process. That is, the analytic continuation can be used to extract a signal which is cluttered with random noise.

Let us discuss this problem further by considering the concept of analytic continuation in the frequency domain. The implementation of the analytic continuation involves a transformation of one frequency domain data into another.

In the analytic continuation process, we first Fourier transform the surface fields $H(x,y)$ to obtain $h(k_x, k_y)$. This information lies on a grid in (k_x, k_y) space between limits of $\pm k_{xn}$ and $\pm k_{yn}$, where the subscript-N refers to the respective Nyquist frequency, as shown in Fig.28. After that, the data is continued downward by convolving with hyperbolic functions which are derived from the Fourier expansion of the Green's function in (k_x, k_y) domain, as shown in Fig. 29.

In Figs. 28 and 29, we note that the amplitude of the high frequency part is amplified more than twice of the original spectrum, while the low frequency part shows a slight increase. This amplification of the high frequency is the main feature of the downward continuation when we continue toward the source.

The spectrum after convolution is almost the same as the theoretical spectrum calculated at the depth, as shown in Figs. 29 and 30. This demonstrates the accuracy of the analytic continuation process in the frequency domain.

Next, we considered the problem of signal enhancement in the frequency domain.

Fig.31 is the amplitude spectrum of the surface data with 10 percent noise. After convolution in the frequency domain, we note that the irregular contour tightens and it becomes identical with the spectrum of the modeling data at the depth, which is shown in Fig.32.

This process is more clear in the three-dimensional picture generated by the SURFII package in Dec-10. Fig.33 is the spectrum of the surface data with 10 percent noise. Fig.34 is the spectrum after convolution in the frequency domain. We observe that the random noise is compensated out after the convolution.

In the geopotential problem, oscillations are generated if the surface field is noisy. However, in the geoelectric problem, three components of electromagnetic fields are stacked in the frequency domain; therefore, the noise is compensated out in the analytic continuation process.

This noise test reveals that the analytic continuation is a good stacking scheme to extract a signal which is cluttered with random noise.

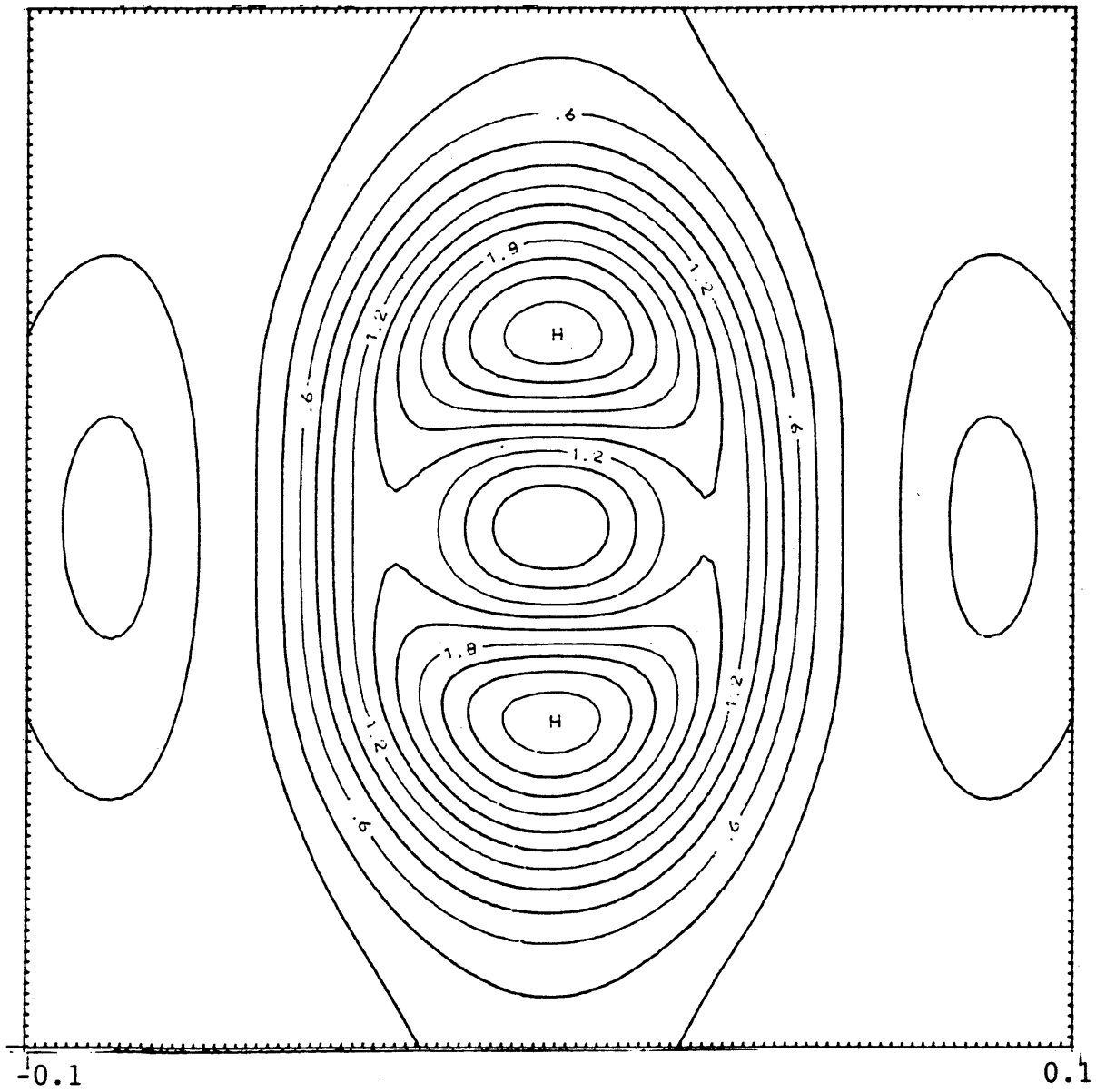


Fig.28. Amplitude spectrum of the surface data. The depth of the dipoles is 120m.

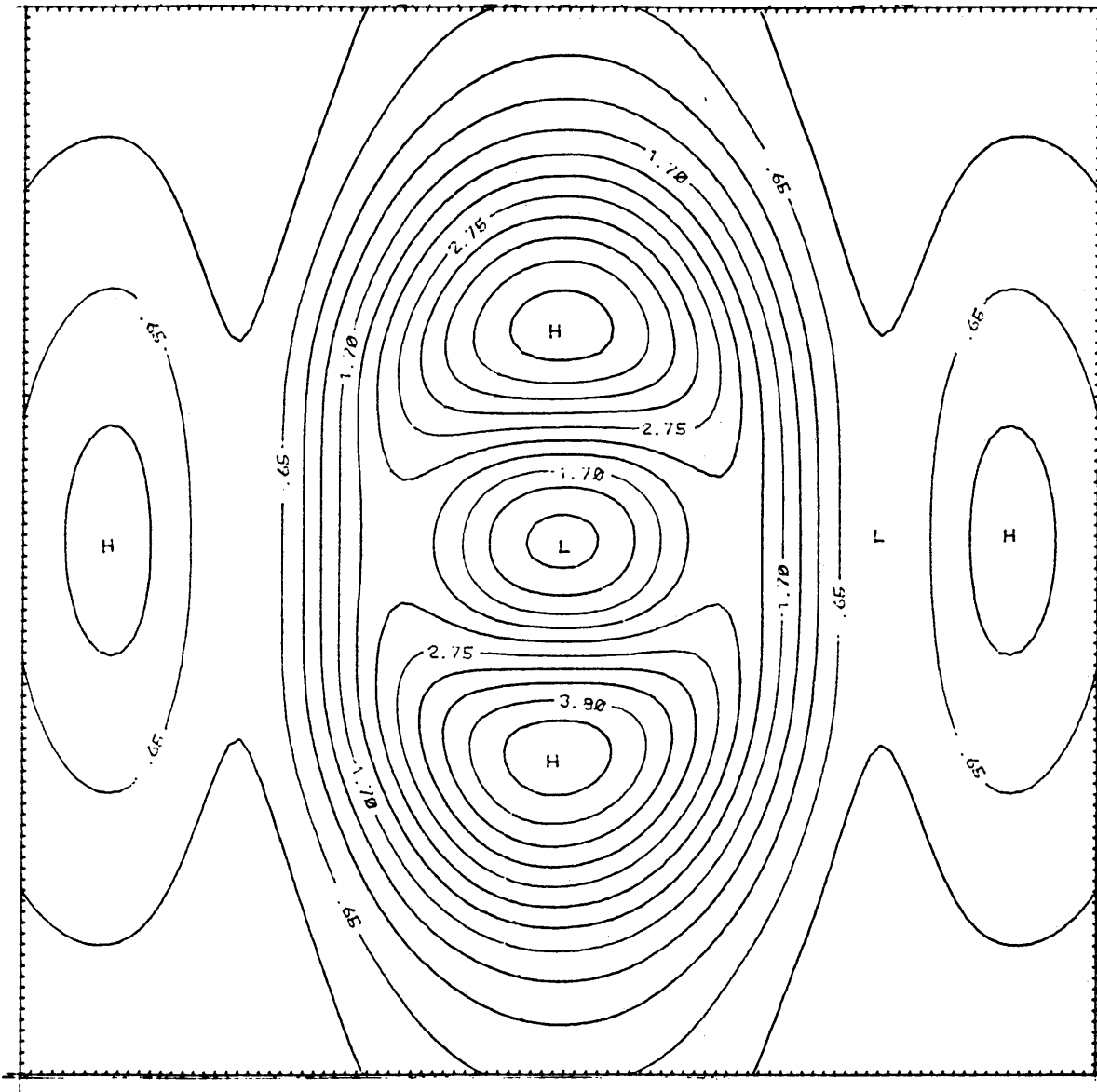


Fig.29. Amplitude spectrum of the surface data after convolution in the frequency domain.

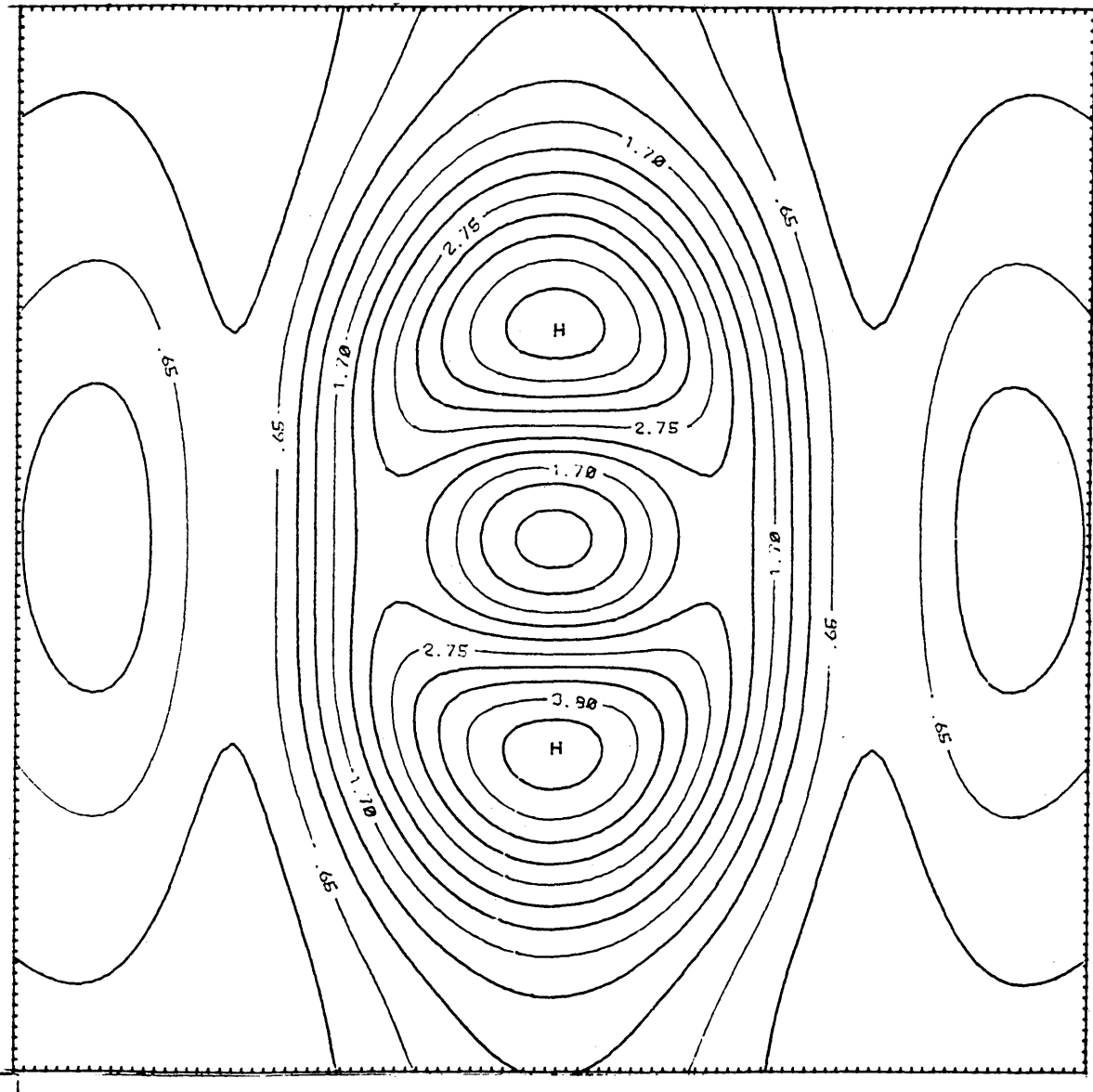


Fig.30. Amplitude spectrum of the modeling data at the depth of 100m.

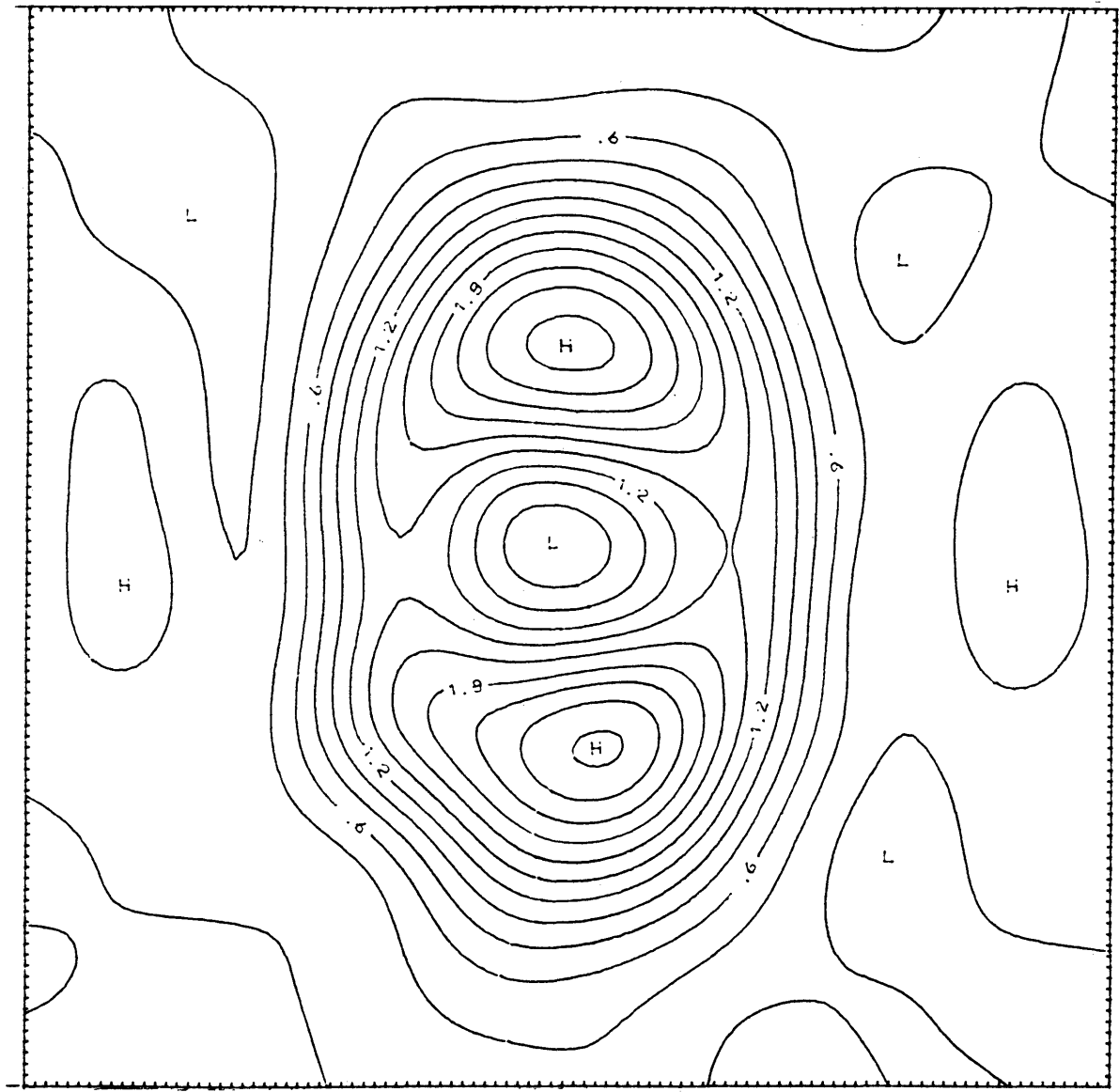


Fig.31. Amplitude spectrum of the surface data with 10 percent noise.

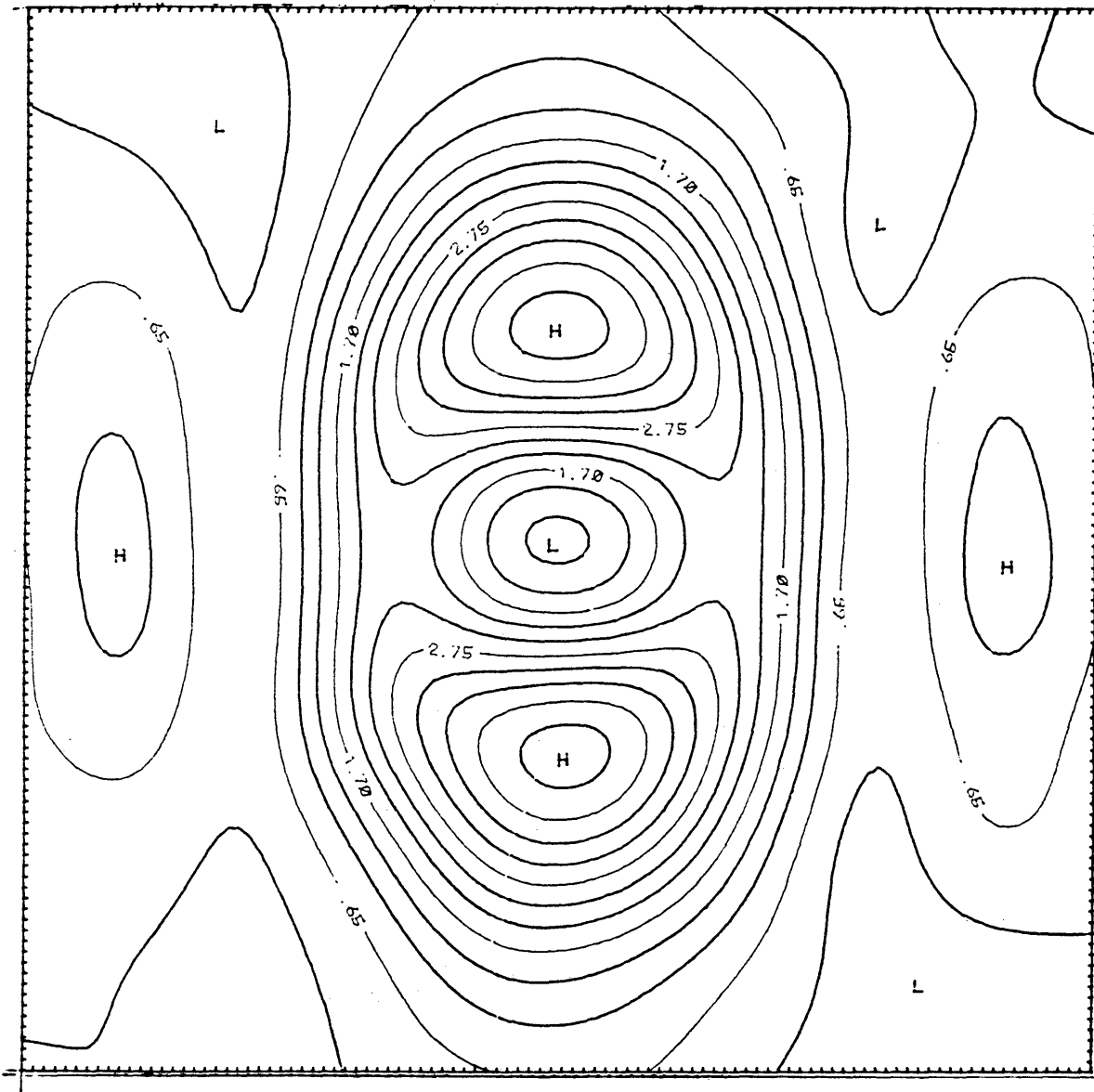


Fig.32. Amplitude spectrum after convolution in the frequency domain.

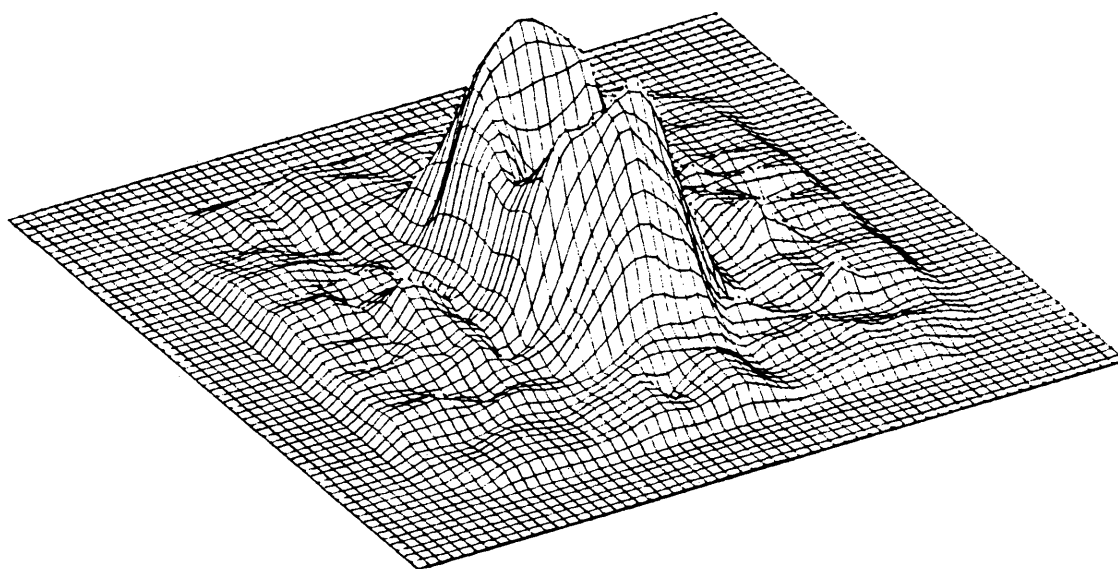


Fig.33. Three-dimensional view of the amplitude spectrum of the surface data with 10 percent noise.

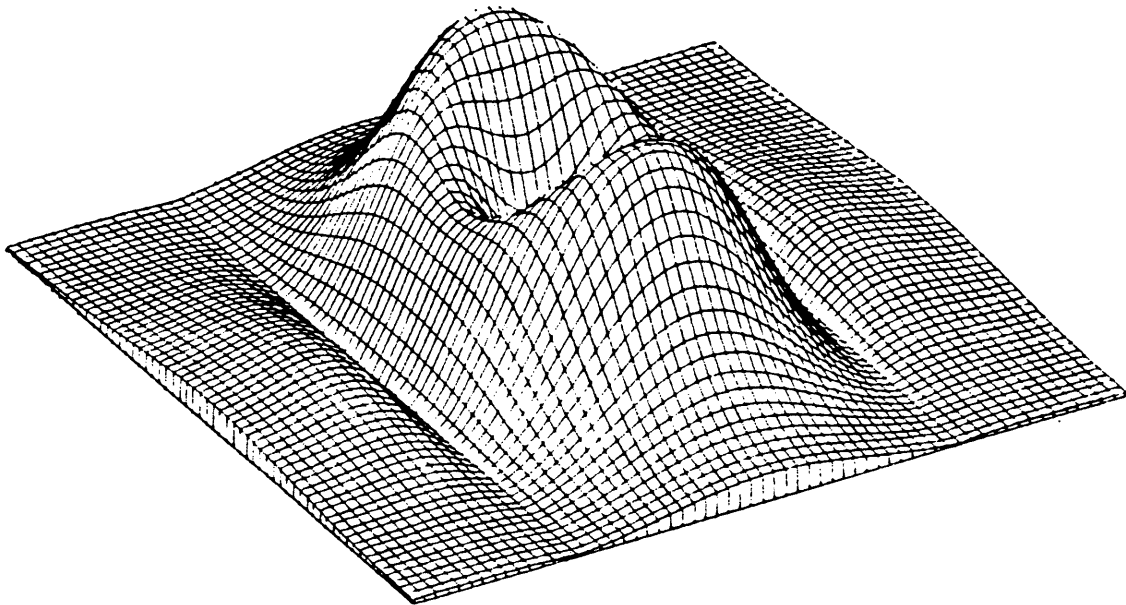


Fig.34. Three-dimensional view of the amplitude spectrum after convolution.

3. Accuracy of scale or computer modeling.

The electromagnetic field over a rectangular thin plate was calculated by a numerical method and used as a test case to measure the accuracy of the numerical modeling.

The plate model is particularly useful for Turam interpretation because of the important effect of conductor size on the Turam response. Several numerical methods to calculate the response of the finite thin plate model has been developed.

The convenient solution of the plate model is the integral equation solution of Annan(1974), because the method can handle any type of EM systems.

Annan computed the set of eigenpotentials, and used these to represent the individual current flow in the plate as a sum of those eigencurrents. After that, the magnetic fields were calculated by summing up those individual current systems using the Biot-Savart law.

The geometry of the model is shown in Fig.35. The electromagnetic field was calculated at a grid interval 20m using the program PLATE (K.D. Kim, 1983) which implemented the integral equation algorithm. For this response, the frequency used was 100 Hz. The width and length of the plate are 100m and the depth is 100m below the grid of

of observation.

The line with o-mark in Fig.36 is the theoretically computed in-phase component of vertical magnetic field produced by a rectangular line source.

The line with x mark is a profile continued downward 20m toward the plate. The continued data shows difference with the curve with ∇ mark which is theoretically computed curve at the depth as shown in Fig.36. To check the accuracy of downward continuation, we double the grid spacing and test the convergence between the two sets of data. In Fig.37, we observe that the two sets of data for grid spacings of 25m and 50m, respectively, converge well.

We already pointed out that the continued data with different grid spacings converges each other except at the source region. Therefore, the difference between the modeling data and the continued data is due to the numerical error in the computer modeling.

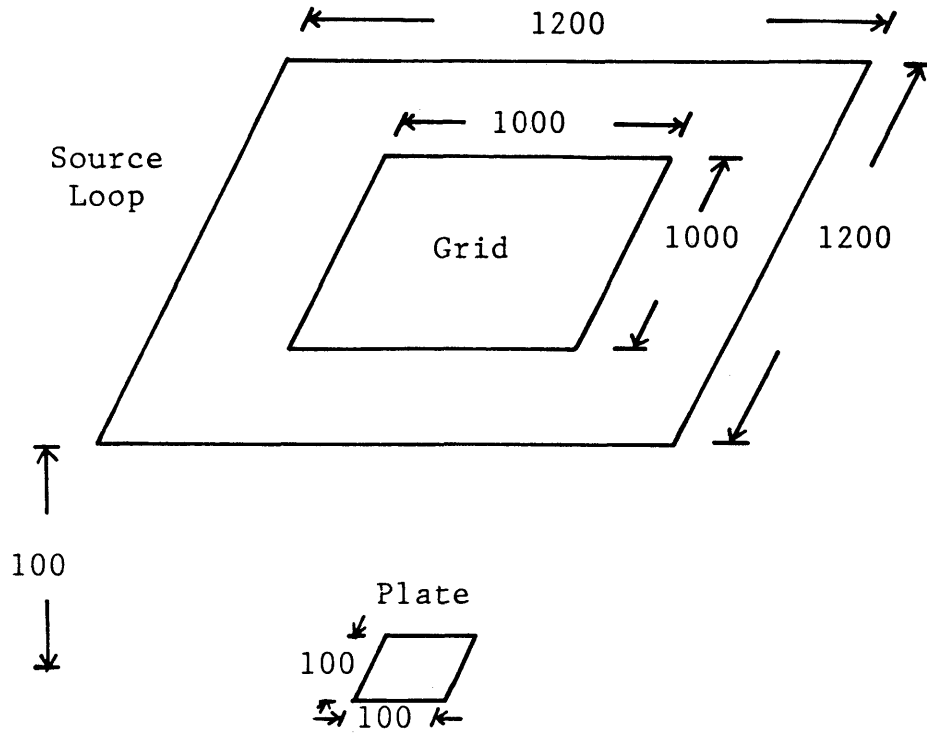


Fig.35. Schematic diagram of the plate model.

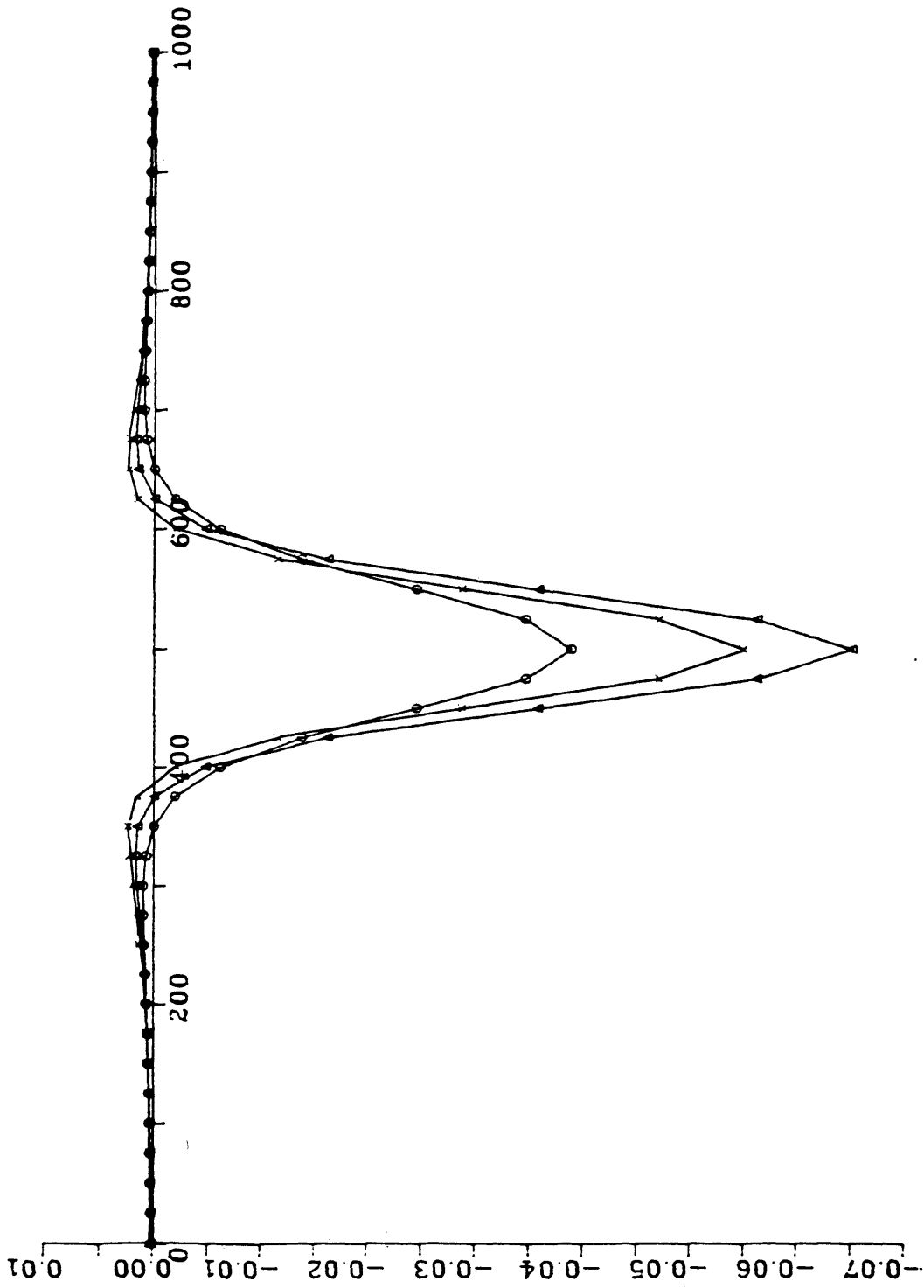


Fig.36 . Comparison between the theoretical data and the continued data.

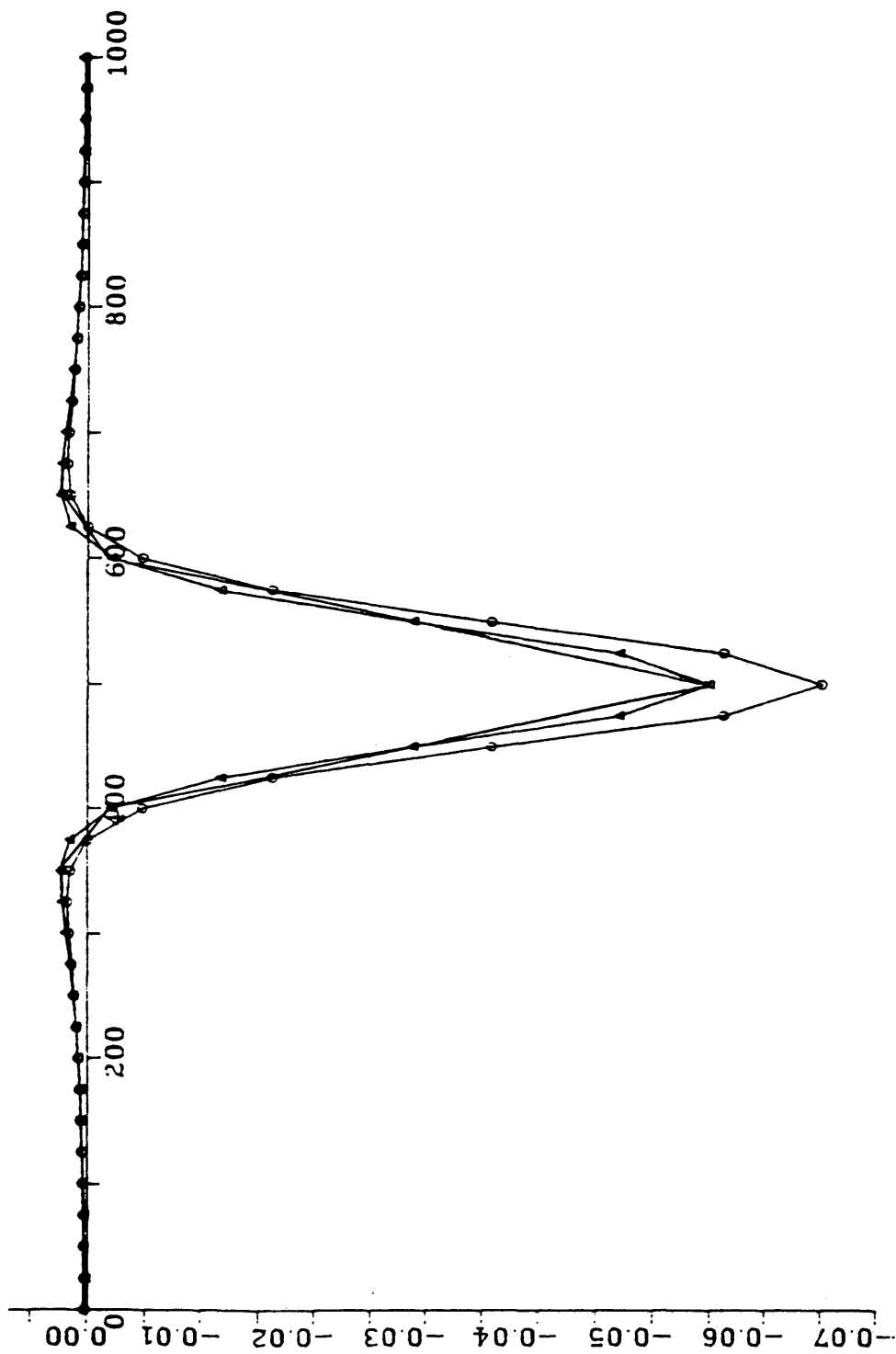


Fig.37 . Convergence of the continued data.

CONCLUSIONS

An interpretation scheme of electromagnetic data using analytic continuation was studied and found to yield results of satisfactory accuracy in several cases tested.

The strength of the method seems to lie in its ability to handle the problems of depth estimation, resolution, signal enhancement, and accuracy of scale or computer modeling. Another advantage is that the method does not require any priori knowledge about the shape of the anomaly-causing body or the source.

Reliability of the analytic continuation depends on the grid interval selected and the depth of continuation. The oscillations are generated if the sampling grid is too fine, or if the field is continued too close to the source of the anomaly. The oscillations generated due to the fine grid can be eliminated by increasing the grid spacing; however, near the source region, the two sets of data does not converge each other. This singular behavior of a field near the source region is a good diagnostics to locate geologic inhomogeneities.

The optimum grid interval is about one-fourth the depth to the top of the anomalous source. A fair estimate of the

depth of the inhomogeneity can be made from a visual examination alone of the continued curves. The log contours are more definitive than the profile to locate the body.

The analytic continuation scheme using the Stratton-Chu integral does not involve any assumptions except the uniformity of medium; therefore, it is a good method for estimating the error of the scale or numerical modeling.

The noise test performed in this thesis reveals that the analytic continuation can be used to extract a signal from a random noise which may be caused by random variation of all parameters of the electromagnetic field. In the geopotential problem, oscillations are generated if the surface field is noisy. However, in the geoelectric problem, three components of electromagnetic fields are stacked in the frequency domain; therefore, the noise which does not satisfy the wave equation is compensated out in the analytic continuation process.

Since analytic continuation works quite well in the problems of depth estimation, resolution, and signal enhancement, it offers a better approach to the interpretation of the geoelectric problems than the method of a reconstruction of the geoelectric cross section is combined as a successive step of analytic continuation.

REFERENCES

- Annan, A. P., 1974: The equivalent source method for EM scattering analysis and its geophysical application, Ph.D Thesis, Memorial Univ. of Newfoundland.
- Hartmann, O., 1963: Behandlung lokaler erdmagnetischer Felder als Randwertaufgabe der potential theore, Ahandlungen der Akad. Wiss. Cottingen. Math. Kl. Beitr. internat. Geophys. Heft 9.
- Kertz, O., 1957: Modelle fur erdmagnetischen induzierte elektrische strome in untergrund., Nachr. Akad. Wiss. Math.-Phys. Klasse.
- Kim, K. D., 1983: Frequency and time domain responses of a rectangular thin plate, Msc thesis, Colorado School of Mines, T-2987.
- Roy, A., 1968: Continuation of electromagnetic field - I, Geophysics, V.33, No.5, P834-837.
- Roy, A., 1969: Continuation of electromagnetic field - II, Geophysics, V.34, No.4, P572-583.
- Markov G. T., 1967: Excitation of electromagnetic waves, Energy, Moscow-Leningrad.
- Morse, F. M. and Feshbach, H., 1953: Methods of theoretical physics, McGraw-Hill, New York.
- Oristaglio, M. L. and Worthington, M. N., 1980: Inversion

of surface and borehole electromagnetic data for two-dimensional conductivity model, *Geophysical Prospecting*, V.28, P.633-637.

Stratton, J. A., 1953: *Electromagnetic theory*, McGraw-Hill, New York.

Weidelt, P., 1975: Inversion of two-dimensional conductivity structure, *Physics of the Earth and Planetary Inter.*, V.10, P.282-291.

Zhdanov, M. S., 1976: *Methods of transformation and interpretation of anomalies of gravitational, magnetic, and transient EM fields of the Earth*, Doctorate, Moscow.

Zhdanov, M. S., 1978: *Supplementary chapters on electrical prospecting*, Minkh, Moscow.

Zhdanov, M. S. and Berdichevsky, M. N., 1982: *Advanced theory of deep geomagnetic sounding*, Academy of Sciences, Moscow University.

APPENDIX A. INTERACTIVE USER'S MANUAL - SAMPLE SESSION FOR
MODELING AND CONTINUATION FOR A MAGNETIC DIPOLE SOURCE.

.EX ACEF1.FOR

TYPE OF MODELING: MAGNETIC DIPOLE, LINE SOURCE, TUNNEL (1ST
LETTER) M

DIFFUSION OR PROPAGATION (1ST LETTER) D

ENTER THE COORDINATE OF STARTING POINT OF THE GRID. THE
POINT IS AT THE LEFT TOP POSITION OF THE GRID.

-500, -500, 100

ENTER THE HORIZONTAL AND VERTICAL LENGTH OF THE GRID ...

.... 1000,1000

ENTER THE HORIZONTAL AND VERTICAL SPACING OF THE GRID ..

.... 50,50

ENTER MOMENT OF DIPOLE, CONDUCTIVITY, AND FREQUENCY ...

.... 10.E6,1.,100

ENTER THE OUTPUT FILE NO. 10

FILE NO.	NX	NY	DELX	DELY
----------	----	----	------	------

10	21	21	50	50
----	----	----	----	----

THE OUTPUT IS READY IN THE FORMAT OF INPUT FOR THE COMPUTER
PROGRAM OF ANALYTIC CONTINUATION. IF YOU WANT PLOT THE
MODELING DATA EXECUTE PLOT.FOR.

END OF EXECUTION

.EX ACEF2.FOR

ANALYTIC CONTINUATION OF EM FIELDS (15/11/84)

TYPE OF DATA: PROFILE OR CONTOUR (1ST LETTER) C

TYPE OF FIELD: DIFFUSION OR PROPAGATION (1ST LETTER) ... D

INPUT THE FILE NO. OF SURFACE DATA 10

ENTER THE NO. OF SURFACE DATA POINTS NX,NY 21,21

ENTER THE SPACING OF RECEIVER DELX, DELY 50,50

ENTER THE CONDUCTIVITY, FREQUENCY, AND RELATIVE DIELECTRIC
CONSTANT 1.,100,1.

ENTER THE DEPTH OF DOWNWARD CONTINUATION 20

ENTER THE NO. OF THE FFT POINTS 64

INPUT THE OUTPUT FILE NO. 11

THE OUTPUT FILE IS STRUCTURED FOR THE PLOTTING PACKAGE
IN DEC-10 AFTER EX PLOT.FOR. IF THE OUTPUT IS PROFILE
R LBY:GRAPH. IF THE OUTPUT IS CONTOUR, DO FOLLOWING
STEPS: R MNL:KGRID, R MNL:FIT, R MNL:TOPO.

END OF EXECUTION

.EX PLOT.FOR

ENTER THE NO. OF DATA POINTS NX,NY 21,21

ENTER THE FILE NO. OF SURFACE DATA. 11

ENTER SPACING DELX, DELY 50,50

IF MODELING DATA, ENTER XM AND D FOR CONTINUED DATA .. D

ENTER THE OUTPUT FILE NO. FOR PLOTTING PACKAGE 12

END OF EXECUTION

APPENDIX C - COMPUTER PROGRAM LISTINGS

CCCCCCCCCCCC

```

*****
      THIS IS A MODELING PROGRAM FOR THE EM
      RESPONSE OF MAGNETIC DIPOLES, LINE SOURCE
      AND TWO DIMENSIONAL SCATTERING OF EM WAVE
      DUE TO TUNNEL.
*****

      INIEGER TYPEM,TYPEP

*****
      SELECT THE TYPE OF MODELING
*****

10  *WRITE(4,10)
11  *FORMAT(1X,'TYPE OF MODELING: MAGNETIC DIPOLE,
12  *      LINE SOURCE, TUNNEL (1ST LETTER)')
20  *READ(4,20)TYPEM
21  *FORMAT(A5)
22  *WRITE(4,30)
30  *FORMAT(1X,'DIFFUSION OR PROPAGAATION (1ST LETTER)')
31  *READ(4,40)TYPEP
32  *FORMAT(A5)
33  *IF(TYPEM.EQ.M)GO TO 50
34  *IF(TYPEM.EQ.L)GO TO 60
35  *IF(TYPEM.EQ.T)GO TO 70
50  *CALL DIPOL(TYPEP)
51  *GO TO 30
60  *CALL LINEM(TYPEP)
61  *GO TO 30
70  *CALL TUNNE(TYPEP)
80  *CONTINUE

*****
      THE OUTPUT IS READY IN THE FORMAT OF INPUT
      FOR THE COMPUTER PROGRAM OF ANALYTIC CONTINUA-
      TION. IF YOU WANT PLOT THE MODELING DATA,
      EXECUTE PLOT.FOR.
*****

90  *WRITE(4,90)
91  *FORMAT(1X,'THE OUTPUT IS READY IN THE FORMAT OF
92  *      INPUT OF THE CONTINUATION PROGRAM
93  *      IF YOU WANT ANALYIIC CONTINUATION,
94  *      EXECUTE ACEF2.FOR. IF YOU WANT PLOT
95  *      THE MODELING DATA, EXECUTE PLOT.FOR.')
96  *STOP
97  *END

```

CCCCCCCC

CCCCCCCC
CCCC

```

SUBROUTINE DIPOL(TYPEP)
*****
SUBROUTINE DIPOL IS DESIGNED FOR THE EM RESPON-
SE OF A MAGNETIC DIPOLE. THE OUTPUT IS PRE-
PARED IN THE ORDER OF HZ, HY, HX, WHICH IS THE
ORDER OF INPUT DATA IN THE PROGRAM FOR ANALYTIC
CONTINUATION.
*****

COMPLEX HX(128,128),HY(128,128),HZ(128,128)
COMPLEX CI,XK,CEX,CEX1,CEX2
INTEGER TYPEP
DIMENSION X(128),Y(128)

*****
INPUT THE PARAMETERS OF GRID AND DIPOLE
*****

WRITE(4,50)
50 FORMAT(1X,'ENTER THE COORDINATE OF STARTING POINT //
1 THE POINT IS AT THE LEFT TOP POSITION //
2 OF THE GRID //')
READ(4,*)DX,DY,DZ
WRITE(4,200)
200 FORMAT(1X,'ENTER THE HORIZONTAL AND VERTICAL LENGTH //
1 OF THE GRID //')
READ(4,*)XLEN,YLEN
WRITE(4,300)
300 FORMAT(2X,'ENTER THE HORIZONTAL AND VERTICAL SPACING //
1 OF THE GRID //')
READ(4,*)DELA,DELY
WRITE(4,500)
500 FORMAT(2X,'ENTER MOMENT, CONDUCTIVITY AND FREQUENCY')
READ(4,*)EMOM,SIG,OME
PAI=3.141592
AMU=4.*PAI/10.**7
CI=(0.,1)
NDX=XLEN/DELA+1
NDY=YLEN/DELY+1
XK=CI*SIG*AMU*2.*PAI*OME
XK=CSQRT(XK)
DO 600 I=1,NDY
DO 600 J=1,NDX
X(J)=DELA*(J-1)+DX
Y(I)=DELY*(I-1)+DY
R=X(J)**2+Y(I)**2+DZ**2
R=SQRT(R)
CEX=CI*XK*R
CEX1=CEXP(CEX)
CEX2=XK**2*R**2

```

```

DENO=4.*PA1*R**5
HX(I,J)=FMOM*X(J)*DZ*CEX1*(3.-3.*CEX-CEX2)/DENO
HY(I,J)=FMOM*Y(I)*DZ*CEX1*(3.-3.*CEX-CEX2)/DENO
HZ(I,J)=FMOM*CEX1*(2.*DZ**2-2.*DZ**2*CEX-
&(1.-CEX-CEX2)*(X(J)**2+Y(I)**2))/DENO
600 CONTINUE
&WRITE(4,100)
100 FORMAT(2X,'ENTER THE TAPE NO. OF MODELING DATA')
&READ(4,*)IPTAPE
&DO 800 I=1,NDY
&WRITE(IPTAPE,*)(HZ(I,J),J=1,NDX)
&WRITE(IPTAPE,*)(HY(I,J),J=1,NDX)
&WRITE(IPTAPE,*)(HX(I,J),J=1,NDX)
800 CONTINUE
&WRITE(4,700)IPTAPE,NDX,NDY,DELX,DELY
700 FORMAT(2X,'FILE OF DATA  NX  NY DELX  DELY',/
&IX,I12,I4,14,F7.3,F7.3)
&RETURN
&END

```

C.C.C.C.C

```

SUBROUTINE LINEM(TYPEP)
*****
SUBROUTINE LINEM IS DESIGNED FOR THE EM RES-
PONSE OF 2-D LINE SOURCE.
*****
COMPLEX EY(100),HX(100),HZ(100)
COMPLEX CK,CUN,CI,CK0,CK1,B,ARG
INTEGER TYPEP
DIMENSION X(100)
WRITE(4,10)
10 FORMAT(1A,'ENTER THE FREQUENCY AND CONDUCTIVITY')
READ(4,*)HERZ,SIG
WRITE(4,20)
20 FORMAT(1A,'ENTER THE STARTING RECEIVER POSITION %/,
AND NO. OF MEASUREMENT
)
READ(4,*)STARTZ,STARTX,RINC,NM
WRITE(4,31)
31 FORMAT(1A,'ENTER THE MOMENT')
READ(4,*)RJ
PAI=3.141592
CI=(0.,1.)
AMU=4.*PAI/(10.**7)
UME=2.*PAI*HERZ
CK=CI*SIG*AMU*UME
CK=CSQRT(CK)
DO 30 I=1,NM
X(I)=STARTX-(I-1)*RINC
30 CONTINUE
DO 40 I=1,NM
R=SQRT(X(I)**2+STARTZ**2)
B=R*CK
BB=REAL(B)
CALL MODBES(BB,CK0,CK1)
EY(I)=-CI*RJ*UME*AMU*CK0/2./PAI
HX(I)=STARIZ*CK*RJ*CK1/2./PAI/R
HZ(I)=X(I)*CK*RJ*CK1/2./PAI/R
40 CONTINUE
WRITE(4,50)
50 FORMAT(1A,'ENTER THE OUTPUT FILE AND OUTPUT FOR PLOT')
READ(4,*)IOUT,IPOUT
WRITE(IOUT,*)(EY(I),I=1,NM)
WRITE(IOUT,*)(HX(I),I=1,NM)
DO 50 I=1,NM
ARG=EY(I)
EYM=SQRT(REAL(ARG)**2+AIMAG(ARG)**2)
X(I)=(I-1)*RINC
50 WRITE(IPOUT,*)X(I),EYM
RETURN
END

```

```
SUBROUTINE MODDES(B,K0,K1)
DOUBLE PRECISION B8,BV(8)
COMPLEX K0,K1
B8=B*1.414213562373095D0
CALL KELVIN(B8,8,BV)
K0=CMPLX(SNGL(BV(3)),SNGL(BV(4)))
K1=CMPLX(-SNGL(BV(8)),SNGL(BV(7)))
RETURN
END
```

```

SUBROUTINE KELVIN(X,M,B)
IMPLICIT DOUBLE PRECISION (A-H,O-Z)
DOUBLE PRECISION B(8),CN(8),SN(8)
DATA CN / .707106781186547500,0.00, -.70710678
*-1.00, -.707106781186547500,0.00, .707106781186547500,1.
*SN / .707106781186547500,-1.00, -.707106781186547500,0.
*-.707106781186547500,-1.00, -.707106781186547500,0.00/
DATA PI4/.785398163397443300/,R22/.707106781186547500/,
*E/1.00D-10/,
*PI1/.3183098861837907/
IF(M.LT.1.UR.M.GT.8.UR.X.LE.0.000)GO TO 9
IF(X.GE.3.JDJ)GO TO 8
X2=0.500*X
I1=-0.2500*X4
S1=T1
T2=0.000
T3=0.000
T4=0.000
T15=0.000
T26=0.000
T75=0.000
T86=0.000
IF(M.EQ.1)GO TO 100
T2=X2**2
S2=T2
IF(M.EQ.2) GO TO 100
T5=1.500
S5=T1*T5
IF(M.EQ.3) GO TO 100
T6=1.000
S6=T2
IF(M.EQ.4) GO TO 100
T3=-0.500*X2**3
S3=T3
T4=X2
S4=T4
IF(M.LE.5) GO TO 100
T7=-0.2500*X2**3
S7=2.000*T7*T5
T9=X2
S8=T8
100 IK=2.000
101 IK2=IK+IK
IK21=IK2-1.000
IK22=IK2-2.000
RK2=1.000/IK2
RK21=1.000/IK21
RK22=1.000/IK22
R1=-X4*(RK21*RK2)**2
T1=T1*R1
S1=S1+T1

```

```

IF(M.EQ.1) GO TO 200
A2=-X4*(RK22*RK21)**2
I2=T2*R2
S2=S2+T2
IF(M.EQ.2) GO TO 200
T5=T5+RK21+RK2
T15=T1*T5
S5=S5+T15
IF(M.EQ.3) GO TO 200
T6=T6+RK22+RK21
I20=T2*I0
S6=S6+T26
IF(M.EQ.4) GO TO 200
T3=T3*(-A4*(RK22*RK21)**2*RK2))
S3=S3+T3
T4=T4*(-X4*PK22**2*RK21/(TK2-3.000))
S4=S4+T4
IF(M.LE.0) GO TO 200
T7=T7*R1
T75=TK2*T7*T5
S7=S7+T75
T8=T8+R22
T80=TK21*T8*T6
S8=S8+T80
200 1K=TK+1.000
* IF(DABS(T1).GT.E.OR.DABS(T2).GT.E.OR.DABS(T15).GT.E.OR.
* DABS(I20).GT.E.OR.DABS(T3).GT.E.OR.DABS(T4).GT.E.OR.
* DABS(T75).GT.E.OR.DABS(T80).GT.E) GO TO 101
B(1)=1.000+S1
IF(M.EQ.1) GO TO 9
B(2)=S2
IF(M.EQ.2) GO TO 9
C=0.115931515658412400-DLOG(X)
B(3)=C*B(1)+PI4*B(2)+S5
IF(M.EQ.3) GO TO 9
B(4)=C*B(2)-PI4*B(1)+S6
IF(M.EQ.4) GO TO 9
B(5)=R22*(S3-S4)
IF(M.EQ.5) GO TO 9
B(6)=R22*(S3+S4)
IF(M.EQ.6) GO TO 9
S7=C*S3-B(1)/X+PI4*S4+S7
S8=C*S4-B(2)/X-PI4*S3+S8
B(7)=R22*(S7-S8)
IF(M.EQ.7) GO TO 9
B(8)=R22*(S7+S8)
RETURN
END
NU=0
A2=P22*X
X8=B.000*X
SX=DSQRT(X)

```

```

EX2=EXP(SNGL(-X2))
C1=1.253314137315500D0*EX2/SX
C2=1.0D0/(2.506628274631001D0*SX*EX2+1.0D-38)
MAXK=30
IF(X.LT.15.0D0) MAXK=X+X
1 XNU=NU
XMU=4.0D0*XNU
ALP=X2+PI4*(XNU+XNU-0.5D0)
BETA=ALP+PI4
CB=DCOS(BETA)
CA=DCOS(ALP)
SB=DSIN(BETA)
SA=DSIN(ALP)
N4=4*NU
FM=0.0D0
FP=0.0D0
GM=0.0D0
GP=0.0D0
TM=1.0D0
TP=1.0D0
K=1
2 TK=K
T=(XMU-(TK+TK-1.0D0)**2)/(TK*X5)
TPL=DABS(TP)
TP=-TP*T
IF(DABS(TP).GT.TPL) GO TO 21
TM=TM*T
N=MOD(K,8)
IF(N.EQ.0) N=8
T1=TP*CN(N)
FP=FP+T1
T2=TM*CN(N)
FM=FM+T2
T3=TP*SN(N)
GP=GP+T3
T4=TM*SN(N)
GM=GM+T4
K=K+1
IF(K.GT.MAXK) GO TO 3
GO TO 2
21 FP=FP-T1
FM=FM-T2
GP=GP-T3
GM=GM-T4
3 FP=FP+1.0D0
FM=FM+1.0D0
B(N4+4)=C1*(-FM*SB-GM*CB)
B(N4+3)=C1*(FM*CB-GM*SB)
B(N4+2)=C2*(FP*SA-GP*CA)+PI1*B(N4+3)
B(N4+1)=C2*(FP*CA+GP*SA)-PI1*B(N4+4)
IF(NU.EQ.1.0D0) GO TO 9

```

```
NU=1  
GO TO 1  
END
```

CCCCCCCC

SUBROUTINE TUNNE(TYPEP)

```

*****
SUBROUTINE TUNNE IS DESIGNED TO CALCULATE THE
EM RESPONSE OF A TUNNEL DUE TO A LINE SOURCE.
THE OUTPUT IS PREPARED IN THE ORDER OF ELECTRIC
FIELD AND HORIZONTAL MAGNETIC FIELD IN THE
DIRECTION OF LINE SOURCE.
*****
COMPLEX HANOS,HANOR,HANOA,IEZ,IHR,THF,HANORD,HANJD,HANMRD
COMPLEX EZ(100),HX(100),HY(100),CI
COMPLEX HRD(100),HFI(100)
COMPLEX HANO,HAND,HANMS,HANMR,HANMA,HANMAD,CONM,CMPLX
INTEGER TYPEP
DIMENSION CYR(100),RHOR(100),FAIR(100),BS1(4),BS2(4)
DIMENSION BS3(1000),BS4(1000),BS5(1000),BS6(1000),FAI(100)
DIMENSION BS7(1000),BS8(1000),BS9(1000),FAID(100),WK(1000)
PAI=3.141592
WRITE(4,10)
10 FORMAT(1X,'ENTER THE FREQUENCY')
READ(4,*)HERIZ
WRITE(4,20)
20 FORMAT(1X,'ENTER THE TUNNEL RADIUS')
READ(4,*)AA
WRITE(4,30)
30 FORMAT(1X,'ENTER THE DIELECTRIC CONST(RELATIVE)')
READ(4,*)RDE
WRITE(4,50)
50 FORMAT(1X,'ENTER THE OUTPUT FILE NO,AND OUTPUT FOR PLOT')
READ(4,*)OUT,IOUT
WRITE(4,60)
60 FORMAT(1X,'ENTER THE SOURCE COORDINATE(X,Y)')
READ(4,*)CX,CY
WRITE(4,70)
70 FORMAT(1X,'ENTER THE STARTING RECEIVER POSITION AND
&INTERVAL X,Y,DELX AND NP
READ(4,*)CAR,CYRR,DELNP,NP
WRITE(4,80)
80 FORMAT(1X,'ENTER THE NUMBER OF SUMMATION')
READ(4,*)MAXM
OME=2.*PAI*HERTZ
SIG=0.0
CI=(0.,1.)
EPC=3.854/10.**12
EPI=RDE*EPJ
AMU=4.*PAI/10.**7
CKOUT=SQRT(OME**2*XMU*EPI)
CKIN=SQRT(OME**2*XMU*EPC)
AIC=1.
DO 100 I=1,NP
CYR(I)=CYRR-(I-1)*DELNP

```

```

      RHOR(I)=SQRT(CXR**2+CYR(I)**2)
      FAIR(I)=ATAN2(CYR(I),CXR)
100 CONTINUE
      RHUS=SQRT(CXS**2+CYS**2)
      FAIS=ATAN2(CYS,CXS)
C   COMPUTE FIELD AT EACH RECEIVER POINT
      DO 1000 I=1,NP
      DELFAI=FAIR(I)-FAIS
      DMAG=RHOS**2+RHOR(I)**2-2.*RHOS*RHOR(I)*COS(DELFAI)
      DMAG=SQRT(DMAG)
      CON=-CKOUT**2*XI/(4.*OME*PI)
C   ARGUMENTS
      ARG1=CKOUT*DMAG
      ARG2=CKOUT*RHOS
      ARG3=CKOUT*RHOR(I)
      ARG4=CKOUT*AA
      ARG5=CKIN*AA
C   CALL IMSL
      CALL MMB SJR(ARG1,0,2,BS1,*K,IER1)
      CALL MMB SYN(ARG1,0,2,BS2,IER2)
      CALL MMB SJR(ARG2,0,MAXM,BS3,*K,IER3)
      CALL MMB SYN(ARG2,0,MAXM,BS4,IER4)
      CALL MMB SJR(ARG3,0,MAXM,BS5,*K,IER5)
      CALL MMB SYN(ARG3,0,MAXM,BS6,IER6)
      CALL MMB SJR(ARG4,0,MAXM,BS7,*K,IER7)
      CALL MMB SYN(ARG4,0,MAXM,BS8,IER8)
      CALL MMB SJR(ARG5,0,MAXM,BS9,*K,IER9)
      WRITE(10,*)IER1,IER2,IER3,IER4,IER5,IER6,IER7,IER8,IER9
C   COMPUTE THE FIRST TERM
      HR1=-BS2(1)
      HANO=CMPLX(BS1(1),HR1)
      HR2=-BS2(3)
      HANB=CMPLX(BS1(3),HR2)
      HR3=-BS4(1)
      HANOS=CMPLX(BS3(1),HR3)
      HR4=-BS6(1)
      HANOR=CMPLX(BS5(1),HR4)
      HR5=-BS8(1)
      HANOA=CMPLX(BS7(1),HR5)
      HR6=-BS6(3)
      HANORD=CMPLX(BS5(3),HR6)
      BS9D=-BS7(3)
      BS7D=-BS7(3)
      HR7=-BS8(3)
      HANOD=CMPLX(BS7(3),HR7)
      ZE=X4U*BS9(1)*CKOUT/CKIN/BS9D
      TEZ=HANOS*HANOR*(BS7(1)-ZE*BS7D)/(HANOA-ZE*HANOD)
      IHR=(0.,0.)
      IHF=HANOS*HANORD*CKOUT*(BS7(1)-ZE*BS7D)/(HANOA-ZE*HANOD)
C   SUM UPTO M=MAXM-1
      MAXM1=MAXM-2

```

```

DO 500 M=2,MAXM1
HR8=-BS4(M+M-1)
HANMS=CMPLX(BS3(M+M-1),HR8)
HR9=-BS6(M+M-1)
HANMR=CMPLX(BS5(M+M-1),HR9)
HR10=-BS8(M+M-1)
HANMA=CMPLX(BS7(M+M-1),HR10)
HR11=-BS9(M+M+1)
HR12=-BS9(M+M+1)
HANMRD=CMPLX(BS5(M+M+1),HR11)+(M-1)*HANMR/ARG3
HANMAD=CMPLX(BS7(M+M+1),HR12)+(M-1)*HANMA/ARG4
BS9D=-BS9(M+M+1)+(M-1)*BS9(M+M-1)/ARG5
BS7D=-BS7(M+M+1)+(M-1)*BS7(M+M-1)/ARG4
ZE=XMU*BS9(M+M-1)*CKOUT/(CKIN*BS9D)
CONM=(BS7(M+M-1)-ZE*BS7D)/(HANMA-ZE*HANMAD)
FAI(I)=(M-1)*(FAIS-FAIR(I))
AEZ=TEZ+2.*COS(FAI(I))*HANMS*HANMR*CONM
THR=THR+2.*(M-1)*SIN(FAI(I))*HANMS*HANMR*CONM
HF=HF+2.*COS(FAI(I))*HANMS*HANMRD*CKOUT*CONM
500 CONTINUE
FAID(I)=FAIS-FAIR(I)
EZ(I)=CON*(HANU-TEZ)
RHO(I)=-1./((CI*OME*XMU*RHOR(I))*CON*(HAND*CKOUT*(-2.))*
$RHOS*RHOR(I)*SIN(FAID(I)))/(2.*UMAG)-THR)
HF1(I)=1./((CI*OME*XMU)*CON*(HAND*(2.*RHOR(I)-
&2.*RHOS*COS(FAID(I)))/(2.*UMAG)-HF)
RX(I)=HRU(I)*COS(FAIR(I))-HF1(I)*SIN(FAIR(I))
HY(I)=HRU(I)*SIN(FAIR(I))+HF1(I)*COS(FAIR(I))
1000 CONTINUE
DO 1010 I=1,NP
1010 CYR(I)=(I-1)*DELNP
DO 3000 I=1,NP
*WRITE(OUT,*) CYR(I),EZ(I)
3000 CONTINUE
DO 4000 I=1,NP
*WRITE(OUT,*) CYR(I),HY(I)
4000 CONTINUE
DO 5000 I=1,NP
REEZ=REAL(EZ(I))
AIEZ=AIMAG(EZ(I))
EEZ=SQRT(REEZ**2+AIEZ**2)
CYR(I)=(I-1)*DELNP
*WRITE(OUT,*)CYR(I),EEZ
5000 CONTINUE
RETURN
END

```

C


```

C
C
C
SUBROUTINE DOWPD(TYPEF)
*****
SUBROUTINE DOWPD IS DESIGNED TO CALCULATE THE
TWO DIMENSIONAL ANALYTIC CONTINUATION FOR TE
MODE EM WAVE.
*****
DOUBLE PRECISION EPS0, EPS1
INTEGER TYPE, I, Q, V, N, OK, R, TYPEF
COMPLEX EZ(64), HCOS, HSIN, SEEZ
COMPLEX HX(64), CI, CON(64), CQ(64)
DIMENSION WCRK(20000), X(64)
DIMENSION AKX(64), AKY(64), REEZ(64), AIEZ(64)
DATA NN/64/
DATA I/'I', Q/'Q', Y/'Y', N/'N', R/'R'/
1 WRITE(4,301)
801 FORMAT(2X, 'INPUT THE FILE NO. OF SURFACE DATA')
READ(4,*) IFILE
REWIND IFILE
WRITE(4,302)
802 FORMAT(2X, 'ENTER THE NO. OF SURFACE DATA POINTS NX')
READ(4,*) NX
WRITE(4,303)
803 FORMAT(2X, 'ENTER THE SPACING OF RECEIVER DELX')
READ(4,*) DELX
WRITE(4,99)
99 1 FORMAT(2X, 'ENTER THE CONDUCTIVITY, FREQUENCY, AND
RELATIVE DIELECTRIC CONSTANT')
IF (TYPEF.EQ.D) RDE=0.0
READ(4,*) SIG, OME, RDE
WRITE(4,304)
804 FORMAT(2X, 'ENTER THE DEPTH OF DOWNWARD CONTINUATION')
READ(4,*) DEP
WRITE(4,305)
805 FORMAT(2X, 'ENTER THE NO. OF FFT POINTS')
READ(4,*) NFFT
CI=(0.,1.)
PAI=3.141592
XMU=4.*PAI/10.**7
EPS0=8.854/(10.**12)
EPS1=RDE*EPS0
CK=(2.*PAI*CKE)**2*XMU*EPS1
NX1=NX+1
NXN=NFFT/2+1
NXN1=NXN+1
DO 41 I=1, NX
41 READ(IFILE,*) S, EZ(I)
DO 42 I=1, NX
42 READ(IFILE,*) S, HX(I)
DO 50 I=1, NX
50 A(I)=(I-1)*DELX
DO 200 I=NX1, NFFT

```

```

EZ(I)=(0.,0.)
HX(I)=(0.,0.)
200 CONTINUE
CALL FOURT(HX,MN,1,-1,1,WORK)
CALL FOURT(EZ,MN,1,-1,1,WORK)
DELKA=2.*PAI/NFFT/DELX
DO 10 J=1,NXN
AKX(J)=(J-1)*DELKX
10 CONTINUE
DO 30 J=NXN1,NFFT
AKA(J)=(NFFT-J+1)*DELKX
30 CONTINUE
DO 600 J=1,NFFT
CQ(J)=AKX(J)**2-CK
600 CONTINUE
DO 700 I=1,NFFI
CUN(I)=DEP*CSQRT(CQ(I))
700 CONTINUE
AKA(NXN)=0.0
DO 100 I=1,NFFI
HCUS=(CEXP(CUN(I))+CEXP(-CUN(I)))/2.
HSIN=(CEXP(CUN(I))-CEXP(-CUN(I)))/2.
EZ(I)=EZ(I)*HCUS-CI*(2.*PAI*JME*XMU
**HA(I))*HSIN
*/CSQRT(CUN(I))
790 CONTINUE
100 CONTINUE
CALL FOURT(EZ,MN,1,1,1,WORK)
DO 850 I=1,NFFI
EZ(I)=EZ(I)/NFFT
850 WRITE(4,904)
904 FORMAT(2X,'INPUT THE OUTPUT FILE NO. FOR PLOT')
READ(4,*)IOUT
DO 960 I=1,NA
EEEZ=EZ(I)
960 REEZ(I)=SQRT(REAL(EEEZ)**2+AIMAG(EEEZ)**2)
DO 1000 I=1,NX
WRITE(IOUT,*)X(I),REEZ(I)
1000 CONTINUE
RETURN
END

```

T-2987

```

WRITE(4,105)
FORMAT(2X,'ENTER THE NO. OF FFT POINTS')
READ(4,*)NFFT
CI=(0.,1.)
PAI=3.141592
AMU=4.*PAI/10.**7

```

CCCCC

```

SUBROUTINE DOWCD(TYPEF)
*****
SUBROUTINE DOWCD IS DESIGNED TO CALCULATE THE
THREE DIMENSIONAL ANALYTIC CONTINUATION.
*****
INTEGER TYPE,I,Q,Y,N,OK,R,TYPEF
COMPLEX HZ(64,64)
COMPLEX HY(64,64),HSIN,HCOS
COMPLEX HX(64,64),HSIN,HCOS
COMPLEX HZ(64,64),HSIN,HCOS
COMPLEX HY(64,64),HSIN,HCOS
COMPLEX HX(64,64),HSIN,HCOS
DIMENSION WORK(2000),NN(2),X(64)
DIMENSION AKX(64),AKY(64),REHZ(64,64),AIHZ(64,64)
101 FORMAT(2X,'INPUT THE FILE NO. OF SURFACE DATA')
READ(4,*)IFILE
WRITE(4,102)
102 FORMAT(2X,'ENTER THE NO. OF SURFACE DATA POINTS NX,NY')
READ(4,*)NX,NY
WRITE(4,103)
103 FORMAT(2X,'ENTER THE SPACING OF RECEIVER DELX,DELY')
READ(4,*)DELA,DELY
99 104 FORMAT(2X,'ENTER THE CONDUCTIVITY, FREQUENCY, AND
RELATIVE DIELECTRIC CONSTANT')
IF(TYPEF.EQ.D)KEEPS=0.0
READ(4,*)SIG,OME,KEEPS
WRITE(4,104)
104 FORMAT(2X,'ENTER THE DEPTH OF DOWNWARD CONTINUATION')
READ(4,*)DZF
WRITE(4,105)
105 FORMAT(2X,'ENTER THE NO. OF FFT POINTS')
READ(4,*)NFFT
CI=(0.,1.)
PAI=3.141592
AMU=4.*PAI/10.**7
EPC=8.854/(10.E12)
EPS=KEEPS*EPC
CK=CI*SIG*AMU*2.*PAI*OME+(2.*PAI*OME)**2*XMU*EPS
NX1=NX+1
NY1=NY+1
NXN=NFFT/2+1
NYN=NFFT/2+1
NXN1=NXN+1
NYN1=NYN+1
50 LC 50 I=1,NY
^ (1)=(1-1)*DELA
LO 100 I=1,NY

```

```

      READ(IFILE,*) (HZ(I,J),J=1,NX)
      READ(IFILE,*) (HY(I,J),J=1,NX)
      READ(IFILE,*) (HX(I,J),J=1,NX)
100  CONTINUE
      DO 200 I=NY1,NFFT
      DO 200 J=NX1,NFFT
      HZ(I,J)=(0.,0.)
      HY(I,J)=(0.,0.)
      HX(I,J)=(0.,0.)
200  CONTINUE
      CALL FOURRT(HX,NN,2,-1,1,WORK)
      CALL FOURRT(HY,NN,2,-1,1,WORK)
      CALL FOURRT(HZ,NN,2,-1,1,WORK)
      DELKX=2.*PAI/NFFT/DELY
      DELKY=2.*PAI/NFFT/DELY
      DO 10 J=1,NXN
      AKX(J)=(J-1)*DELKX
10  CONTINUE
      DO 20 J=NXN1,NFFT
      AKX(J)=(NFFT-J+1)*DELKX
20  CONTINUE
      DO 30 I=1,NYN
      AKY(I)=(I-1)*DELKY
30  CONTINUE
      DO 40 I=NYN1,NFFT
      AKY(I)=(NFFT-I+1)*DELKY
40  CONTINUE
      DO 500 I=1,NFFT
      DO 500 J=1,NFFT
      CQ(I,J)=AKX(J)**2+AKY(I)**2-CK
600  CONTINUE
      DO 700 I=1,NFFT
      DO 700 J=1,NFFT
      CUN(I,J)=DEP*CSQRT(CQ(I,J))
700  CONTINUE
      AKX(NXN)=0.C
      AKY(NYN)=0.C
      DO 800 I=1,NFFI
      DO 800 J=1,NFFI
      IF(SIG.EQ.J.AND.I.EQ.1.AND.J.EQ.1) GO TO 790
      HCOS=(CEXP(CUN(I,J))+CEXP(-CUN(I,J)))/2.
      HSIN=(CEXP(CUN(I,J))-CEXP(-CUN(I,J)))/2.
      HZ(I,J)=HZ(I,J)*HCOS+CI*(AKX(J)
      *HA(I,J)+AKY(I)*HY(I,J))*HSIN
      *CSQRT(CQ(I,J))
790  CONTINUE
800  CONTINUE
      CALL FOURRT(HZ,NN,2,1,1,WORK)
      DO 850 I=1,NFFT
      DO 850 J=1,NFFT
850  HZ(I,J)=HZ(I,J)/NFFT/NFFT
      WRITE(4,904)

```

```
904 FORMAT(2X, 'INPUT THE OUTPUT FILE NO. FOR PLOT')
      READ(4,*)IOUT
      DO 1000 I=1,NY
      *WRITE(IOUT,*)(HZ(I,J),J=1,NX)
1000 CONTINUE
      RETURN
      END
```

CCC

```

SUBROUTINE FLURT(DATA,NN,NDIM,ISIGN,IFORM,WORK)
C
  DIMENSION DATA(1),NN(1),IFACT(32),WORK(1)
  DATA TWGPI/6.25318530717967/,RTHLF/0.70710678118655/
  NP1=0
  NP2=0
  IF(NDIM-1)1190,10,10
  10  NTOT=2
     DO 20 IDIM=1,NDIM
  20  IF(NN(IDIM))1190,1190,20
     NTOT=NTOT*NN(IDIM)
     NP1=2
C
C   MAIN LOOP FOR EACH DIMENSION
C
  DO 1180 IDIM=1,NDIM
  N=NN(IDIM)
  NP2=NP1*N
  IF(N-1)1190,1170,30
C
C   IS N A POWER OF TWO AND IF NOT, WHAT ARE ITS FACTORS
C
  30  M=N
     NTWO=NP1
     IF=1
     IDIV=2
  40  IQUOT=M/IDIV
     IREM=M-IDIV*IQUOT
     IF(IQUOT-IDIV)120,50,50
  50  IF(IREM)70,60,70
  60  NTWO=NTWO+NTWO
     IFACT(IF)=IDIV
     IF=IF+1
     M=IQUOT
     GO TO 40
  70  IDIV=3
     INJN2=IF
  80  IQUOT=M/IDIV
     IREM=M-IDIV*IQUOT
     IF(IQUOT-IDIV)140,90,90
  90  IF(IREM)110,100,110
  100 IFACT(IF)=IDIV
     IF=IF+1
     M=IQUOT
     GO TO 90
  110 IDIV=IDIV+2
     GO TO 80
  120 INJN2=IF
     IF(IREM)140,130,140
  130 NTWO=NTWO+NTWO
     GO TO 150

```

```

140  IF ACT(IF)=4
      SEPARATE FOUR CASES--
      1. COMPLEX TRANSFORM OR REAL TRANSFORM FOR THE 4TH,
          DIMENSIONS.
      2. REAL TRANSFORM FOR THE 2ND OR 3RD DIMENSION.
          TRANSFORM HALF THE DATA, SUPPLYING THE OTHER
          JUGATE SYMMETRY.
      3. REAL TRANSFORM FOR THE 1ST DIMENSION, N ODD.
          SET THE IMAGINARY PARTS TO ZERO.
      4. REAL TRANSFORM FOR THE 1ST DIMENSION, N EVEN.
          TRANSFORM A COMPLEX ARRAY OF LENGTH N/2 WHOSE
          ARE THE EVEN NUMBERED REAL VALUES AND WHOSE
          ARE THE ODD NUMBERED REAL VALUES. SEPARATE
          THE SECOND HALF BY CONJUGATE SYMMETRY.

150  ICASE=1
      IFMIN=1
      IIRNG=NP1
160  IF (IDIM-1) 160, 210, 210
170  IF (IFORM) 170, 170, 210
      ICASE=2
      IIRNG=NP0*(1+NPREV/2)
180  IF (IDIM-1) 180, 180, 210
      ICASE=3
      IIRNG=NP1
190  IF (NTWO-NP1) 190, 210, 190
      ICASE=4
      IFMIN=2
      NTWO=NTWO/2
      N=N/2
      NP2=NP2/2
      NTOT=NTOT/2
      I=1
      DO 200 J=1, NTOT
      DATA(J)=DATA(I)
200  I=I+2
      SHUFFLE DATA BY BIT REVERSAL, SINCE N=2**K. AS THE
      CAN BE DONE BY SIMPLE INTERCHANGE, NO WORKING ARRAY

210  IF (NTWO-NP2) 210, 220, 220
220  NP2HF=NP2/2
      J=1
      DO 230 I2=1, NP2, NP1
      IF (J-I2) 230, 250, 250
230  I1MAX=I2+NP1-2
      DO 240 I1=12, I1MAX, 2
      DO 240 I3=11, NTOT, NP2
      J3=J+I3-I2
      IEMPR=DATA(I3)

```

```

TEMP1=DATA(I3+1)
DATA(I3)=DATA(J3)
DATA(I3+1)=DATA(J3+1)
DATA(J3)=TEMP1
240 DATA(J3+1)=TEMP1
250 M=NP2/HP
260 IF(J-M) 230,250,270
270 J=J-M
M=M/2
280 IF(M-NP1) 230,250,260
J=J+M
GO TO 370

C
C SHUFFLE DATA BY DIGIT REVERSAL FOR GENERAL N
C
290 NWORK=2*N
DO 360 I1=1, NP1, 2
DO 360 I3=I1, N/OT, NP2
J=I3
DO 350 I=1, NWORK, 2
300 IF(ICASE-3) 300, 310, 300
WORK(I)=DATA(J)
WORK(I+1)=DATA(J+1)
GO TO 320
310 WORK(I)=DATA(J)
WORK(I+1)=J.
320 IFP2=NP2
IF=IFMIN
330 IFP1=IFP2/IFACT(IF)
J=J+IFP1
340 IF(J-I3-IFP2) 350, 340, 340
J=J-IFP2
IFP2=IFP1
IF=IF+1
350 IF(IFP2-NP1) 350, 350, 330
CONTINUE
I2MAX=I3+NP2-NP1
I=1
DO 360 I2=I3, I2MAX, NP1
DATA(I2)=WORK(I)
DATA(I2+1)=WORK(I+1)
360 I=I+2

C
C MAIN LOOP FOR FACTORS OF TWO. PERFORM FLURIER TRANSFORMS
C LENGTH FOUR, WITH ONE OF LENGTH TWO IF NEEDED.
C W=EXP(ISIGN*2*PI*SQRT(-1)*M/(4*MMAX)). CHECK FOR
C AND REPEAT FOR W=W*(1+ISIGN*SQRT(-1))/SQRT(2).
C
370 IF(NTWO-NP1) 680, 680, 380
380 NP1TW=NP1+NP1
IPAP=NTWO/NP1

```

```

390  IF(IPAR-2)430,410,400
400  IPAR=IPAR/4
      GO TO 390
410  DO 420 I1=1,IIRNG,2
      DO 420 K1=I1,NTOT,NP1TW
      K2=K1+NP1
      TEMPR=DATA(K2)
      TEMPI=DATA(K2+1)
      DATA(K2)=DATA(K1)-TEMPR
      DATA(K2+1)=DATA(K1+1)-TEMPI
420  DATA(K1)=DATA(K1)+TEMPR
430  DATA(K1+1)=DATA(K1+1)+TEMPI
440  MMAX=NP1
450  IF(MMAX-NTW0/2)450,680,680
      LMAX=MAX0(NP1TW,MMAX/2)
      DO 670 L=NP1,LMAX,NP1TW
      M=L
      L=LMAX-1,LMAX,0,500,460
      M=L
      IF(MMAX-NP1)500,500,460
460  THETA=-TWOPI*FLOAT(L)/F
      IF(ISIGN)480,470,470
470  THETA=-THETA
480  WR=COS(THETA)
      *2I=2.*NR*WI
      *3R=*2R*NR-W2I*WI
      *3I=*2R*WI+W2I*WR
500  DO 630 I1=1,IIRNG,2
      KMIN=I1+IPAR*M
      IF(MMAX-NP1)510,510,520
510  KMIN=I1
520  KDIF=IPAR*MMAX
530  KSTEP=4*KDIF
      IF(KSTEP-NTW0)540,540,630
540  DO 620 K1=KMIN,NTOT,KSTEP
      K2=K1+KDIF
      K3=K2+KDIF
      K4=K3+KDIF
      IF(MMAX-NP1)550,550,580
550  U1R=DATA(K1)+DATA(K2)
      U1I=DATA(K1+1)+DATA(K2+1)
      U2R=DATA(K3)+DATA(K4)
      U2I=DATA(K3+1)+DATA(K4+1)
      U3R=DATA(K1)-DATA(K2)
      U3I=DATA(K1+1)-DATA(K2+1)
560  U4R=DATA(K3+1)-DATA(K4+1)
      U4I=DATA(K4)-DATA(K3)
      GO TO 510
570  U4R=DATA(K4+1)-DATA(K3+1)
      U4I=DATA(K3)-DATA(K4)

```



```

C
680 IF (NTWO-NP2) 690, 900, 900
690 IFP1=NTWO
    IF=INON2
    NP1HF=NP1/2
700 IFP2=IFACT(IF)*IFP1
    J1MIN=NP1+1
    IF (J1MIN-IFP1) 710, 710, 760
710 DO 750 J1=J1MIN, IFP1, NP1
    THETA=-TWOPI*FLOAT(J1-1)/FLOAT(IFP2)
    IF (ISIGN) 730, 720, 720
720 THETA=-THETA
730 *SIPR=COS(THETA)
    *SIP1=SIN(THETA)
    WR=WSTPR
    WI=WSTPI
    J2MIN=J1+IFP1
    J2MAX=J1+IFP2-IFP1
    DO 750 J2=J2MIN, J2MAX, IFP1
    I1MAX=J2+I1RNG-2
    DO 740 I1=J2, I1MAX, 2
    DO 740 J3=I1, NTOT, IFP2
    TEMPR=DATA(J3)
740 DATA(J3)=DATA(J3)*WR-DATA(J3+1)*WI
    DATA(J3+1)=TEMPR*WI+DATA(J3+1)*WR
    TEMPR=WR
    WR=WR*WSTPR-WI*WSTPI
750 WI=TEMPR*WSTPI+WI*WSTPR
760 THETA=-TWOPI/FLOAT(IFACT(IF))
    IF (ISIGN) 730, 770, 770
770 THETA=-THETA
780 *SIPR=COS(THETA)
    *SIP1=SIN(THETA)
    J2RNG=IFP1*(1+IFACT(IF)/2)
    DO 890 I1=1, I1RNG, 2
    DO 890 I3=I1, NTOT, NP2
    J2MAX=I3+J2RNG-IFP1
    DO 880 J2=I3, J2MAX, IFP1
    J1MAX=J2+IFP1-NP1
    DO 850 J1=J2, J1MAX, NP1
    J3MAX=J1+NP2-IFP2
    DO 850 J3=J1, J3MAX, IFP2
    JMIN=J3-J2+I3
    JMAX=JMIN+IFP2-IFP1
    I=1+(J3-I3)/NP1HF
    IF (J2-I3) 790, 790, 820
790 SUMR=0.
    SUMI=0.
    DO 810 J=JMIN, JMAX, IFP1
800 SUMR=SUMR+DATA(J)
810 SUMI=SUMI+DATA(J+1)

```

```

      WCRK(I)=SUMR
      WCRK(I+1)=SUMI
      GO TO 850
820  ICONJ=1+(IFP2-2*J2+I3+J3)/NP1HF
      J=JAMX
      SUMR=DATA(J)
      SUMI=DATA(J+1)
      ULDSR=0.
      ULDSI=0.
      J=J-IFP1
830  TEMPR=SUMR
      TEMPI=SUMI
      SUMR=TWCNR*SUMR-ULDSR+DATA(J)
      SUMI=TWCNR*SUMI-ULDSI+DATA(J+1)
      ULDSR=TEMPR
      ULDSI=TEMPI
      J=J-IFP1
      IF(J-JMIN)340,340,830
840  TEMPR=WR*SUMR-ULDSR+DATA(J)
      TEMPI=WI*SUMI
      WCRK(I)=TEMPR-TEMPI
      WCRK(ICONJ)=TEMPR+TEMPI
      TEMPR=WR*SUMI-ULDSI+DATA(J+1)
      TEMPI=WI*SUMR
      WCRK(I+1)=TEMPR+TEMPI
      WCRK(ICONJ+1)=TEMPR-TEMPI
850  CONTINUE
      IF(J2-I3)860,860,870
860  WR=WSTPR
      WI=WSTPI
      GO TO 880
870  TEMPR=WR
      WR=WR*WSTPR-WI*WSTPI
      WI=TEMPR*WSTPI+WI*WSTPR
880  TWCNR=WR+NR
      I=1
      I2MAX=I3+NP2-NP1
      DO 890 I2=I3,I2MAX,NP1
      DATA(I2)=WCRK(I)
      DATA(I2+1)=WCRK(I+1)
890  I=I+2
      IF=IF+1
      IFP1=IFP2
      IF(IFP1-NP2)700,900,900
CCC
      COMPLETE A REAL TRANSFORM IN THE 1ST DIMENSION, N EVEN,
      JUGATE SYMMETRIES.
900  GO TO (1170,1090,1170,910),ICASE
910  NHALF=N
      N=N+N

```

```

      THETA=-T*UPI/FLOAT(N)
      IF (ISIGN) 930, 920, 920
920  THETA=-THETA
930  *SIPR=COS(THETA)
      *SIPI=SIN(THETA)
      *R=WSTPR
      *I=WSTPI
      IMIN=3
      JMIN=2*NHALF-1
      GO TO 960
940  J=JMIN
      DO 950 I=IMIN, NTOT, NP2
      SUMR=(DATA(I)+DATA(J))/2.
      SUMI=(DATA(I+1)+DATA(J+1))/2.
      DIFR=(DATA(I)-DATA(J))/2.
      DIFI=(DATA(I+1)-DATA(J+1))/2.
      TEMPR=*R*SUMI+*I*DIFR
      TEMPI=*I*SUMI-*R*DIFR
      DATA(I)=SUMR+TEMPR
      DATA(I+1)=DIFI+TEMPI
      DATA(J)=SUMR-TEMPR
      DATA(J+1)=-DIFI+TEMPI
950  J=J+NP2
      IMIN=IMIN+2
      JMIN=JMIN-2
      TEMPR=*R
      *R=*R*WSTPR-*I*WSTPI
      *I=TEMPR*WSTPI+*I*WSTPR
960  IF (IMIN-JMIN) 940, 970, 1000
970  IF (ISIGN) 980, 1000, 1000
980  DO 990 I=IMIN, NTOT, NP2
990  DATA(I+1)=-DATA(I+1)
1000 NP2=NP2+NP2
      NTOT=NTOT+NTOT
      J=NTOT+1
      IMAX=NTOT/2+1
1010 IMIN=IMAX-2*NHALF
      I=IMIN
      GO TO 1030
1020 DATA(J)=DATA(I)
      DATA(J+1)=-DATA(I+1)
1030 I=I+2
      J=J-2
      IF (I-IMAX) 1040, 1040, 1040
1040 DATA(J)=DATA(IMIN)-DATA(IMIN+1)
      DATA(J+1)=0.
      IF (I-J) 1050, 1080, 1080
1050 DATA(J)=DATA(I)
      DATA(J+1)=DATA(I+1)
1060 I=I-2
      J=J-2

```

```

1070 IF (I-IMIN) 1070, 1070, 1050
      DATA(J)=DATA(IMIN)+DATA(IMIN+1)
      DATA(J+1)=0.
      IMAX=IMIN
      GO TO 1010
1080 DATA(1)=DATA(1)+DATA(2)
      DATA(2)=0.
      GO TO 1170

```

```

C
C COMPLETE A REAL TRANSFORM FOR THE 2ND OR 3RD DIMENSION BY
C CONJUGATE SYMMETRIES.

```

```

1090 IF (I1RNG-NP1) 1100, 1170, 1170
1100 DO 1160 I3=1, NPOT, NP2
      I2MAX=I3+NP2-NP1
      DO 1160 I2=I3, I2MAX, NP1
      IMIN=I2+I1RNG
      IMAX=I2+NP1-1
      JMAX=2*I3+NP1-IMIN
      IF (I2-I3) 1120, 1120, 1110
1110 JMAX=JMAX+NP2
1120 IF (IDIM-2) 1150, 1150, 1130
1130 J=JMAX+NP0
      DO 1140 I=IMIN, IMAX, 2
      DATA(I)=DATA(J)
      DATA(I+1)=-DATA(J+1)
1140 J=J-2
1150 J=JMAX
      DO 1160 I=IMIN, IMAX, NP0
      DATA(I)=DATA(J)
      DATA(I+1)=-DATA(J+1)
1160 J=J-NP0

```

```

C
C END OF LOOP ON EACH DIMENSION

```

```

1170 NP0=NP1
      NP1=NP2
1180 NPREV=N
1190 RETURN
      END

```

```

C
C *****
C PROGRAM PLOT.FOR IS DESIGNED FOR THE OUTPUT IN
C THE FORMAT OF PLOTTING PACKAGE. FOR THE PRO-
C FILE OUTPUT, RUN LBY:GRAPH. FOR THE CONTOUR
C DO FOLLOWING SEQUENCE: R MNL:KGRID, R MNL:FIT,
C R MNL:TJPC.
C *****

```

```

ANIEGER D, AM, TYPE
COMPLEX HZ(64, 64)

```

```

COMPLEX HY(64,64),HSIN,HCOS
COMPLEX HX(64,64)
DIMENSION X(64),Y(64)
DIMENSION AKX(64),AKY(64),REHZ(64,64),AIHZ(64,64)
DATA D/'D',AM/'AM',XM/'XM'
101 *WRITE(4,101)
    FORMAT(2X,'INPUT THE FILE NO. OF SURFACE DATA')
    READ(4,*)IFILE
    *IND IFILE
102 *WRITE(4,102)
    FORMAT(2X,'ENTER THE NO. OF SURFACE DATA POINTS NX,NY')
    READ(4,*)NX,NY
    *WRITE(4,998)
998 *FORMAT(2X,'ENTER DELX,DELY')
    READ(4,*)DELX,DELY
    *WRITE(4,999)
999 *FORMAT(2X,'IF MODEL DATA, ENTER XM AND D FOR DOWN DATA')
    READ(4,999)TYPE
103 *FORMAT(A4)
    DO 50 I=1,NY
    50 X(I)=(I-1)*DELX
    DO 100 I=1,NX
    READ(IFILE,*) (HZ(I,J),J=1,NY)
    IF (TYPE.EQ.D) GO TO 100
    READ(IFILE,*) (HY(I,J),J=1,NY)
    READ(IFILE,*) (HX(I,J),J=1,NY)
100 CONTINUE
993 CONTINUE
148 DO 901 I=1,NX
    DO 901 J=1,NY
    REHZ(I,J)=REAL(HZ(I,J))
    AIHZ(I,J)=AIMAG(HZ(I,J))
901 CONTINUE
    DO 775 I=1,NX
    775 Y(I)=(I-1)*DELY
    *WRITE(4,904)
904 *FORMAT(2X,'INPUT THE OUTPUT FILE NO. FOR PLOT')
    READ(4,*)IOUT
    DO 777 I=1,NX
    DO 777 J=1,NY
    WRITE(IOUT,*)X(J),Y(I),REHZ(I,J)
777 CONTINUE
STOP
END

```

C.C.C.C.C

```

*****
PROGRAM RANDOM IS DESIGNED TO GENERATE THE
PANDA WHITE NOISE.
*****

```

```

COMPLEX NOISE1(128,128),NOISE2(128,128),NOISE3(128,128)

```

```

IBIG=99999
*WRITE(4,100)
100 FORMAT(1X,'ENTER NX AND NY')
*READ(4,*)NX,NY
*WRITE(4,200)
200 FORMAT(1X,'ENTER OUTPUT FILE')
*READ(4,*)IOUT
*WRITE(4,300)
300 FORMAT(1X,'ENTER THE SIGNAL STRENGTH HZ HY HX')
*READ(4,*)AAA1,AAA2,AAA3
*WRITE(4,400)
400 FORMAT(1X,'ENTER THE SIGNAL TO NOISE RATIO')
*READ(4,*)SNR
DO 10 I=1,NX
DO 10 J=1,NY
NOISE1(I,J)=CMPLX(RAN(IBIG)-0.5,RAN(IBIG)-0.5)
NOISE2(I,J)=CMPLX(RAN(IBIG)-0.5,RAN(IBIG)-0.5)
NOISE3(I,J)=CMPLX(RAN(IBIG)-0.5,RAN(IBIG)-0.5)
10 CONTINUE
AA1=0.
AA2=0.
AA3=0.
DO 30 I=1,NX
DO 30 J=1,NY
A1=REAL(NOISE1(I,J))**2+AIMAG(NOISE1(I,J))**2
A2=REAL(NOISE2(I,J))**2+AIMAG(NOISE2(I,J))**2
A3=REAL(NOISE3(I,J))**2+AIMAG(NOISE3(I,J))**2
AA1=A1+AA1
AA2=A2+AA2
AA3=A3+AA3
30 CONTINUE
REC1=AAA1/SNR/AA1
REC2=AAA2/SNR/AA2
REC3=AAA3/SNR/AA3
DO 101 I=1,NX
DO 101 J=1,NY
NOISE1(I,J)=NOISE1(I,J)*SQRT(REC1)
NOISE2(I,J)=NOISE2(I,J)*SQRT(REC2)
NOISE3(I,J)=NOISE3(I,J)*SQRT(REC3)
101 CONTINUE
DO 20 I=1,NX
*WRITE(IOUT,*)(NOISE1(I,J),J=1,NY)
*WRITE(IOUT,*)(NOISE2(I,J),J=1,NY)
*WRITE(IOUT,*)(NOISE3(I,J),J=1,NY)
20 CONTINUE
AA1=0.
AA2=0.
AA3=0.
DO 31 I=1,NX
DO 31 J=1,NY
A1=REAL(NOISE1(I,J))**2+AIMAG(NOISE1(I,J))**2

```

```
A2=REAL( NOISE2(I,J))**2+AIMAG( NOISE2(I,J))**2
A3=REAL( NOISE3(I,J))**2+AIMAG( NOISE3(I,J))**2
AA1=A1+AA1
AA2=A2+AA2
AA3=A3+AA3
31 CONTINUE
*WRITE(4,*) AA1, AA2, AA3
STOP
END
```